Versuchsanstalt für Wasserbau
Hydrologie und Glaziologie
der Eidgenössischen
Technischen Hochschule Zürich

Mitteilungen 214

Dye tracing and modelling jökulhlaups

Mauro A. Werder

Zürich, 2009

Herausgeber: Prof. Dr. Robert Boes

Zitiervorschlag für VAW-Mitteilungen:

Werder, M.A. (2009).
Dye tracing and modelling jökulhlaups.
Mitteilungen 214, Versuchsanstalt für Wasserbau, Hydrologie und Glaziologie (VAW),
R. Boes, Hrsg., ETH Zürich.

Im Eigenverlag der
Versuchsanstalt für Wasserbau,
Hydrologie und Glaziologie
ETH Zürich
CH-8092 Zürich

Tel.: +41 - 44 - 632 4091
Fax: +41 - 44 - 632 1192
e-mail: info@vaw.baug.ethz.ch

Zürich, 2009

ISSN 0374-0056

Presently Baedeker [the guidebook] was found again, and I hunted eagerly for the time-table. There was none. The book simply said the glacier was moving all the time. This was satisfactory, so I shut up the book and chose a good position to view the scenery as we passed along. I stood there some time enjoying the trip, but at last it occurred to me that we did not seem to be gaining any on the scenery. I said to myself, “This confounded old thing’s aground again, sure,”—and opened Baedeker to see if I could run across any remedy for these annoying interruptions. I soon found a sentence which threw a dazzling light upon the matter. It said, “The Gorner Glacier travels at an average rate of a little less than an inch a day.” I have seldom felt so outraged. I have seldom had my confidence so wantonly betrayed. I made a small calculation: 1 inch a day, say 30 feet a year; estimated distance to Zermatt, 3 1–18 miles. Time required to go by glacier, *a little over five hundred years!* I said to myself, “I can *walk* it quicker—and before I will patronize such a fraud as this, I will do it.”

When I revealed to Harris the fact that the passenger-part of this glacier,—the central part,—the lightning-express part, so to speak,—was not due in Zermatt till the summer of 2378, and that the baggage, coming along the slow edge, would not arrive until some generations later, he burst out with,—

“That is European management, all over! An inch a day—think of that! Five hundred years to go a trifle over three miles! But I am not a bit surprised. It’s a Catholic glacier. You can tell by the look of it. And the management.”

Mark Twain, A Tramp Abroad, 1880

Preface

Jökulhlaups, an islandic term for the sudden drainage of glacier dammed lakes, pose one of the greatest and far reaching glacier related hazards. These lakes have the tendency to drain rapidly once an initial drainage pathway has been established. Gornersee is a typical example of such a lake. It is located at the confluence area between Gorner- and Grenzgletscher above Zermatt, Valais. In this thesis, the author presents an experimental study of the glacier drainage system of Gornergletscher. The measurements are interpreted using existing and newly developed models of jökulhlaups, with the ultimative goal to predict the timing and magnitude of jökulhlaups.

The author first presents results from dye-tracing experiments using at least six moulins over three field seasons and related hydrological measurements. Interestingly, the outburst flood drainage conditions for each of the three years differed considerably: subglacial in the first year, followed by a supraglacial event in the second year and a mixed one in the third year. During the outburst in 2006, the author was able to directly inject dye tracer into the drainage channel of Gornersee during the onset of its outburst and measure the flow speed of the lake water on its passage through the glacier. This made it possible to test a jökulhlaup model not only against discharge measurements, but for the first time also against measured water flow speeds. The author shows that the the ability of the jökulhlaup model to match discharge hydrographs provides only a weak test of whether that model produces a satisfactory representation of reality. The present work shows that there is a mismatch between the simulated water velocity and those inferred by dye tracing. Furthermore, the author points out that the onset part of the flood hydrograph is not well represented by the jökulhlaup model. These are important new results which should help to motivate the glaciological community to improve existing jökulhlaup models.

The newly formed supraglacial lake on Unterer Grindelwaldgletscher shows that new glacier lakes can develop rapidly due to glacier change. Model calculations performed by the author have shown that the destructive potential of the expected floods in the next years is considerable. The performed predictions of maximal discharge for 2008 were successful and lay within the uncertainty range. These uncertainties are due to poorly known external factors, such as lake water temperature and roughness of the water channel within the glacier.

The present work illustrates that the onset time of a jökulhlaup can not be predicted yet. This is because small scale processes, like the development of small cracks, may either be sufficient or not to initiate a drainage before the lake fills to or above flotation level. It seems unlikely that such small scale processes can be detected by some measurement techniques anytime soon. However, the results of this study have shown that jökulhlaups can be used as natural experiments which probes the non-equilibrium behaviour of subglacial processes due to the large perturbation caused by the heightened discharge. Thus, new insights can be gained of processes governing the interaction of the glacier drainage system with the glacier dynamics and vice-versa.

Zürich, December 2009 Martin Funk

Contents

List of Figures

List of Tables

Abstract

This thesis is part of a large project conducted by our group on Gornergletscher, Switzerland, to investigate the yearly jökulhlaups (glacier lake outburst floods) occurring there. The culprit of these outburst floods is Gornersee, an ice marginal lake. The focus of this thesis lies in the hydrological and hydraulic aspects of the drainage of this lake. Naturally, other aspects of the hydrology of Gornergletscher were also studied, as well as a hazard assessment study of the newly formed supraglacial lake on Unterer Grindelwaldgletscher, Switzerland.

The evolution of Gornergletscher's drainage system was studied with dye tracer experiments and complementary hydrological measurements. A clear seasonal evolution of the drainage system could be seen which, in 2005, coincided with the lake drainage, suggesting a causal relationship. During the jökulhlaups, tracer transit speeds double and there is evidence that subglacial water storage processes during the flood are due to lateral spreading of water at the glacier bed. Water transit speed in the main subglacial drainage channel can be estimated from these tracer experiments and the results show that, even during the jökulhlaup, they are lower than predicted by models. The puzzling observational fact, that transit speeds are highest after the peak of the flood, is caused by tracer retardation in the injection moulin.

During the supraglacial lake drainage in 2006, I conducted a series of high frequency tracer injections during 55 hours to investigate the diurnal variability of the drainage system. The discharge conditions of the moulin were exceptionally stable because Gornersee was steadily draining into it, contrasting to existing measurements from Unteraargletscher where such a series was performed using an ordinary moulin, fed by a meltwater stream with large diurnal fluctuations. On Gornergletscher, I found two daily transit speed maxima and minima whereas on Unteraargletscher only one maximum and minimum was observed. I devised a simple two component model of the en- and subglacial drainage system which can simulate the qualitatively different results from the Gorner- and Unteraargletscher experiments.

In 2006, due to special circumstances, I was able to directly inject dye tracer into the drainage channel of Gornersee during the onset of its outburst and measure the transit speed of the lake water on its passage through the glacier. This made it possible to test an established jökulhlaup model, not only against discharge measurements, but for the first time also against water flow speeds inferred from measurements. In order to fit the model, the sinuosity or heat transfer needed to be increased. However, the inferred flow speeds during the first 12 hours cannot be fitted by the model leading to the conclusion that initially the drainage path is not a usual subglacial channel (R channel).

The newly formed lake on Unterer Grindelwaldgletscher is threatening the communities downstream with severe floods. A hazard assessment study was conducted which estimates the increase in lake volume, predicts maximal future flood discharges and advanced warning times over the next five years. An early warning system was set up and this study was used to decide on preventative measures to be taken.

Zusammenfassung

Diese Doktorarbeit ist ein Teil eines grossen Projekts unserer Forschungsgruppe, welches die alljährlichen Gletscherseeausbrüche am Gornergletscher untersucht. Verursacher dieser sogenannten Gletscherläufe ist der eismarginale Gornersee. Der Schwerpunkt dieser Arbeit liegt in den hydrologischen und hydraulischen Aspekten solcher Flutwellen, aber natürlich werden auch andere Themen beleuchtet, unter anderem eine Gefahrenbeurteilung des neu entstandenen Sees auf dem Unteren Grindelwaldgletscher.

Die Zeitentwicklung des glazialen Abflusssystems des Gornergletschers wurde mit Färbversuchen und ergänzenden hydrologischen Experimenten untersucht. Eine deutliche saisonale Entwicklung wurde beobachtet, welche im Jahr 2005 zeitlich mit dem Anfang des Gletscherlaufes zusammenfiel und dadurch auf einen Kausalzusammenhang schliessen lässt. Während des Gletscherlaufs verdoppeln sich die Tracerdurchgangsgeschwindigkeiten, jedoch liegen die abgeschätzten Fliessgeschwindigkeiten im subglazialen Abflusssystem tiefer als Modelvorhersagen. Die Durchgangsgeschwindigkeiten sind nach der Seeentleerung am höchsten, was mit der Verzögerung des Tracers in der Injektionsmühle erklärt werden kann. Die beobachteten Wasserspeicherungsprozesse während des Ausbruchs werden durch eine sich ausbreitende Wasserschicht am Gletscherbett verursacht.

Eine Serie von Färbeversuchen über 55 Stunden wurde während der supraglazialen Entleerung des Sees im Jahr 2006 durchgeführt um die tageszeitliche Variabilität des Abflusssystems zu untersuchen. Der Abfluss in die Injektionsmühle war ausserordentlich stabil, weil sich der See durch diese entleerte. Die Ergebnisse werden mit solchen von zwei vorliegenden Messreihen vom Unteraargletscher verglichen, welche eine normale Mühle mit hohen tageszeitlichen Abfluss-schwankungen für die Injektionen verwendeten. Die Durchgangsgeschwindigkeiten der Messungen vom Gornergletscher zeigen zwei tägliche Maxima und Minima, wohingegen die vom Unteraargletscher nur jeweils ein solches aufweisen. Ich habe ein Zweikomponentenmodell des en- und subglazialen Abflusssystems entwickelt, welches die qualitativ unterschiedlichen Resultate vom Unteraar- und Gornergletscher reproduziert.

Im Jahr 2006 war es dank ungwöhnlicher Umstände möglich, das Wasser des auslaufenden Sees direkt mit Tracer zu markieren und damit seine Durchgangsgeschwindigkeit zu ermitteln. Dies ermöglicht erstmals ein Gletscherlaufmodell nicht nur mit gemessenen Abflüssen sondern auch mit abgeschätzten Fliessgeschwindigkeiten zu testen. Um das Modell anpassen zu können, müssen entweder die Kanalrauigkeit oder die Wärmeleitung zwischen Wasser und Eiskanalwand erhöht werden. Jedoch können die sehr tiefen abgeschätzten Fliessgeschwindigkeiten der ersten 12 Stunden des Ausbruchs nicht vom Modell reproduziert werden, was schliessen lässt, dass anfänglich der Abfluss nicht durch einen normalen subglazialen Kanal (R channel) führt.

Der neu entstandene See auf der Zunge des Unteren Grindelwaldgletschers bedroht die flussabwärts gelegenen Gemeinden. Eine Gefahrenabschätzungsstudie wurde durchgeführt, in welcher der Anstieg des Seevolumens in den nächsten fünf Jahren abgeschätzt wird und die zukünfitgen Spitzenabflüsse und Vorwarnzeiten prognostiziert werden. Ein Vorwarnsystem wurde installiert, und anhand dieser Studie wurden bauliche Massnahmen beschlossen.

Chapter 1

Introduction

Jökulhlaups, also known as glacier lake outburst floods, pose one of the greatest and far reaching glacier related hazards. Ice-dammed lakes have the tendency to drain rapidly once an initial drainage path has been established. This can be attributed to two factors: First, ice has a 10% lower density than water, thus an ice dam can be lifted up once the lake level reaches 90% of the dam height. This type of lake drainage initiation leads to jökulhlaups with the most rapidly rising discharge. Second, once a small drainage path is established, it enlarges due to melting on its walls because of positive lake water temperature and because of dissipation of potential energy. This is a runaway process and leads to a progressively increasing lake discharge. Both of these processes lead to glacier lake outburst floods.

Our group investigated two ice-dammed lakes, both located in Switzerland. Gornersee, an ice marginal lake, on Gornergletscher is situated upstream of Zermatt, Valais (Fig. 1.1, 1.2). Before the installation of a water catchment station in the 1960s by a hydroelectric power company, the drainage of Gornersee regularly caused damage in Zermatt. The water catchment station effectively limits the peak discharge flowing through Zermatt. However, the combination of a heavy rainfall or very warm weather with the lake outburst could potentially still lead to damage.

The newly formed supraglacial lake on Unterer Grindelwaldgletscher, Bernese Oberland (Fig. 1.3) has much greater hazard potential. This lake first formed in 2005 and its basin has been increasing in size ever since. This increase is caused by larger ice surface lowering rates in the lake basin compared to on the debris-covered dam. The outburst of this lake will likely cause severe floods if no damage prevention measures are taken.

Of course, jökulhlaups are by themselves an interesting phenomenon meriting study and have for many years captured the attention of glaciologists (e.g. Thorarisson, 1939; Mathews, 1965; Nye, 1976; Clarke, 1982; Ng et al., 2007). They are one of the most dynamic large scale glacial process and illustrate dramatically the interaction of the glacier drainage system with the ice mass of the glacier and vice versa. The recent discovery of active subglacial lakes in Antarctica (e.g. Wingham et al., 2006) has sparked new interest in the subject.

Figure 1.1: *Watercolour by Bruno Nedela of Monte Rosa (2006), enclosed by Gornergletscher (left) and Grenzgletscher (right), and Gornersee in their confluence as seen from our field camp.*

Many of the processes driving jökulhlaups are still poorly understood, especially the triggering mechanisms and early stages of the outbursts. To predict the onset time of a jökulhlaup both of these processes need better understanding. The evolution of the flood can be modelled by lake discharge flowing through en- and subglacial channels, so-called R channels (Röthlisberger, 1972), as done by e.g. Clarke (2003), possibly coupled to subglacial sheet flow (Flowers et al., 2004). However, models which take the interaction of the jökulhlaup with the rest of the glacier drainage system into account, e.g. existing R channels or en- or subglacial water storage, are not well developed (Kessler and Anderson, 2004). Hydrofracturing of the ice has been observed (Roberts et al., 2000; Waller et al., 2001) in the field but no existing theories take this process into account. The lake drainages observed in Antarctica seem to be more gradual with a constant discharge over several month to years (Wingham et al., 2006). This cannot be explained with current theories of subglacial drainage as they all predict a progressively increasing discharge.

1.1 Aim

The project of our group on Gornergletscher has been one of, if not the most, comprehensive field study of a jökulhlaup to date. The project can be split into three parts, each of which is the topic of a doctoral thesis: Fabian Walter's (2009) thesis concentrates on ice quakes during the jökulhlaup, Patrick Riesen's (in progress) thesis studies the ice flow perturbations due to the jökulhlaup and my thesis is on the hydrological and hydraulic aspects of the jökulhlaup.

The aim of my part of the project was

1. to experimentally study the glacier drainage system of Gornergletscher,
2. to apply existing and newly developed models to Gornergletscher jökulhlaups,
3. and to predict the timing and magnitude of the jökulhlaups.

1.1.1 Experimental investigation

The Gornersee jökulhlaups were experimentally studied using numerous methods: lake level measurement; lake bathymetry and surface topography from aerial photography; bed topography from radar echo soundings; surface flow speed and ablation measurements at stakes; subglacial water pressure, ice deformation and temperature measurements in boreholes; discharge, conductivity and turbidity measurements in the proglacial stream Gornera; meteorological measurements; active and passive source seismology; and tracer experiments, which are the focus of this thesis.

I conducted over 200 dye tracer experiments during three field campaigns on Gornergletscher (2005–2007). Dye tracer experiments are quite a simple kind of measurement (Käss, 1998): dye is poured into the water of which the flow characteristics should be determined. The dye content of the water is monitored somewhere downstream, in my case in the proglacial stream, by an instrument called fluorometer. The breakthrough curve is the result of the experiment: a time series of the dye concentration at the detection site, which then needs to be interpreted. The main difficulty in the interpretation is that the breakthrough curve is an integrated measure of the conditions the tracer encountered on the whole flow path.

Figure 1.2: *Photograph of the filled Gornersee in 2004. The lake is situated in the confluence area of the Gorner- and Grenzgletscher tributaries. The right part of the lake is covered in icebergs whereas the left part is mostly open water.*

Figure 1.3: *Photograph of the filled supraglacial lake on Unterer Grindelwaldgletscher in 2008. The completely debris covered glacier is situated in the valley bottom.*

The dye tracer experiments I conducted, complemented with the lake level, proglacial discharge and subglacial water pressure measurements, were used to study:

- the seasonal evolution of the drainage system and its interrelationship with the jökulhlaup,
- the catchment structure of Gornersee on its Grenzgletscher side,
- the englacial drainage system within the lake dam and its interaction with the filling lake,
- the influence of the jökulhlaups on the glacier drainage system,
- the lake water transit speeds during the onset of the 2006 jökulhlaup,
- and the diurnal variability of the glacier drainage system during the exceptional circumstances of the subsequent supraglacial overspill lake drainage in 2006.

The strategy I employed to achieve the first of above points was the following: each year I chose one or two main moulins which were used for frequent tracer injections, i.e. with an interval of 1 to 7 days. I injected tracer always at 14:00 CEST at the time of highest surface melt to make them comparable to each other. These injections were used to study the evolution of the flow path of the water entering the moulin due to the seasonal changes and the jökulhlaup. In 2005, the main moulin was M1, located about 600 m downglacier of the lake (c.f. Fig. 2.2). In 2006, the main moulins were M4, located right beside the lake, and M2, 500 m downglacier of the lake. In 2007, the main moulins were again M2 and also M3, located on the Grenzgletscher side of the lake dam. Additionally, I also used some other moulins for tracer injections albeit at a lower frequency, like M0 situated above the lake.

To determine the catchment of Gornersee on its Grenzgletscher side, I injected tracer into many of the moulins situated on the lake dam. I associated them with the lake catchment if no dye was registered at the fluorometer, i.e. the water flowed into the lake.

The last of above points was assessed by injecting dye at an interval of 3 h into moulin M4, into which the lake drained supraglacially in 2006. These experiments were inspired by a similar series of experiments of Schuler et al. (2004) on Unteraargletscher to which they are compared.

1.1.2 Modelling the jökulhlaup

Quantitative evaluation of tracer experiments was made possible by interpreting them with the help of simple models of the glacial drainage system, e.g. the diurnal variability of the glacier drainage system was captured in a two component model of the en- and subglacial water flow reproducing the measured transit speeds and allowing to infer subglacial transit speeds. The measurements during the onset of the lake drainage in 2006 were compared one to one to the established jökulhlaup model of Clarke (2003).

1.1.3 Flood magnitude prediction

Furthermore, the appearance and fast growth of the new supraglacial lake on Unterer Grindelwaldgletscher and its outbursts spurred a hazard assessment investigation where my task was to predict future flood magnitudes. This was achieved by applying Clarke's 2003 model to the situation on Unterer Grindelwaldgletscher. The comparison of model results to observations showed that the outburst of glacier lakes can be more complicated than what current models describe; as was also the case with the Gornergletscher jökulhlaups. Nevertheless, estimates of the flood magnitude and duration were possible to make, however, predicting the timing of the onset remains an unsolved problem.

1.2 Structure

Three of this thesis' Chapters 5, 6 and 7 are derived from publications in peer reviewed journals (Werder et al., 2009; Werder and Funk, 2009; Werder et al., 2010), Chapter 4 is in preparation to be submitted (Werder et al., submitted). Thus, those four chapters are self contained. To keep with this structure the two additional chapters (2 and 3) and were also set up to be self contained.

Part I: Dye tracing jökulhlaups

Chapter 2
Seasonal evolution of the glacier drainage system
The seasonal evolution of the glacier drainage system of Gornergletscher is investigated using dye tracer experiments and complementary hydrological measurements. I interpret the evolution of double peaked dye breakthrough curves with the help a model of two competing R channels.

Chapter 3
Catchment of Gornersee and hydraulics of the lake dam
The drainage system within the ice dam of Gornersee on its Grenzgletscher side was probed with tracer experiments: I determined the catchment structure of Gornersee and observed how two large calving events disturbed the englacial drainage system within the lake dam.

Chapter 4
Short term variations of tracer transit speed on Alpine glaciers
The supraglacial overspill of Gornersee in 2006 lasting three weeks lead to very stable discharge conditions in the moulin into which it drained. We conducted a series of tracer injections into this moulin over a diurnal discharge cycle to investigate the effects of these stable discharge conditions on tracer transit speeds. The findings are compared to existing measurements using a 'normal' moulin with large diurnal discharge fluctuations. A two component model of the en- and subglacial drainage system is devised to calculate tracer transit speeds and is fitted to our and the existing measurements.

Chapter 5
Dye tracing a jökulhlaup:
Subglacial water transit speed and water storage mechanism
We investigated the influence of the Gornersee jökulhlaups in 2005 and 2007 on the glacier drainage system with dye tracer experiments. For their interpretation, we use a model of tracer retardation inside the injection moulin due to inflow modulation. We see evidence for water storage at the glacier bed and we can give bounds on the subglacial flow speed of the lake water during the 2005 jökulhlaup.

Part II: Modelling jökulhlaups

Chapter 6
Testing a jökulhlaup model against flow speeds inferred from measurements

In 2006, the lake drained by overspilling into a moulin on its shore and thus we were able to inject dye into the lake outlet. During the first 1.5 days of the drainage, fully pressurised flow conditions prevailed in the lake outlet channel allowing us to simulate this situation with a jökulhlaup model. For the first time, this made it possible to compare measured and modelled water flow speeds of a jökulhlaup.

Chapter 7
Hazard assessment investigations in connection with the formation of a lake on the tongue of Unterer Grindelwaldgletscher, Bernese Alps, Switzerland

The newly formed glacier lake on Unterer Grindelwaldgletscher is threatening the villages downstream with flooding. We conducted a hazard assessment study to quantify the growing flood risks. A jökulhlaup model was run assuming different scenarios using estimates of the future evolution of the lake hypsometry to predict maximal lake discharges and advance warning times.

Part I

Dye tracing jökulhlaups

Chapter 2

Seasonal evolution of the glacier drainage system

Abstract During the three field seasons 2005–2007 on Gornergletscher, I was able to study the winter–summer and, in one instance, the beginning of the reverse transition of the glacier drainage system. I inferred tracer transit speeds as low as $0.03\,\mathrm{m\,s^{-1}}$ in the inefficient winter regime and up to $0.75\,\mathrm{m\,s^{-1}}$ during the summer regime. In 2007, I observed double peaked tracer return curves from two moulins which evolved synchronously over five days. I interpreted this to be due to water flowing through two distinct pathways and modelled this process successfully with a lumped element model of two competing R channels. In 2005, the onset of the jökulhlaup coincided with the winter–summer transition of the glacier drainage system near the lake, suggesting a causal relationship. It has been proposed before that such a transition could triggering a jökulhlaup for which I show evidence.

2.1 Introduction

The glacier drainage system adjusts its capacity to the prevailing meltwater discharge conditions. In winter, it is inefficient as it carries little discharge. In spring, with increased meltwater flux, the drainage system adjusts its capacity and becomes more efficient and, in autumn, the reverse transition takes place. I conducted dye tracer experiments during these transition phases which are the focus of this chapter. The seasonal evolution of the drainage system has been studied before by dye tracer experiments (e.g. Bingham et al., 2005), and Nienow et al. (1998) observed that the transition area from inefficient to efficient migrates upglacier with the receding snowline.

This chapter is organised as follows: I describe the field site, terminology and location and sizes of the moulins used for tracer injections presented in this chapter and Chapter 3. To interpret some of the findings, I introduce a lumped element model describing two competing subglacial channel, so called R channels (Röthlisberger, 1972). I present results from 31 tracer injections in 2005–2007 using six moulins. The winter–summer and reverse transition are discussed with a series of injections conducted in 2005. In 2007, I observed the evolution of double peaked breakthrough curves from tracer experiments conducted using two different moulins at the same time and interpret this with the lumped element model. Finally, I discuss the possibly causal relationship between the lake outburst in 2005 and the winter–summer transition.

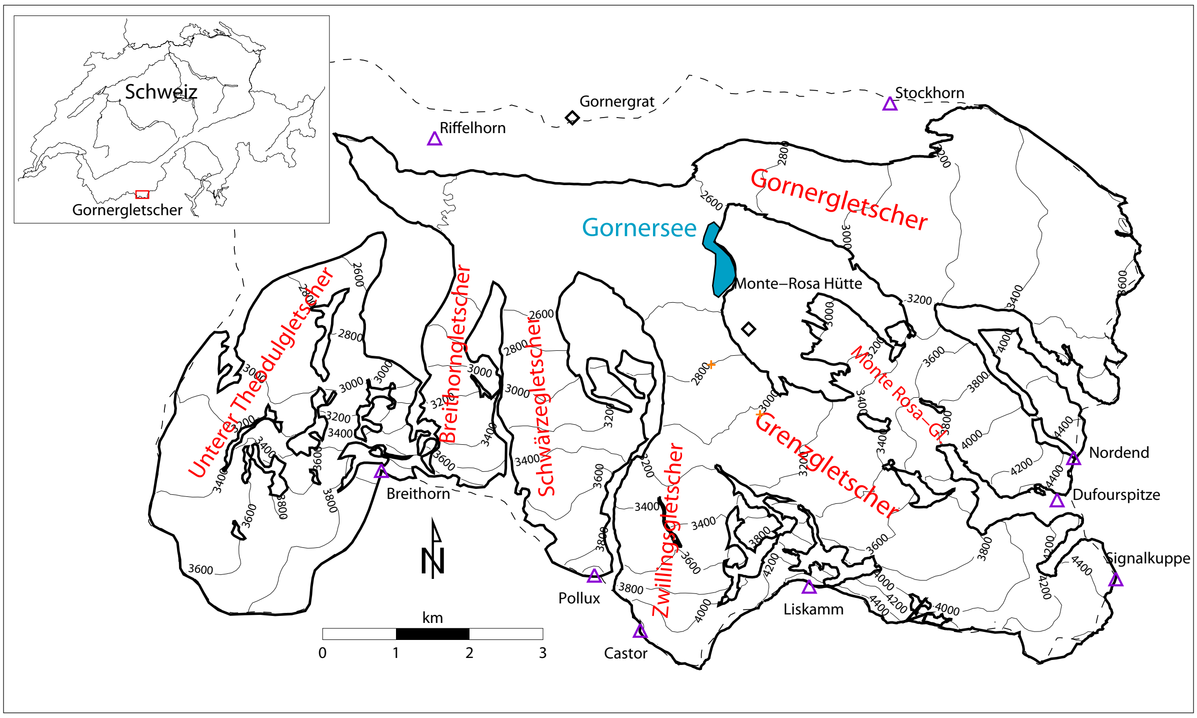

Figure 2.1: *Overview map of Gornergletscher and its tributaries. Contour line interval is 200 m, the catchment is outlined with the dashed line, triangles mark mountain summits and huts are marked with diamonds.*

2.2 Field site

Gornergletscher is a large valley glacier in the Swiss Alps with a surface area of $\sim$60 km^2 and a length of 14 km (Fig. 2.1). Its accumulation area lies on the slopes of several 4000 m peaks including the highest summit in Switzerland, Monte Rosa/Dufourspitze 4634 m. It has six major tributaries, Gornergletscher (giving its name to the whole glacier system), Monte Rosagletscher, Grenzgletscher (the largest one), Zwillingsgletscher, Schwärzegletscher and Breithorngletscher; the two Theodulgletscher do not connect to Gornergletscher anymore. Gornergletscher is one of the few polythermal valley glacier in the Alps (Ryser, 2009) due to the high altitude of some of its accumulation area. The terminus is currently located at $\sim$2200 m a.s.l. where a single proglacial stream, the Gornera, exits the glacier. The tongue reaches up to $\sim$2550 m a.s.l. and its surface is characterised by large canyons and small ponds, so called entonnoirs (Renaud, 1936). The ice thickness reaches up to 450 m in the overdeepened part of the tongue (Fig. 2.2). Gornersee, an ice marginal lake, is located in the confluence area of Gorner- and Grenzgletscher at 2530 m a.s.l. Gornersee fills every spring and drains in summer, normally as a jökulhlaup (glacier lake outburst flood) but supraglacial overspill has also been observed. In the past years the maximal volume of the lake basin was estimated to be $\sim 4.5\times10^6$ m^3 and peak discharge from the lake is $\sim$20 m^3 s^{-1}. The jökulhlaup lasts for about two to seven days, depending on the lake volume and the exact outburst mechanism.

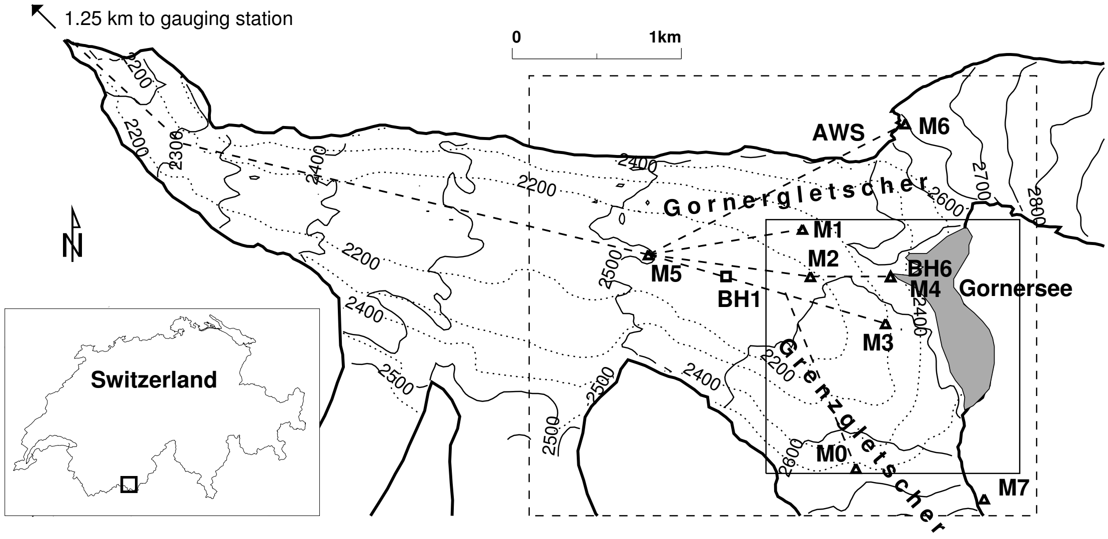

Figure 2.2: *Map of the tongue of Gornergletscher with solid contours of surface elevation and dotted contours of bed elevation. The moulins used for tracer injections are marked by triangles and labelled by M0–M7, their transit distance is measured along the dashed lines. The subglacial water pressure was measured in the boreholes marked BH1 and BH6. The automatic weather station is at the northern glacier margin (AWS). The dashed box bounds the inset displayed in the result Figures 2.5–2.10 and the solid box the detail in Figure 3.1.*

2.3 Background and methods

Our group has conducted field studies on Gornergletscher during the years 2004–2008. Apart from those in the first and last years, the field studies included dye tracer experiments which can be divided into three types: experiments to study the evolution of the drainage system on a diurnal time scale (Chapter 4), due to the seasonal evolution (the focus of this chapter), due to the jökulhlaup (Chapter 5 and 6) and injections to study the configuration of the lake catchment (Chapter 3). Complementing measurements included: lake level and temperature, proglacial discharge (provided by Grande Dixence SA, a hydro-electric power company) and water temperature, subglacial water pressure in boreholes (Huss et al., 2007), surface ice flow speed measured with GPS and theodolite at more than 30 stakes (Sugiyama et al., 2007, 2008), active and passive seismology (Walter, 2009), air temperature, precipitation, weather observations, surface topography from photogrammetry and bed topography from radar echo soundings.

The fluorescent dyes Rhodamine WT and Uranine were used for tracer injections which were conducted manually at 14:00 CEST. The dye was registered at the water catchment station of Grande Dixence SA, 1.25 km downstream of the glacier terminus with a Tuner 10-AU and a BackScat fluorometer, which both allowed continuous dye detection. The proglacial discharge was measured at the catchment station by Grande Dixence SA. The ventilated off-ice air temperature and precipitation was registered at the automatic weather station (AWS in Fig. 2.2). Subglacial water pressure was measured in the boreholes BH1 and BH6 (Fig. 2.2). The field methods are described in more detail in Section 5.4.

From the tracer breakthrough curves I extracted the *residence time* (t), defined as the time interval between the injection time and the time of maximal tracer concentration at the detection site. The *transit distance* ($\hat{l}$) is defined as the shortest possible horizontal travel distance of the tracer (marked with dashed lines in Fig. 2.2). The *transit speed* is then defined by the ratio $\hat{v} = \hat{l}/t$. Note that the transit speed is a lower bound on the mean, channel cross-section averaged tracer flow speed, as the transit distance is the shortest possible flow path length of the tracer (for a more in-depth discussion of these terms refer to Sections 5.2 and 6.2). Furthermore, the breakthrough curves were fitted by an advection-dispersion model with storage term (van Genuchten and Wierenga, 1976; Smedt et al., 2005) giving the additional characterising parameters of dispersion D, fraction of mobile water β and exchange coefficient between mobile and immobile water ω (not presented). The fraction of returned tracer mass M can be calculated by integrating the dye concentration multiplied by the proglacial discharge. The presented breakthrough curves are normalised. The normalised tracer load C_{norm} is defined as tracer mass flux divided by the injected mass. This allows the comparison of breakthrough curves from experiments conducted with different injected tracer masses and during different proglacial stream discharge conditions. For a more in-depth description of the data processing and definitions of terms refer to Section 5.4.1.

2.3.1 Injection sites

The moulins used for tracer injections are marked on the map in Figure 2.2. With their description, I give a qualitative attribute of maximal discharge into the moulin using the following classification: “small” with maximum discharge smaller than about 0.1 $\mathrm{m^3\,s^{-1}}$, “medium” with maximum discharge in the range 0.1–0.4 $\mathrm{m^3\,s^{-1}}$ and “large” with maximum discharge >0.4 $\mathrm{m^3\,s^{-1}}$. M5 (large, transit distance $\hat{l} = 5\,\mathrm{km}$) was used in 2005 and is located 2 km downglacier of the lake. M0 (medium, $\hat{l} = 7\,\mathrm{km}$) was used in all years for injections and is located about 1 km upglacier of the lake on the Grenzgletscher tributary. M1 (large, $\hat{l} = 6\,\mathrm{km}$) was used in 2005 and is located about 600 m downglacier of the lake . M4 (small, $\hat{l} = 6.5\,\mathrm{km}$), used in 2006, is situated beside lake; it was the moulin into which the lake overspilled and drained in 2006 (see Chapter 6). M3 (small, $\hat{l} = 6.5\,\mathrm{km}$), used in 2007, is located about 200 m from the lake, just at the edge of the ice dam on the Grenzgletscher side. M2 (large, $\hat{l} = 6\,\mathrm{km}$) used in 2006 and 2007 is located about 500 m downglacier of the lake, probably closer to the main drainage channel than M1 used in 2005 (see Chapter 6 for a discussion on the location of the main drainage channel). M6 (large, $\hat{l} = 6\,\mathrm{km}$) is situated on the Gornergletscher tributary. In the presentation of the results, I use the abbreviations expM0–expM6 to refer to a tracer experiment using M0–M6 as injection site.

2.3.2 Lumped element model

In 2007, tracer injections from two moulins yielded double peaked return curves for the duration of a week. This phenomenon is commonly attributed to being caused by two alternative flow paths of the tracer. In a glacier this could be due to two parallel, competing channels in the ice or at the glacier bed, so called R channels (Röthlisberger, 1972). These R channels adjust their size according to the discharge and effective pressure conditions, they can grow by ice melt at the R channel wall and shrink by creep closure of the ice. As their hydraulic conductivity and growth rate increase with size, larger R channels can capture the discharge of smaller R channels and grow at their expense. I set up a simple lumped element model (Fig. 2.3) to simulate this type of evolution and will compare it to the evolution of the measured double peaked breakthrough curves.

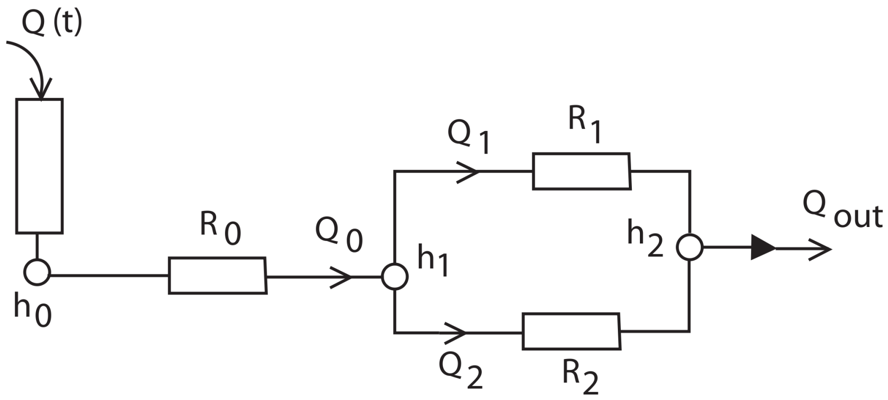

Figure 2.3: *Sketch of the lumped element model containing two competing R channels used for residence time calculation. R_i are the R channel elements, Q_i the discharges and h_i the hydraulic heads (i=0. . . 2). The leftmost element represents the injection moulin.*

Table 2.1: *Compilation of physical constants used in the lumped element model*

Constant	Variable	Value
Ice flow exponent	n	3
Constant 1	C_1	$2.2\times10^{-5}\,\mathrm{m}^{-1}$
Constant 2	C_2	$3.7\times10^{-13}\,\mathrm{m}^{-n}\,\mathrm{s}^{-1}$
Latent heat of fusion	L	$333.5\,\mathrm{kJ\,kg}^{-1}$
Pressure melting coefficient	c_t	$7.5\times10^{-8}\,\mathrm{K\,Pa}^{-1}$
Specific heat capacity of water	c_p	$4180\,\mathrm{J\,kg}^{-1}\,\mathrm{K}^{-1}$
Gravitational acceleration	g	$9.8\,\mathrm{m\,s}^{-2}$
Density of water	ρ_w	$1000\,\mathrm{kg\,m}^{-3}$
Density of ice	ρ_i	$900\,\mathrm{kg\,m}^{-3}$
Ice flow constant	B	$5.3\times10^{-24}\,\mathrm{Pa}^{-n}\,\mathrm{s}^{-1}$

The model follows Clarke (1996) and I will reference equations therein in this paragraph. To simulate R channels, I use Röthlisberger resistors (Eqn. 27) for circular R channels. Note that in this chapter the resistance parameter R is equivalent to Clarke's F_T defined by his Equation 17. I use his Equation 5 to model the moulin which is fed by an ideal discharge generator (Eqn. 2).

The model (Fig. 2.3) consists of a moulin element and three R channel elements, two of which are in parallel. The moulin element has a filling height h_0 and a cross-sectional area A. The R channel elements have resistance R_i, cross-sectional area S_i and length l_i. The upper boundary condition is the discharge into the moulin Q and the lower boundary condition is given by the hydraulic head $h_2 = 0$ (atmospheric pressure), where the water of the two R channel merges again. This leads to the following system of differential algebraic equations for h_1, h_2, Q_i and S_i $(i = 0 \ldots 2)$

$$\frac{dh_0}{dt} = \begin{cases} \frac{Q-Q_0}{A_{\text{small}}} & \text{if } h_0 \leq h_{\text{min}}, Q \leq Q_0 \\ 0 & \text{if } h_0 \geq h_{\text{max}}, Q \geq Q_0 \\ \frac{Q-Q_0}{A} & \text{otherwise} \end{cases} \tag{2.1}$$

$$h_0 - h_1 = R_0 Q_0^2 \tag{2.2}$$

$$h_1 - h_2 = R_1 Q_1^2 \tag{2.3}$$

$$h_1 - h_2 = R_2 Q_2^2 \tag{2.4}$$

$$Q_0 = Q_1 + Q_2 \tag{2.5}$$

$$\frac{dS_i}{dt} = C_1 \frac{Q_i \Delta h_i}{l_i} - C_2 (h_i^* - \bar{h}_i)^n S_i, \tag{2.6}$$

where $C_1 = (1 - \rho_{\text{w}} c_{\text{p}} c_{\text{t}}) \frac{\rho_{\text{w}} g}{\rho_{\text{i}} L}$ and $C_2 = 2B \left(\frac{\rho_{\text{w}} g}{n}\right)^n$ are constants, h_{max} and h_{min} are the maximum and minimum filling height of the moulin, A_{small} is the cross-sectional area of the connection of the moulin to the next element (chosen such that its volume is small compared to the discharge carried), Δh_i are the pressure drops in the R channels, $h_i^* = \rho_{\text{ice}} h_{\text{ice}\,i} / \rho_{\text{w}}$ is the hydraulic head corresponding to flotation pressure above the R channels and $\bar{h}_i$ is the mean hydraulic head in the R channels. The values used for physical constants are given in Table 2.1. The resistance R_i is calculated from S_i with the Gauckler-Manning-Strickler formulation (Chow et al., 1998) and assuming a circular cross-section

$$R_i = 2^{4/3} \pi^{2/3} \, n_{\text{man}}^2 \, l \, S_i^{-8/3}, \tag{2.7}$$

where n_{man} is the Manning roughness. If a semi-circular channel was used, R would increase by about 10% for the same S. In fact, digressing somewhat, the resistance R of a channel with a cross-sectional geometry of a circular segment with central angel θ (Fig. 2.4), introduced by Hooke et al. (1990), can also be calculated. For an arbitrary cross section we have

$$R = \frac{n_{\text{man}}^2 l}{S^2 R_{\text{h}}^{4/3}}, \tag{2.8}$$

where R_{h} is the hydraulic radius of the conduit, defined as the ratio of S to the wetted perimeter. The hydraulic radius of a Hooke-channel is given in terms of S and θ by

$$R_{\text{h}}(S, \theta) = \frac{\sqrt{(\theta - \sin\theta) S}}{\sqrt{2}(\theta + \sqrt{2 - 2\cos\theta})} \tag{2.9}$$

and thus R can be calculated as a function of S and θ by plugging Equation (2.9) into (2.8).

The system of differential algebraic equations (2.1)–(2.6) can be solved with MATLAB's ode15s solver. Once the hydraulic problem is solved, the modelled residence time in the moulin element t_{m} can be calculated approximately by

$$t_{\text{m}} = \frac{A}{Q_0} h_0, \tag{2.10}$$

assuming constant discharge conditions during the passage of the tracer. Similarly, the modelled residence time in an R channel element i is approximated by

$$t_i = \frac{S_i}{Q_i} l \tag{2.11}$$

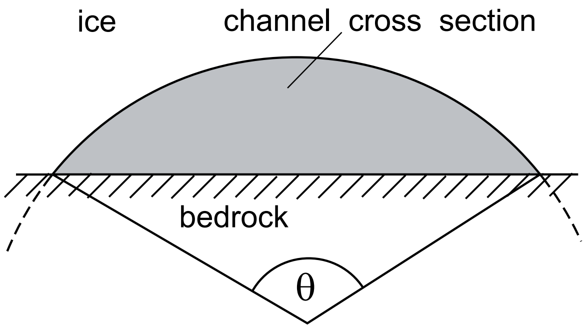

Figure 2.4: *Cross section of a Hooke-channel which has the shape of a circular segment with central angel θ.*

and the sum

$$t = t_{\mathrm{m}} + \sum_i t_i \tag{2.12}$$

is the modelled residence time. For a more complete description of the calculation of residence time and transit speed see Section 4.3.4.

2.4 Observations

The results of tracer experiments are presented in figures displaying both the tracer breakthrough curves and parameters describing those curves (transit speed $\hat{v}$, dispersion D, fraction of mobile water β and fraction of returned tracer mass M). There is a small inset in each plot showing the location of the used moulin. The results from the expM4s, expM2s and expM6s are complemented with additional hydrological and related measurements.

Figure 2.5 shows the results of expM0s in 2005. Transit speed increases from $0.1\,\mathrm{m\,s^{-1}}$ to $0.8\,\mathrm{m\,s^{-1}}$ between 10 and 23 of June. Dispersion decreases from more than $15\,\mathrm{m^2\,s^{-1}}$ to less than $2\,\mathrm{m^2\,s^{-1}}$ between 10 June and 4 August. The last expM0 was conducted in September after a snowfall when there was very little melt. The transit speed decreased to values lower than what the first expM0 produced, whereas the dispersion stayed below $2\,\mathrm{m^2\,s^{-1}}$. M5 was located $\sim$2 km downglacier of M0. expM5s (Fig. 2.6) yielded a transit speed above $0.5\,\mathrm{m\,s^{-1}}$ from the beginning of the experiments, except for the expM5 on 17 September, after the snow fall, yielding a transit speed of $0.32\,\mathrm{m\,s^{-1}}$. The fraction of returned tracer mass increased steadily over the summer season and the dispersion decreased.

M4 started conducting water a few days before I conducted the first expM4 on 10 June 2006. Transit speeds of the expM4s increase from 0.14 to only $0.4\,\mathrm{m\,s^{-1}}$ (Fig. 2.7), half of the transit speed of the expM0s in 2005. Between 15 and 20 June the breakthrough curves are double peaked. Note that this is the moulin into which the lake spilled over in 2006 from 5 July onwards which is the focus of Chapters 4 and 6.

Figures 2.8 and 2.9 show the results in 2007 of expM2s and of expM6s, respectively. Again a pronounced overall increase in transit speed is seen from $0.2\,\mathrm{m\,s^{-1}}$ to $0.75\,\mathrm{m\,s^{-1}}$ and $0.2\,\mathrm{m\,s^{-1}}$ to $0.5\,\mathrm{m\,s^{-1}}$, respectively. The decrease in transit speed of expM2s from 27 to 29 May coincided with a snowfall and cold weather period. Between 9 and 15 June the breakthrough curves of

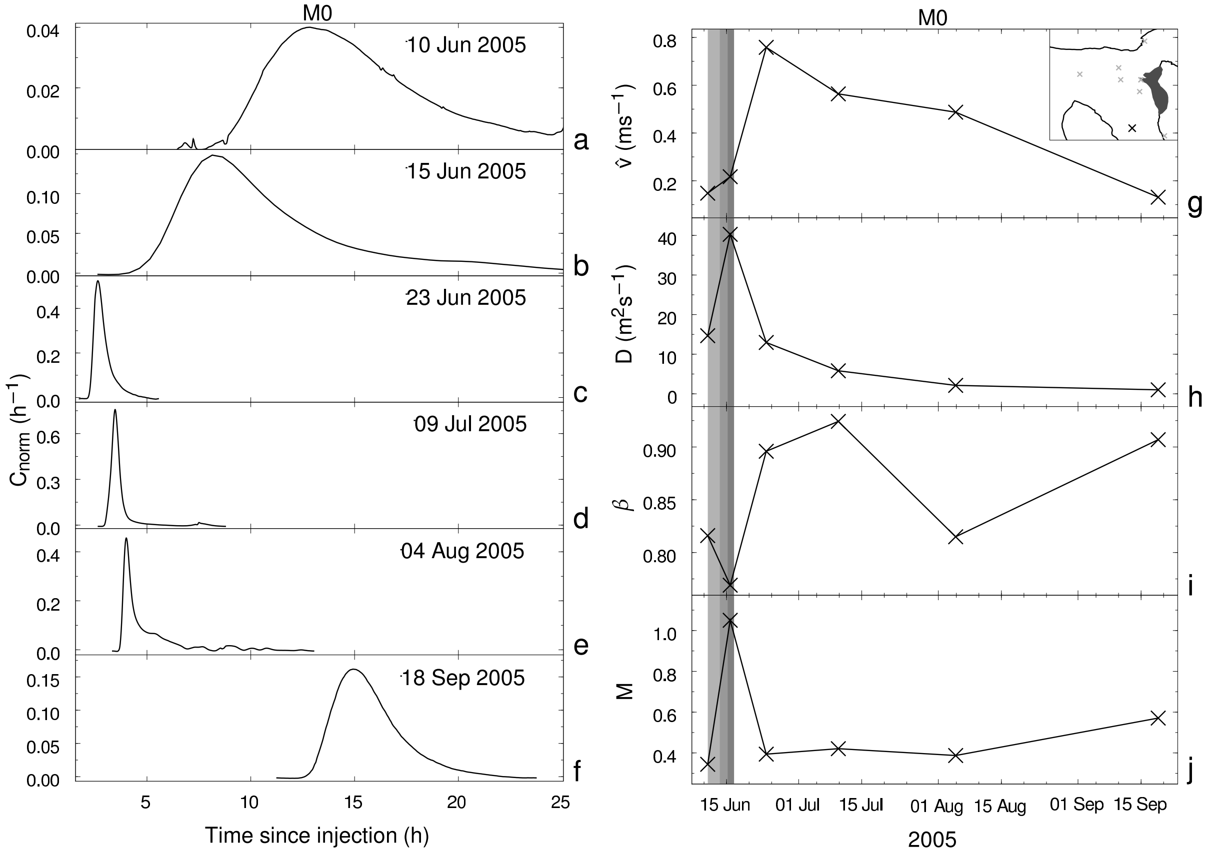

Figure 2.5: *Tracer experiments in 2005 using M0 (expM0s). (a–f) normalised breakthrough curves, (g) transit speed* $\hat{v}$*, (h) dispersion* D*, (i) fraction of mobile water* β *and (j) fraction of returned tracer mass* M*. The grey shading marks the time of the jökulhlaup and is identical to the shading in Figure 5.4. On map inset (g) the location of M0 is marked.*

both expM2s and expM6s are double peaked. In Table 2.2 the most relevant data concerning the evolution of the double peaks are summarised and they are also plotted in Figure 2.11 (right panel). The time difference between the first and second peak increases slightly for the expM2s (1.0–1.2 h) and a bit more for the expM6s (0.9–1.6 h). The ratio of the tracer load of the first to that of the second peak is 0.8 when the two peaks appear and progressively increases to >5 before the second peak disappears. To put this into a wider context, Figure 2.10 presents results of complementary measurements conducted prior and during the appearance of the double peaks, consisting of proglacial discharge, subglacial water pressure data from BH1, air temperature and precipitation. The proglacial discharge increases and its diurnal fluctuations become larger. At first, the subglacial water pressure increases, showing only minimal diurnal fluctuations. They start to become apparent on 9 June, the same day the double peaks were first observed and then become larger over the period when the double peaks are observed. Note the low subglacial water pressure on 14 June coinciding with cloudy weather and the high subglacial water pressure the day after coinciding with a rainfall event.

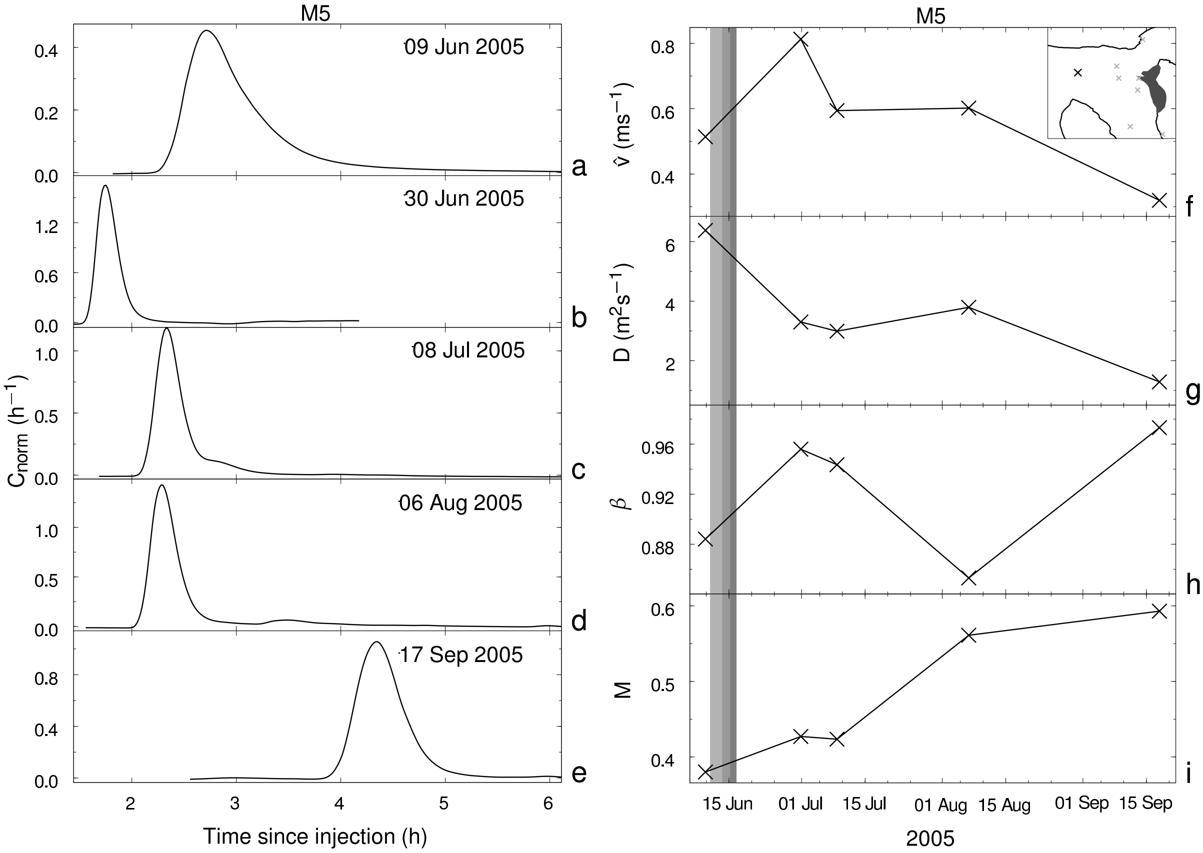

Figure 2.6: *Tracer experiments in 2005 using M5 (expM5s). (a–e) normalised breakthrough curves, (f) transit speed $\hat{v}$, (g) dispersion D, (h) fraction of mobile water β and (i) fraction of returned tracer mass M.*

Table 2.2: *Key observations of the evolution of the double peaks in expM2s (Fig. 2.8c–g) and expM6s (Fig. 2.9b–f): The residence times corresponding to the first (t_1) and second (t_2) peak, the respective transit speeds ($\hat{v}_1, \hat{v}_2$), the time difference between the peaks ($t_2 - t_1$) and the ratio of the first to second peak concentration (r_h)*

Date	t_1 (h)	$\hat{v}_1$ ($\mathrm{m\,s^{-1}}$)	t_2 (h)	$\hat{v}_2$ ($\mathrm{m\,s^{-1}}$)	$t_2 - t_1$ (h)	r_h
expM2s						
5 June	-	-	6.6	0.25	-	-
9 June	4.3	0.39	5.4	0.31	1.1	0.8
12 June	3.1	0.54	4.1	0.41	1.0	1.2
15 June	2.45	0.68	3.65	0.47	1.2	5.9
18 June	2.45	0.68	-	-	-	-
expM6s						
6 June	-	-	9	0.18	-	-
10 June	5.7	0.29	6.6	0.25	0.9	0.8
11 June	4.65	0.36	5.8	0.29	1.15	1.3
14 June	4.3	0.39	5.9	0.28	1.6	5.1
26 June	3.2	0.52	-	-	-	-

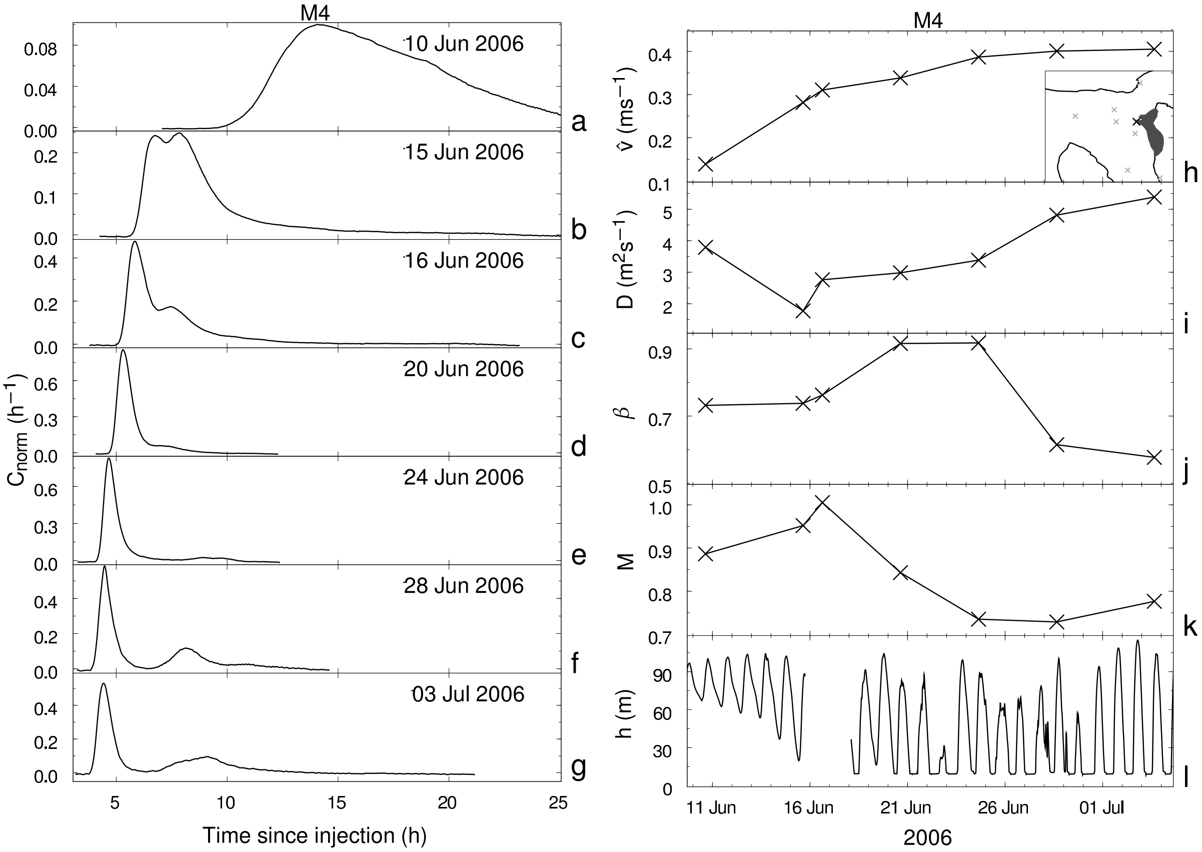

Figure 2.7: *Tracer experiments in 2006 using M4 (expM4s) and subglacial water pressure in borehole BH6 (located 50 m beside M4). (a–g) normalised breakthrough curves, (h) transit speed $\hat{v}$, (i) dispersion D, (j) fraction of mobile water β, (k) fraction of returned tracer mass M and (l) water pressure head h in BH6.*

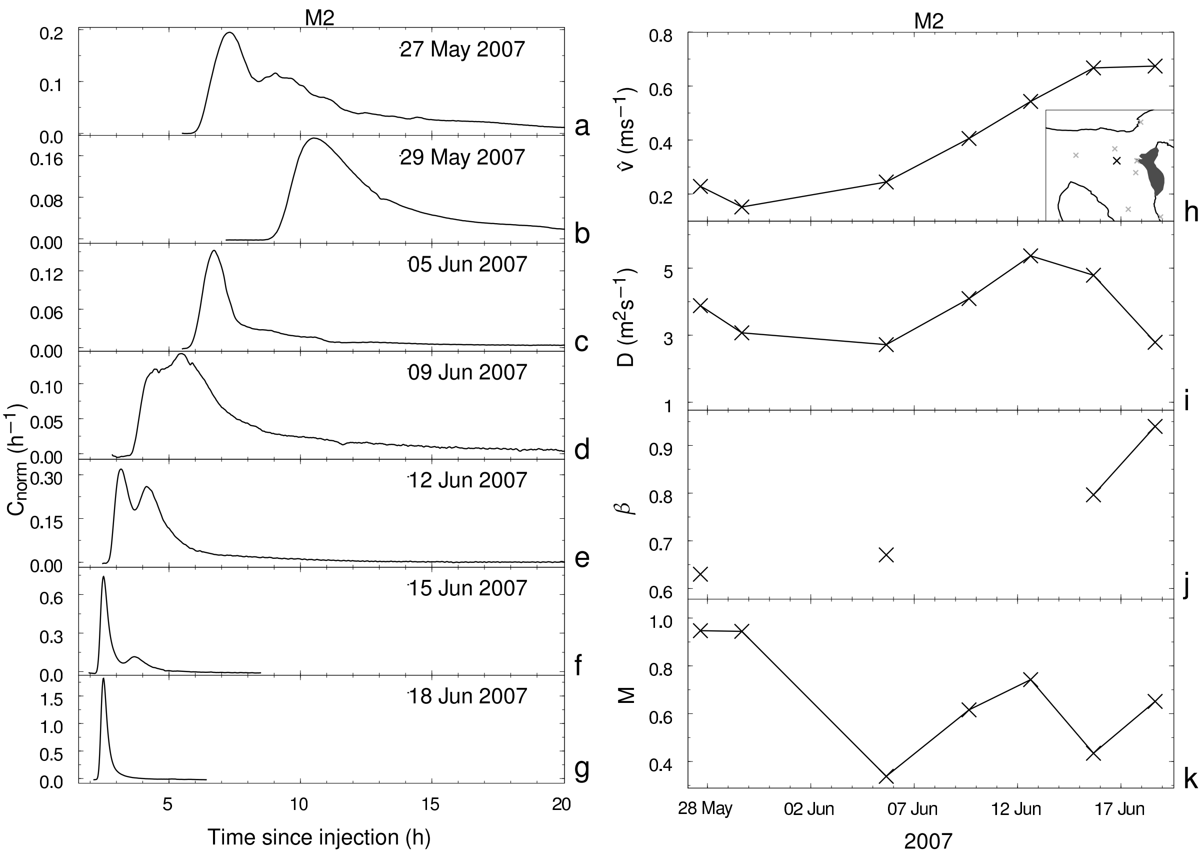

Figure 2.8: *Tracer experiments in 2007 using M2 (expM2s). (a–g) normalised breakthrough curves displaying double peaks, (h) transit speed $\hat{v}$, (i) dispersion D, (j) fraction of mobile water β and (k) fraction of returned tracer mass M.*

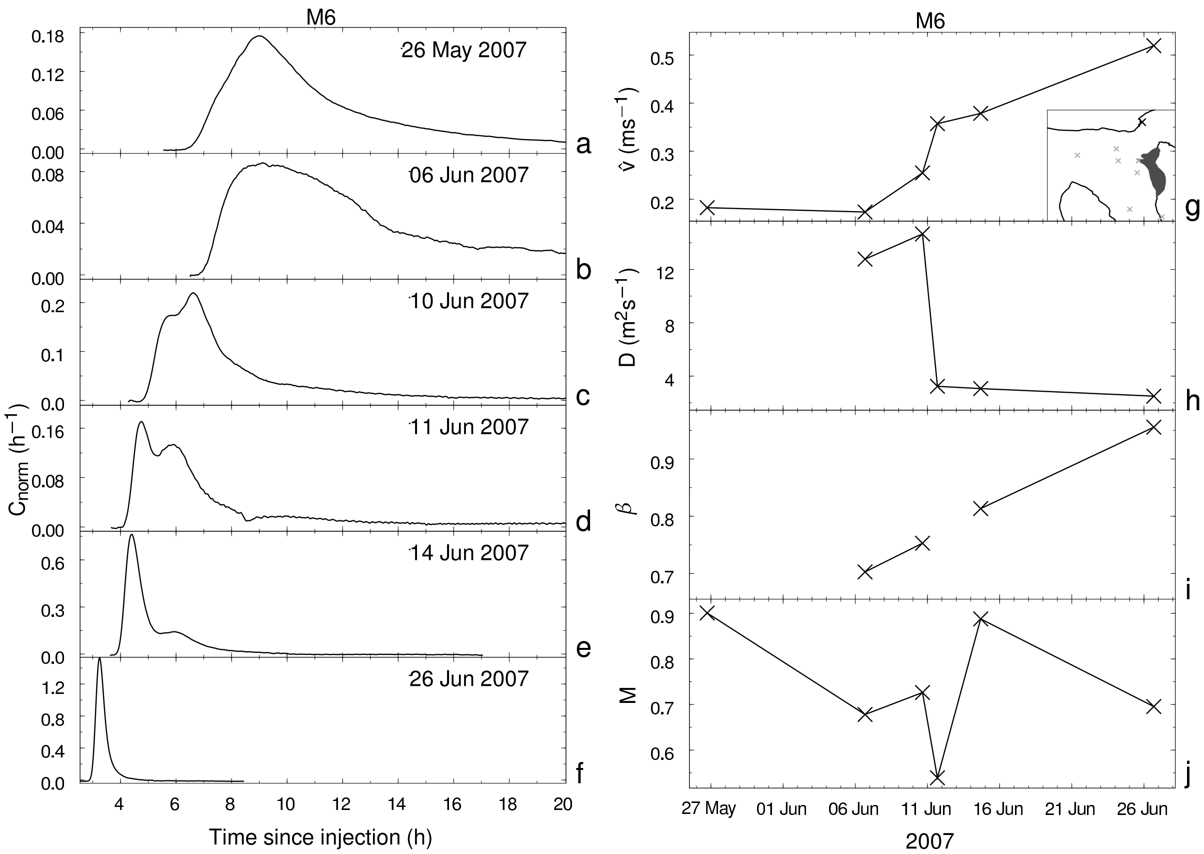

Figure 2.9: *Tracer experiments in 2007 using M6 (expM6s). (a–f) normalised breakthrough curves displaying double peaks, (g) transit speed $\hat{v}$, (h) dispersion D, (i) fraction of mobile water β and (j) fraction of returned tracer mass M.*

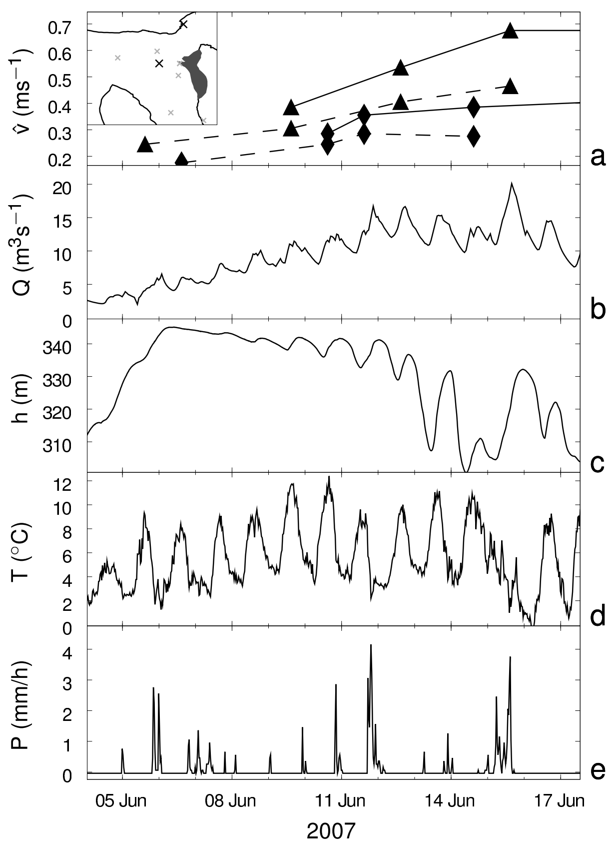

Figure 2.10: *Measurements complementing expM2s (Fig. 2.8) and expM6s (Fig. 2.9). (a) Transit speeds ($\hat{v}_1, \hat{v}_2$) corresponding to the two peaks in expM2s (triangles, Fig. 2.8) and expM6s (diamonds, Fig. 2.9), (b) proglacial discharge, (c) subglacial water pressure head in borehole BH1, (d) ventilated air temperature measurements off-ice at weather station AWS and (e) precipitation at AWS.*

Table 2.3: *Parameters used for the lumped element model*

Parameter	Variable	Value
Channel 1 length	l_0	1000 m
Channel 2 length	l_1	3000 m
Channel 3 length	l_2	1000 m
Ice thickness	h_{ice}	300 m
Moulin cross-sectional area	A	5 m^2
Min. filling height	h_{min}	200 m
Max. filling height	h_{max}	300 m
Manning roughness factor	n_{man}	0.031 m$^{-1/3}$s
Lower boundary hydraulic head	h_2	0 m

2.5 Model results

I interpret the evolution of the double peaks seen in the expM2 and expM6 in 2007 (Fig. 2.8 and 2.9) using the lumped element model (Fig. 2.3). The model is run using the parameters given in Table 2.3. The moulin element is fed by a constant discharge of 0.3 m^3 s^{-1} for the first five days and then a discharge varying diurnally with increasing amplitude (Fig. 2.11d). The constant discharge mimics the effect of meltwater retention in snow cover. The length of the two parallel R channels R_1 and R_2 had to be chosen differently to achieve the observed discrepancy in residence time. To calculate the *modelled transit speed* I use the length of the shorter channel as the transit distance. The hydraulic head h_2 below the two competing R channels is set to zero (air pressure) to simulate the proglacial outlet. The initial conditions for the channel cross-sections are $S_0 = 0.2\,\text{m}^2$, $S_1 = 0.3\,\text{m}^2$ and $S_2 = 0.02\,\text{m}^2$, i.e. the longer channel has an initially larger cross section. The other initial conditions are not critical to the model output and were chosen such that the simulation is numerically stable.

Figure 2.11 shows the results of the simulation compared to the results of expM6s. The model results have large diurnal fluctuations and for comparison to the tracer experiments we plotted the modelled transit speed, discharge ratio and residence time at 14:00 (Fig. 2.11a–c), whereas discharge and subglacial water pressure head are plotted continuously (Fig. 2.11d, e), like the measurements. The two dashed vertical lines indicate the boundaries of the time period used for comparison between measurements and model results: the modelled discharge ratio increases from 0.8 to 8 corresponding roughly to the increase in the ratio of the peak heights observed in the expM6 between 10 and 14 June (r_h in Table 2.2); the modelled transit speed increases from 0.55 m s^{-1} to 0.9 m s^{-1} in the shorter R_2 and only very slightly from 0.4 m s^{-1} to 0.5 m s^{-1} in R_1 (Fig. 2.11a); the modelled time difference increases from 21 to 27 minutes (Fig. 2.11c); and the modelled pressure has diurnal fluctuations once the input discharge starts to vary diurnally, becoming larger as the amplitude of the discharge increases (Fig. 2.11e,d).

2.6 Discussion

The highly dynamic subglacial drainage system adjusts itself to water influx. During winter, when there is little water input into the system, it is inefficient and probably distributed. During summer, when there is high meltwater input, the system is efficient and probably channelised

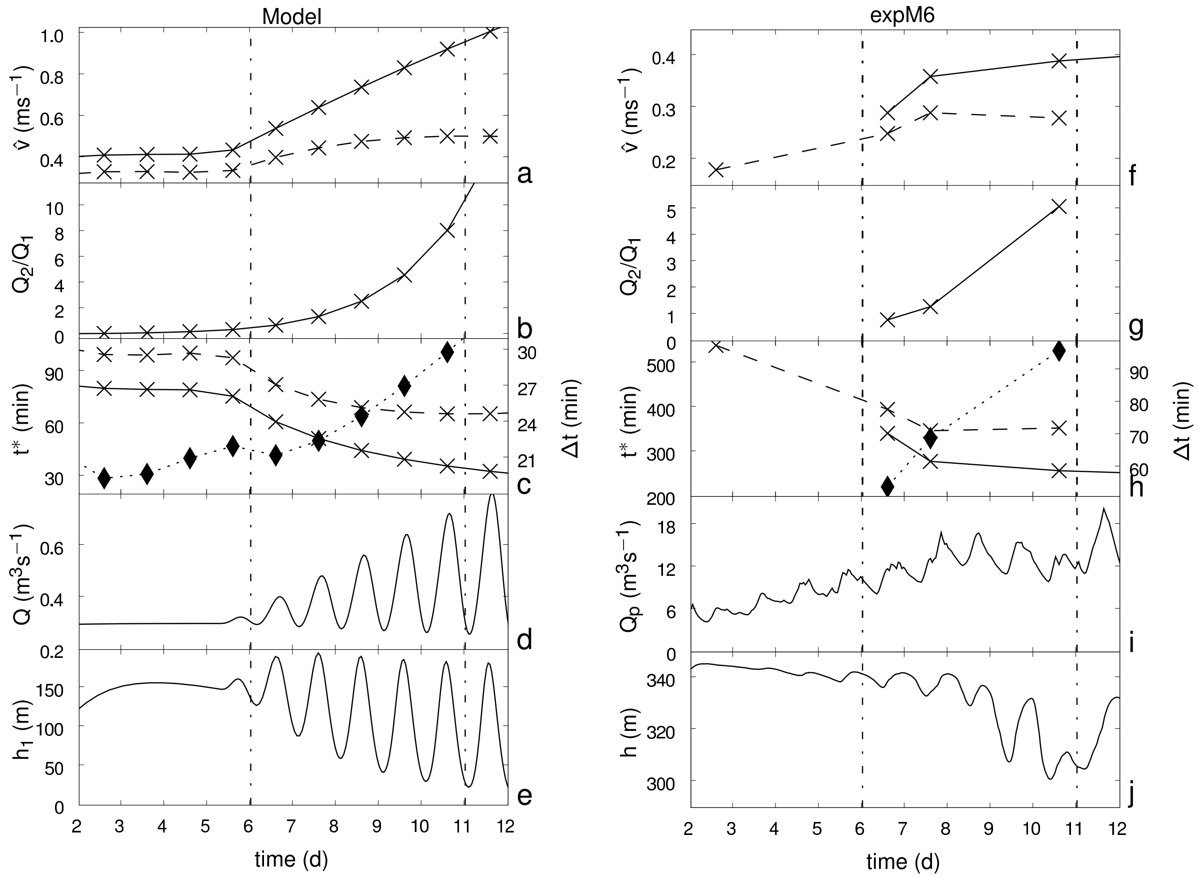

Figure 2.11: *One-to-one comparison of the lumped element model (left panel, c.f. Fig. 2.3) and measurements from M6 (right panel, c.f. Tab. 2.2): (a) modelled transit speed in the shorter ($\hat{v}_1$, solid) and the longer ($\hat{v}_2$, dashed) channel at 14:00, (f) transit speed of faster ($\hat{v}_1$, solid) and slower ($\hat{v}_2$, dashed) peak; (b) ratio of discharges in the shorter to longer channel at 14:00, (g) ratio of height of first to second peak; (c) residence time in the shorter channel (solid) and longer channel (dashed) and their difference (diamonds, right scale) at 14:00, (h) residence time of first (solid) and second (dashed) peak and their difference (diamonds, right scale); (d) model input discharge into the moulin, (i) measured proglacial discharge; and (e) modelled subglacial hydraulic head, (j) measured subglacial hydraulic head in BH1. Crosses mark 14:00 in the model (left) and the time of injection (right).*

(Fountain and Walder, 1998). The transition between these two regimes happens at the beginning of summer and is reversed in autumn (Hubbard and Nienow, 1997). In all years, a pronounced transition from a winter to a summer drainage system configuration is observed. The expM0s (Fig. 2.5) illustrate this particularly nicely: During the winter–summer transition the transit speed increases from $0.1\,\mathrm{m\,s^{-1}}$ on 10 June to $0.75\,\mathrm{m\,s^{-1}}$ on 23 June. At M5, about 2 km downglacier of M0, the drainage system is already quite efficient on 9 June as the corresponding expM5 has a transit speed of $0.5\,\mathrm{m\,s^{-1}}$ (Fig. 2.6f). If we assume that downglacier of M5 the tracer of expM0 on 10 June travels at the transit speed measured in M5, then its transit speed in the upper part must be lower than $0.03\,\mathrm{m\,s^{-1}}$. This low transit speed and the large dispersion ($>15\,\mathrm{m^2\,s^{-1}}$) indicate that the drainage system between M0 and M5 was in an inefficient, probably distributed configuration, e.g. linked cavities or a very braided system. These low transit speed compare well to the transit speed measured by Nienow et al. (1998) with tracer experiments and to what Kamb (1987) derives for a linked cavities drainage system. Two weeks later on 23 June, the drainage system has become efficient downglacier of M0 and the transit speed are as high as $0.75\,\mathrm{m\,s^{-1}}$. The last expM0 on 18 September shows the first stages of the reverse transition in autumn. Dye was injected one day after a snow fall which covered the whole ablation area. The transit speed is again slow ($0.1\,\mathrm{m\,s^{-1}}$) but the small dispersion ($1.3\,\mathrm{m^2\,s^{-1}}$) shows that the system is still channelised. As meltwater input was small, the tracer presumably travelled the whole distance at around $0.1\,\mathrm{m\,s^{-1}}$.

The fraction of returned tracer mass M does not increase with the winter–summer transition for all the experiment series, except the expM5s. This is an indication that storage processes are important throughout the summer season. Dye was injected at 14:00 during peak meltwater input which in turn led to sufficiently high subglacial water pressures that lateral spreading of the water at the bed is possible (c.f. Chap. 5). It is plausible that the stored tracer was released during the low subglacial water pressure at nighttime (Hock et al., 1999). However, due to the high frequency of injections and low amount of injected tracer, I did not see any signals from these release events.

In relation to the jökulhlaup, the winter–summer transition in 2005 was important: The initiation of the lake drainage coincided with the winter–summer transition of the drainage system in the vicinity of the lake (Huss et al., 2007). Subglacial water pressure data from borehole BH1 shows diurnal fluctuations from 31 May onwards and the expM0s show that downglacier of M0 the transition occured between 10 and 23 June. Thus, near the lake the transition must have occurred sometime in between 31 May and 23 June as did the onset of the jökulhlaup on 11 June. This temporal concurrence suggests a causal relationship: Probably there was an existing leak with the potential to become an R channel; this happened once the pressure in the drainage system nearby was low enough to allow water to flow, i.e. after its transition to a summer configuration. Hence, the trigger for a jökulhlaup can be some small englacial opening. However, in the years 2004, 2006 and 2007 the lake continued to fill long after the drainage system was efficient near the lake. Thus, in those years such a predecessor to an R channel probably did not exist, even though I have evidence for a small leak in 2006: during a cold spell lake level dropped by 0.03 m overnight but afterwards the lake continued to fill for another month. These observations indicate that there is little hope to ever predict the onset time of a jökulhlaup such as the one on Gornergletscher, as it seems almost impossible to device measurements techniques which could resolve such a small dam breach. The causal relation between winter–summer transition and onset of a jökulhlaup was suggested by Anderson et al. (2003) and Kessler and Anderson (2004) modelled this scenario.

In 2007, double peaked return curves were observed from 9 June until 15 June in both expM2s and expM6s (Fig. 2.8, 2.9 and Table 2.2). Double peaks can either arise from two different flow paths or from storage and release of water. One striking feature is that the time difference between the arrival of the peaks is quite constant even though the residence time almost halved. This removes storage-release processes as a possibility: the water in storage is released during the times of low subglacial water pressure and hence the second peak would appear during the night or in the morning (Hock et al., 1999, e.g.). Continuous storage-release processes can also be ruled out as they lead to a single peaked curve with a long tail.

This leaves the possibility of two distinct drainage pathways. One is growing at the expense of the other: the ratio of first to second peak heights increases from 0.8 to above 5 (r_{h} in Table 2.2), which should be close to the ratio of discharges carried. We conjecture that the double peaks originate from a part of the drainage system which conducts the water from both moulins as evolution of the double peaks is very similar for the expM2s and expM6s. The main discrepancy is that the time difference between arrival of the two peaks of the expM6 on 14 June (1.6 h) is considerably larger than those of the others experiments (0.9-1.2 h). This could be due to the slightly altered hydraulic conditions on 14 June, especially the low subglacial water pressure (Fig. 2.10c) which was caused by reduced meltwater input in the afternoon due to cloudy sky.

The two distinct drainage pathways could be two competing R channels. At the same pressure difference the larger R channel conducts more water which leads to more melt enlargement. Conversely, the smaller channel conducting less water starts to shrink as the reduced melt rates can not keep up with ice creep closure. Thus the larger channel captures the discharge of the smaller channel (Röthlisberger, 1972).

In Figure 2.11 the results of the lumped element model (Fig. 2.3) simulating two competing R channels are compared to the expM6s. Note that these lumped element calculations are not accurate enough to quantitatively describe the drainage system nor do I have all the necessary field data to drive the model. Thus, the model was not tuned to the measurements and I only give a semi-quantitative interpretation. The aim was to reproduce the following characteristics: the daily subglacial water pressure fluctuations become larger, both drainage paths conduct water faster and the residence time difference between the two flow paths increases.

The subglacial water pressure measured in BH1 is simulated well by the model (Fig. 2.11e,j). The lack of diurnal pressure fluctuations in the model is caused by the lack thereof in the meltwater input during the first five days of the simulation. This is what actually happened, as before the appearance of the double peaks the glacier was snow covered. This snow cover stores meltwater and releases it slowly over the course of the whole day. However, once the diurnal fluctuations commence, the modelled pressure increases above previous values which is not what was measured. The measured subglacial water pressure was close to ice overburden pressure, beyond which it can not rise without lateral spreading of the water at the glacier bed and thus reducing the pressure. This process is not included in the model.

The modelled transit speeds for the faster channel increase from $0.5\,\mathrm{m\,s^{-1}}$ to $0.8\,\mathrm{m\,s^{-1}}$ in the fife day period considered (vertical lines in Fig. 2.11), compared to the measured transit speeds which increase from 0.4 ms to $0.7\,\mathrm{m\,s^{-1}}$ for the expM2s and $0.3\,\mathrm{m\,s^{-1}}$ to $0.4\,\mathrm{m\,s^{-1}}$ for the expM6s between 9 and 15 June (Fig. 2.11a,f). Some of the increase in modelled transit speed, and possibly also of the measured transit speed, is due to changing inflow modulation in the moulin because of increasing discharge into it (see Chapter 4). The model reproduces the increase of transit speed reasonably well, which suggests that the water flowed indeed through

R channels when the double peaks occured. However, with this model it was not possible to simulate the slow transit speed ($<0.2\,\mathrm{m\,s^{-1}}$) measured at the end of May. This failure indicates that then the drainage system was in a distributed configuration.

The residence times of the model and measurements (Fig. 2.11c,h) agree well qualitatively. The modelled residence time difference between the channels is between 20 and 30 min, still shorter than the observed one 50–100 min. Such a large time difference in the model can only be achieved by two channels of different length. The length difference could be attributed to different sinuousities: as both channels need to cover the same horizontal distance, the longer channel has a three times larger sinuosity than the shorter one. The modelled time difference increases during the comparison period by a factor of 1.3 which is close to the factor 1.2 measured in M2 and 1.8 in M6 (Table 2.2).

Another plausible interpretation of the evolution of the double peaks is, that part of the water moves through a distributed drainage system, like linked cavities (Kamb, 1987), and the other part through a channelised drainage system. This could be simulated by a model similar to the one used by Flowers (2008). It would be interesting to see if such a model could reproduce flow conditions as inferred from the evolution of the double peaks.

2.7 Summary

I observed the transition of the glacier drainage system of Gornergletscher from an inefficient winter to an efficient summer configuration with tracer experiments and subglacial water pressure data. I show that during this transition, water transit speeds can increase by a factor of 25 from 0.03 to $0.75\,\mathrm{m\,s^{-1}}$ and infer from the decreasing dispersion that water flow becomes channelised. The observed evolution of double peaked breakthrough curves shows that there can be concurring drainage paths and that the more efficient path grows at the expense of the less efficient one as predicted by the theory of R channels. In 2005, the lake drained as the subglacial drainage system in its vicinity became efficient, suggesting that the jökulhlaup can be triggered by the winter–summer transition and thus illustrating that the whole glacier drainage system needs to be considered when studying jökulhlaups.

Chapter 3

Catchment of Gornersee and hydraulics of the lake dam

Abstract The drainage system within the ice dam of Gornersee, an ice marginal lake, was investigated using tracer experiments. These show that (a) the water flows englacially inside the lake dam, in direction of the crevasses, for up to 500 m before it reaches the lake; (b) the catchment boundary of the lake is very sharp: moulins only separated by one crevasse spacing of about 20 m can belong to different catchments. Repeated experiments using one moulin on the lake dam, conducted before during and after two large calving events, show that the drainage pathway inside the dam was mechanically disturbed by these events. This is direct evidence that such an event can trigger the lake outburst by modifying the drainage system in the lake dam, as was likely the case in the 2004 Gornersee jökulhlaup.

3.1 Introduction

Englacial water flow has not been studied extensively and little is known about it (Fountain et al., 2005; Gulley and Benn, 2007). However, it plays an important role in the routing of water through the glacier, as exemplified by inflow modulation, a process whereby meltwater is delayed inside a moulin (c.f. Chapters 2, 4 and 5). Huss et al. (2007) show that 0.1–10% of Gornergletscher's volume consists of englacial voids, i.e. cavities either filled by water or air. It is not known how many of these voids are conducting water and how many contain stagnant water (Fountain et al., 2005).

During the filling of Gonersee in 2006, I conducted dye tracer experiments using some of the numerous moulins found in the dam of Gornersee on its Grenzgletscher side (Fig. 2.2). The aim was to determine the catchment of the lake. I was expecting that the moulins very close to the lake would drain into it whereas the ones lying further afield would not.

The lake dam on the Grenzgletscher side is heavily crevassed and my experiments show that englacial conduits abound within it. Once a glacial-lake dam has a leak, Nye's 1976 theory predicts that the leak quickly enlarges due to dissipation of potential energy. It is thus remarkable that Gornersee often is so resilient to draining. In the second part of this chapter, I present four dye tracer experiments using a moulin in the lake dam, one conducted before, two in between and one after two large calving events in 2007. These experiments show that this calving event influenced the drainage system within the lake dam.

3.2 Methods

I used the fluorescent dyes Rhodamine WT and Uranine for tracer injections which I injected manually in a short pulse. The detection was done with two fluorometers (Turner 10-AU and BackScat) installed in the proglacial stream at the gauging station of Grande Dixence SA, where proglacial discharge was also measured. The tracer experiments conducted to determine the lake catchment were evaluated according to the binary scheme: If the dye was detected in the proglacial stream, the moulin must be connected to the subglacial drainage system. If no dye was detected, it was assumed that the moulin drained into the lake. I conducted these injections at any time of the day as their results are not compared to one another. No additional evaluation of those experiments was done. The dye concentration in the lake due to these experiments remained low enough to not interfere with the experiments during the lake drainage, presented in Chapter 4 and 6. After having determined which moulins drained into the lake, I mapped the surface watershed of the streams feeding these moulins using a hand-held GPS.

The tracer experiments conducted before, in-between and after the two calving events were all done at 14:00 CEST using the moulin M3. In this chapter I present the normalised breakthrough curves, the tracer transit speed and M, the fraction of returned tracer mass. M is defined as the ratio of injected to detected tracer mass. For a more detailed description of the measurement procedure refer to Chapters 2 and 5.

The structure of the subglacial drainage system can be modelled using the “upstream area” approach (Flowers and Clarke, 1999; Fischer et al., 2005). Water is assumed to flow in the direction of steepest descent of the hydraulic potential. This potential is defined as

$$\phi = z_\mathrm{b} + f_\mathrm{float} \frac{\rho_\mathrm{i}}{\rho_\mathrm{w}} (z_\mathrm{s} - z_\mathrm{b}), \tag{3.1}$$

where z_b and z_s are the bed and surface elevation (Fig. 2.2), respectively, ρ_i and ρ_w the densities of ice and water and f_float is the fraction of the subglacial-water to ice-overburden pressure (see Fig. 6.1 for a plot of the hydraulic potential). The glacier bed was divided into a grid of 25 m spacing. For each grid cell, the upstream area model calculates the sum of grid cells which lie upstream. For this calculation I used a program provided by Gwenn Flowers (Flowers and Clarke, 1999).

3.3 Results

3.3.1 Lake catchment

The map in Figure 3.1 shows the lake catchment and its surroundings. The moulins used for the dye tracer experiments conducted to map the catchment are marked according to whether they belong to the lake catchment nor not. Moulins situated up to 300 m away from the lake belong to its catchment which shows that water does not only enter the lake via surface streams but that also water flows en- or subglacially to reach the lake. The boundary between moulins draining into the lake and those draining to the proglacial stream is sharp as they lie in neighbouring crevasses which are separated by about 20 m. M8 was used for four injections in the time span between 5 June and 22 July 2007; all four injections showed that M8 belonged to the lake catchment. The southernmost moulin, M7 (marked in Fig. 2.2), situated higher than the others on the eastern glacier margin drains to the proglacial stream. The region of the lake catchment south of the marked moulins is devoid of moulins and water flow occurs in large surface streams (discernible in Fig. 3.1).

The map in Figure 3.2 shows the same area as the map in Figure 3.1 but underlain with the result from the upstream area calculation. Red grid-cells receive water from many other grid-cells and blue ones do not. The calculation was done assuming a subglacial water pressure equal to 90% of ice overburden pressure, the bed and surface topography used to calculate the hydraulic potential (Eqn. 3.1) are plotted in Figure 2.2. The results show that there is a hydraulic barrier near the lake shore (blue area). Downglacier of that barrier, water drains towards the centre-line of the glacier (increasingly red towards centre-line). The surface water shed (blue dashed line) and most of the moulins draining into the lake (green diamonds) lie several hundred meters downglacier of this barrier.

3.3.2 Hydraulics of the lake dam

In 2007, two large calving events preceded the jökulhlaup by a week. The first event happened on 30 June which resulted in a lake level drop of 0.1 m corresponding to about $1.5\times10^5\,\mathrm{m}^3$ of ice floating up. The larger, second event occurred the day after, during which about $10^6\,\mathrm{m}^3$ of ice floated up, thereby lowering the lake level by 0.6 m (Fig. 3.4 a). On the photograph in Figure 3.3, the ice mass which was involved in the second event can be seen: the ice to the right of the large, circa 500 m long, crevasse calved off and lifted by as much as 10 m.

Figure 3.4b–e shows the breakthrough curves from tracer experiments conducted using moulin M3 (marked in Fig. 3.1). The experiment three days before the first calving event, on 27 June, produced a sharply peaked breakthrough curve and resulted in a fraction of returned tracer mass M of 0.75. The experiment performed on the day of the first calving event, on 30 June, returned a breakthrough curve with three peaks, much wider than the one obtained on 27 June with $M = 0.89$. The day after, when the bigger event happened (1 July), the injection returned a breakthrough curve similar to the one of 27 June apart from small secondary peaks and had $M = 0.58$. On 2 July, the residence time was shorter than for the previous experiments and there were no more secondary peaks, the fraction of returned tracer mass M was 0.72. (Other tracer experiments using M3 during the lake drainage are discussed in Chapter 5).

3.4 Discussion

The determination of the lake catchment shows that water transits sub- or englacially for long distances before reaching the lake. The location and orientation of the watershed near the lake suggests that water flow is in the direction of the crevasses as theorised by Fountain and Walder (1998). This implies that sub- or englacial flow distance reaches up to 500 m. The ice thickness in the area between the lake and the moulins draining into the lake is between 100 and 250 m (c.f. Fig. 2.2). If the water reached the bed, it seems improbable that it could reascend to the lake because this would necessitate water pressures at the bed which are higher than the ice overburden pressure. This argument is supported by the upstream area model (Fig. 3.2), which shows that all but the easternmost moulin would drain to the proglacial stream, provided their water would reach the glacier bed directly below the moulin. Thus I conclude that water flow must be englacial.

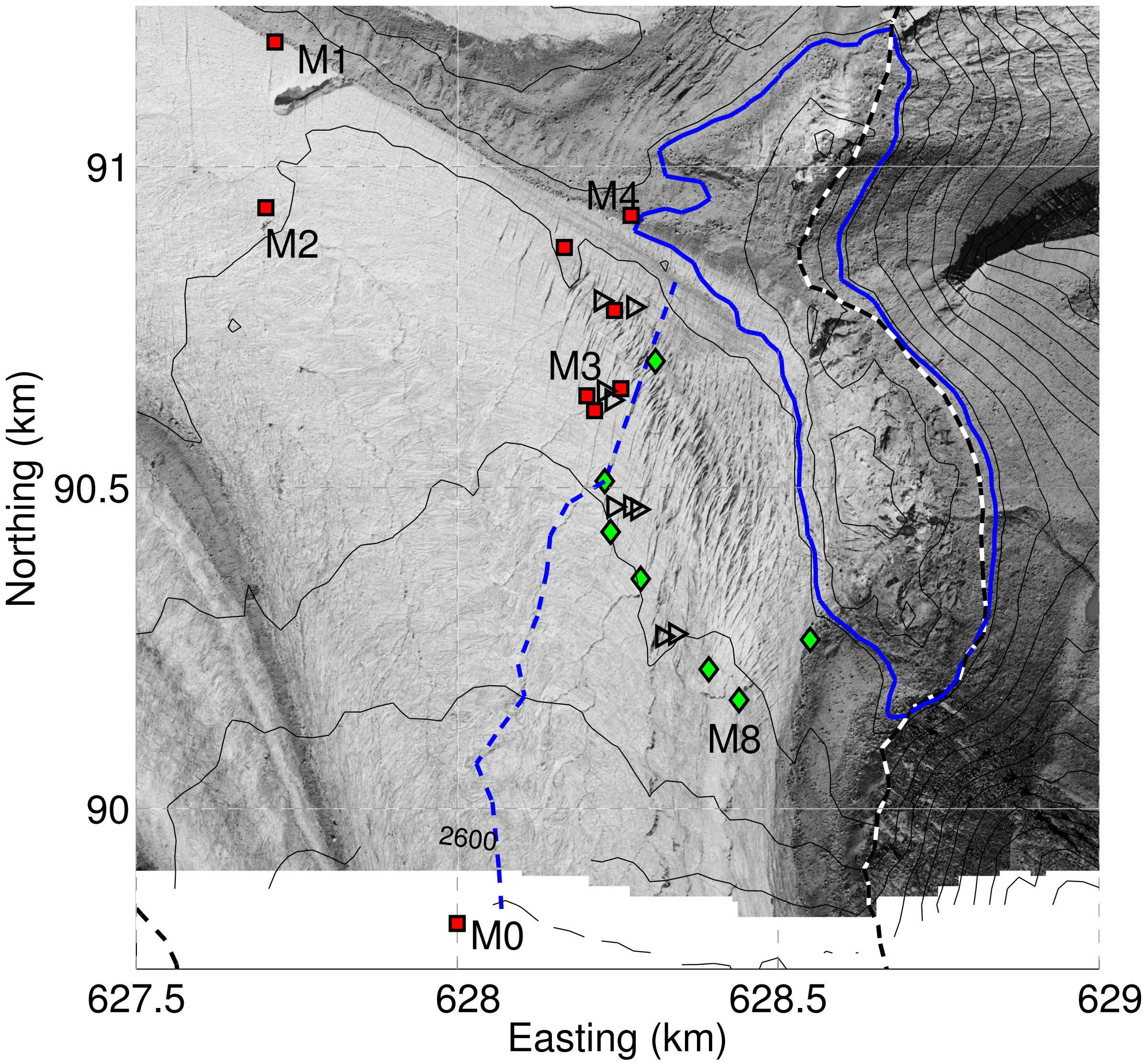

Figure 3.1: *Map of the surroundings of the lake Gornersee (outlined blue) with surface contours and an orthophoto as background. The black-white dashed line marks the outline of the glacier. Moulins marked by red squares drain to the proglacial stream; marked by green diamonds drain into the lake; marked by empty triangles were not traced. Moulins used for multiple injections are labelled M0–M4 and M8 (c.f. Chap. 2, 5). The dashed blue line indicates the surface watershed between proglacial stream and lake.*

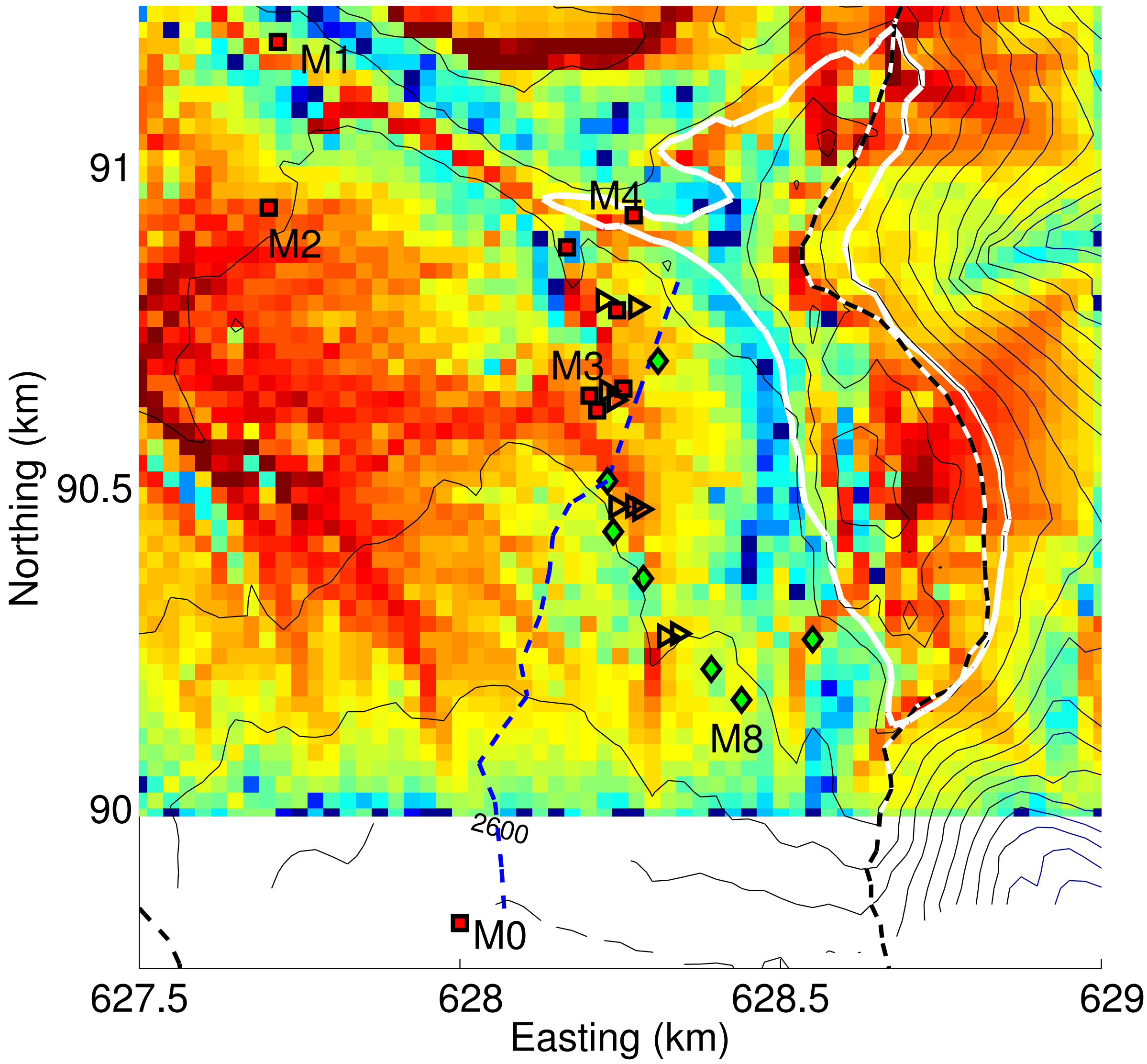

Figure 3.2: *Map of the calculated upstream area near the lake with surface elevation contours, the extent is identical to Figure 3.1. The outline of the glacier (black-white dashed) and the lake (white) are marked. The moulins and the surface water shed are marked as in Figure 3.1. The calculated upstream area of a cell is colour coded: blue corresponds to a small and red to a large upstream area.*

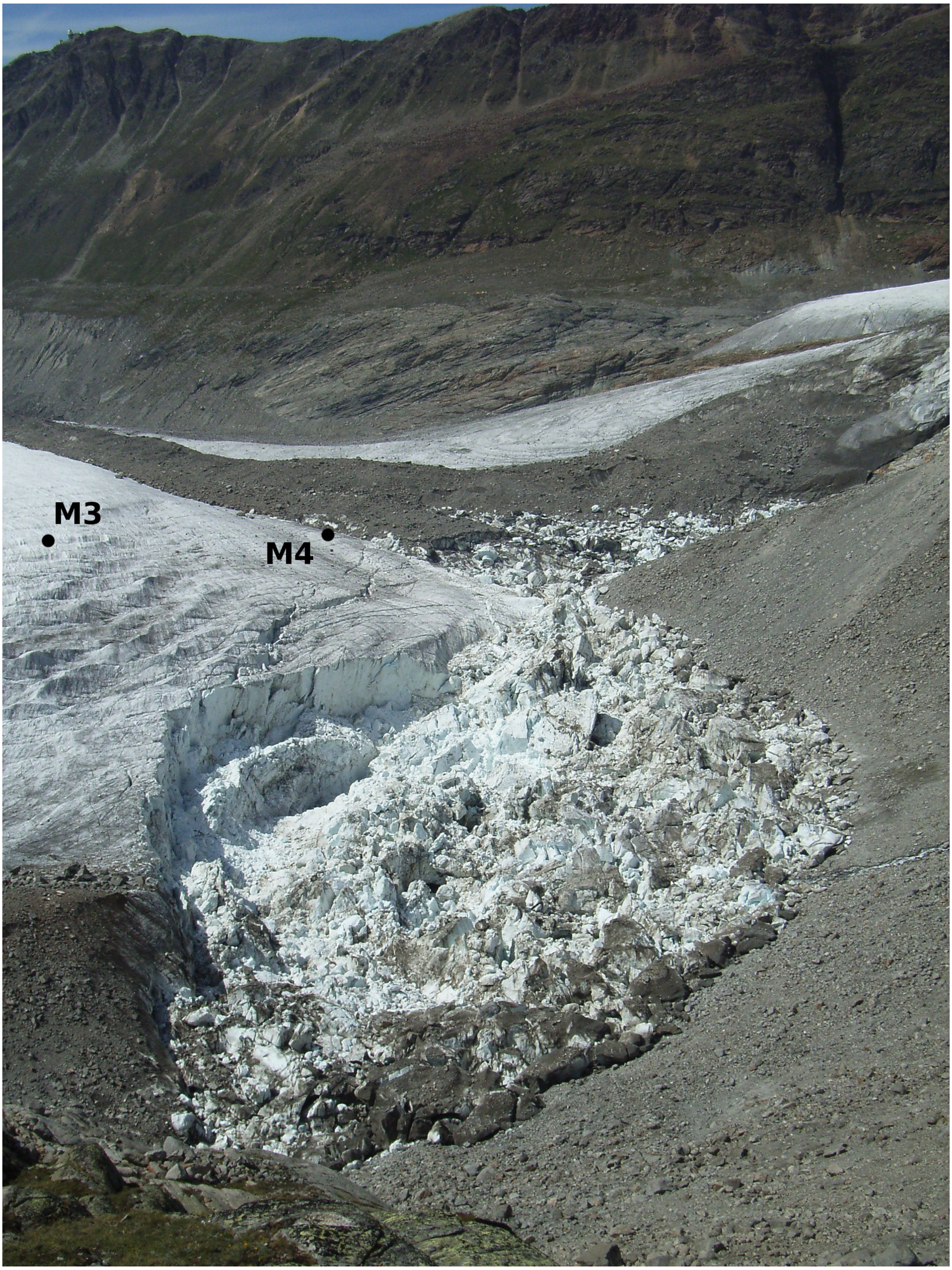

Figure 3.3: *Photograph of the empty Gornersee in 2007. Grenzgletscher is on the left, Gornergletscher at the back. The moulins M3 and M4 are marked. The big crevasse, caused by the big calving event on 1 July, runs from the ice cliff towards M4.*

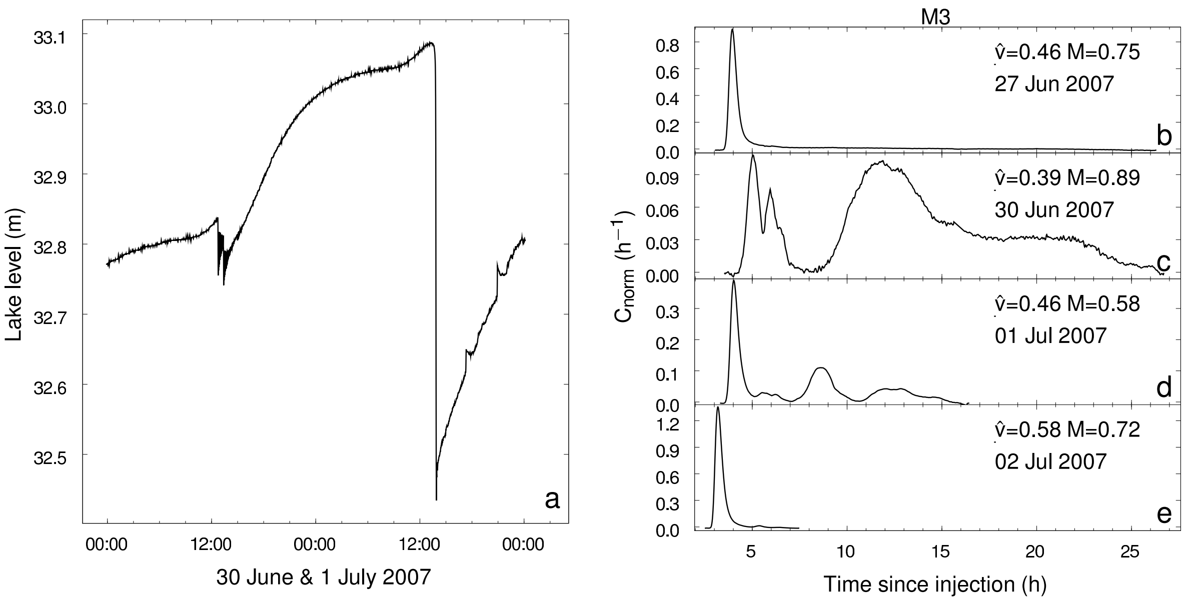

Figure 3.4: *(a) Lake level. Tracer breakthrough curves from M3 in 2007 before (b) during (c, d) and after (e) the big calving events which preceded the jökulhlaup by a week. The legend gives the tracer transit speed $\hat{v}$, the fraction of returned tracer mass M and the injection date. All injections were done at 14:00 (CEST).*

The four traces conducted using moulin M8 over the time span of almost two month show that the catchment structure does not change rapidly. I conclude that the moulins do not readily switch from one catchment to the other and that the structure of the catchment is likely similar from year to year.

The trace done using M7 (Fig. 2.2) showed that this moulin drains to the proglacial stream. Hence, water on the surface in the southwestern part of the lake catchment and water at the bed at the same location belong to different catchment basins. This illustrates that there can be a complex three dimensional watershed structure in glaciers.

The separation of crevasses containing the moulins draining in different directions is only 20 m (Fig. 3.1 near M3). This shows that the ice barrier in the dam area of the lake is very narrow in some places. It is remarkable that the lake dam remains watertight during the filling of the lake subjecting it to large stresses and strains (Riesen, 2007), as exemplified by the disruption of the drainage system within the dam due to the calving event (Fig. 3.4). The ice near the lake dam is cold (Ryser, 2009) which makes it possible that small dam breaches could self-seal due to freezing water.

Before the calving event, the breakthrough curve indicates a well developed drainage path of M3 (Fig. 3.4a). The first calving event disrupted the drainage path of M3 as is shown by the multi-peaked breakthrough curve in Figure 3.4b with the maximal normalised tracer load diminished by a factor of 10 compared to the injection on the day before. The following day, just after the larger second event, the breakthrough curve was almost back to normal and on the subsequent day no more secondary peaks were observed. This shows that the calving events can mechanically influence the lake dam and the drainage system within, however the exact mechanism is not deductible from the tracer experiments. Even though the calving events disrupted the drainage system on the downglacier side of the dam, they did not lead to an immediate outburst of the lake, unlike in 2004 when the lake started to drain after a big calving event.

Chapter 4

Short term variations of tracer transit speed on Alpine glaciers

Abstract We present and interpret the results and interpretation of a series of tracer experiments conducted on an Alpine glacier over a diurnal discharge cycle. For these injections, a moulin was used into which an ice marginal lake was draining, providing a relatively constant discharge. Measured tracer transit speeds show two diurnal maxima and minima. These findings are qualitatively different from existing observations from two series of injections at another site using a moulin fed by supraglacial meltwater with a high diurnal variability, which displayed one diurnal maximum and minimum. We use a simple two-component model of the glacier drainage system, comprising a moulin and a channel element, to simulate the measured transit speeds for all three injection series. The model successfully reproduces all the observations and shows that the same underlying processes can produce the qualitatively different behaviour depending on the different moulin input discharge regimes. Using the model, we asses the relative importance of the different measurement parameters, show that frequent measurements of moulin input discharge are indispensable and propose an experiment design to monitor the development of the drainage system over several weeks.

4.1 Introduction

The glacier drainage system governs how meltwater is routed through the glacier, which in turn influences ice flow dynamics by affecting sliding rates. Due to the virtual inaccessibility of the glacier interior and glacier bed, the investigation of the subglacial drainage system relies on observations of products and the subsequent inference of the underlying processes (Clarke, 2005). Characteristics of the drainage system have been deduced from point measurements such as borehole water levels, slug tests (e.g. Iken et al., 1996), geophysical methods (e.g. Walter et al., 2008) or from bulk information such as discharge recession analysis and hydrograph separation (e.g. Collins, 1979).

Dye tracer experiments proved to be a powerful tool to study the sub- and englacial drainage system and have been performed to characterise the firn aquifer (e.g. Lang et al., 1979), to investigate the drainage system on a seasonal time scale (e.g. Nienow et al., 1998) and on a diurnal time scale (e.g. Nienow et al., 1996; Schuler et al., 2004). The measured tracer transit speed is the quantity most readily compared to models of glacier hydraulics (e.g. Kohler, 1995). The high frequency tracer experiments by Nienow et al. (1996) and Schuler et al. (2004) revealed covariations between tracer transit speed and supraglacial discharge input into the injection moulin. Modulation of inflow from the tributary into a main channel has been suggested as a possible explanation for this. However, the partitioning of the total residence time into contributions from the tributary and main channel remained unresolved until recently (Schuler and Fischer, 2009).

During 2004–2008, the yearly jökulhlaups (glacier lake outburst floods) of the ice marginal lake Gornersee, located on Gornergletscher, Switzerland, were studied using an integrated approach that employed a range of different measurements (e.g. Huss et al., 2007; Sugiyama et al., 2007; Walter et al., 2008), including tracer experiments (c.f. other chapters). The present paper focuses on a series of tracer injections conducted over 24 hours at intervals of about 3 hours followed by two further injections on the subsequent day. These experiments were performed during the slow and steady drainage of Gornersee in 2006. The lake drained slowly because it spilled over into a moulin on its shore which was used for the tracer injections described in this paper. This situation provided a continuously high discharge input into the moulin with a relatively small diurnal amplitude and therefore prompted a comparison to similar experiments where the supraglacial discharge had a pronounced diurnal cyclicity (Schuler et al., 2004). To interpret the observations, we introduce a two component hydraulic model that simulates tracer transport through a moulin and a subglacial channel. We apply this model to investigate the hydraulic context leading to the observed variations of tracer transit speed, in both our observations at Gornergletscher and those of Schuler et al. (2004) at Unteraargletscher.

4.2 Setting

Gornergletscher is a $\sim$60 km^2 valley glacier in the Valais Alps, Switzerland. It covers an altitude range from 2200 $\mathrm{m\,a.s.l.}$ to 4600 $\mathrm{m\,a.s.l.}$ and has a length of 14 km (Huss et al., 2007). Gornersee is an ice marginal lake located in the confluence area of the two main tributaries Gorner- and Grenzgletscher (Fig. 4.1). The lake has an elevation of 2530 $\mathrm{m\,a.s.l.}$ and lies 5.25 km upglacier from the terminus. The greatest ice thickness of 450 m was measured 1 km downglacier of the lake (Sugiyama et al., 2008). The experimental data presented in this paper was collected during a field campaign in 2006 when the lake filled until its shore reached a small moulin (marked M4 on map in Fig. 4.1) into which the lake spilled over. The lake level then gradually lowered by incising a canyon into the ice. The moulin adjusted its capacity over one and a half days after the onset of the outburst (Chapter 6); afterward the lake discharge stabilised and was limited by the rate of spillway incision (Raymond and Nolan, 2000). The rate of lake level lowering was slightly more than 1 m per day, translating into a discharge between 1 and 5 $\mathrm{m^3\,s^{-1}}$. It took about three weeks for the lake to empty. At the end of this time, the canyon was about 200 m long, 5 m wide and up to 50 m deep.

4.3 Methods

4.3.1 Field Methods

Details of the experimental design are described in the two previous papers on tracer experiments on Gornergletscher Chapters 5 and 6. Proglacial discharge was measured by a hydro-

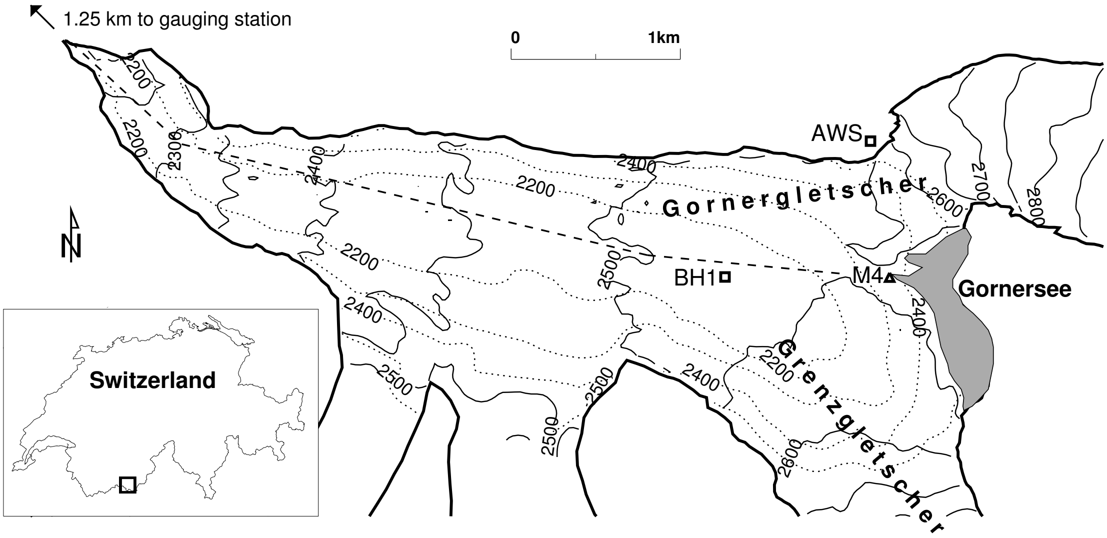

Figure 4.1: *Map of the tongue of Gornergletscher with solid contours of surface elevation and dotted contours of bed elevation (Sugiyama et al., 2008). Marked are the moulin used for tracer injections (M4), the tracer transit distance $\hat{l}$ (dashed line), the maximum extent of the lake (grey shaded area), the borehole used for subglacial water pressure measurements (BH1), and the automatic weather station (AWS).*

power company at a gauging station 1.25 km downstream of the glacier terminus. We manually injected Uranine dye at 3 h intervals between 11:00 on 18 July and 14:00 on 19 July and on 20 July at 14:00 and 17:00. The dye was injected into the lake outlet stream, close to its entry into the moulin M4. The flushing of the dye was always good as discharge was high. The detection of the dye at the gauging station was fully automated using a BackScat submersible fluorometer. A borehole (BH1, Fig. 4.1) was hotwater drilled in 2005 and equipped with a vibrating-wire pressure transducer (Geokon 4500). Air temperature and precipitation were measured by an automatic weather station (AWS, Fig. 4.1) at the northern margin of the glacier. The lake level was measured with a Keller pressure transducer (DCX-22). All times are given in Central European Summer Time (CEST, UTC+2).

4.3.2 Terminology

In order to describe and discuss the tracer experiments and the accompanying model, a few concepts need to be elucidated and terms defined. The same definitions are used as in Chapter 5. We assume that the tracer and the water travel at the same velocity, thus the following definitions apply to both.

The time interval between the passage of the maximum concentration of the tracer cloud at two locations is the *residence time* (Δt, sometimes called the dominant residence time). The shortest possible horizontal distance between those two locations is the *transit distance* ($\hat{l}$), and accordingly, the *transit speed* is the ratio of the transit distance and residence time ($\hat{v} = \hat{l}/\Delta t$). The actual distance travelled by the tracer is the *flow path length* (l). Of course, the time to traverse the *flow path* is also the residence time. Note that the flow path length will, in general, be longer than the transit distance due to the vertical distance covered, the geometry and sinuosity of the flow path. The transit speed is therefore a lower bound on the channel cross-section averaged *flow speed* ($v = l/\Delta t$).

Note that hydraulic models, including the one presented in this paper, use the flow path length and calculate flow speed, not transit distance and speed. For this reason, care must be taken when comparing experimental and model results.

4.3.3 Data processing

Processing of the experimental data follows Schuler et al. (2004) and Chapter 5. We fitted an advection dispersion with storage model to the tracer return curves (Toride et al., 1999). This model returns four parameters characterising the tracer experiment of which we present the dispersion and fraction of mobile water. We correct the transit speed, as defined above, for the time the tracer spent in the proglacial stream (see Chapter 6). Thus, the presented transit speeds are as if the fluorometer was positioned right at the glacier snout. This correction reduces the transit speed by about 0.05 to $0.1\,\mathrm{m\,s^{-1}}$ at low and high proglacial discharge, respectively. The error in transit speed, including the correction, is about 4% (Chapter 6).

The lake discharge Q_m into the moulin was calculated from

$$Q_\mathrm{m} = Q_\mathrm{melt} - \frac{dh_\mathrm{lake}}{dt} A_\mathrm{lake}(h_\mathrm{lake}), \tag{4.1}$$

where Q_melt is the meltwater input into the lake, h_lake is the lake level and A_lake is the hypsometry of the lake. Q_melt is calculated from a distributed temperature index model (Hock, 1999) coupled to a linear-reservoir model as applied to Gornersee by Huss et al. (2007). This model is driven by the measured air temperature from the automatic weather station and was calibrated during the filling period of the lake by matching the measured and calculated lake level. The hypsometry of the lake was determined by photogrammetry. The error in the lake discharge Q_m can be estimated by comparing the measured and modelled filling rate of the lake before the drainage initiated. The absolute error is up to $1\,\mathrm{m^3\,s^{-1}}$ and varies diurnally due to shortcomings of the linear-reservoir model.

4.3.4 Model

Our aim is to simulate the passage of the tracer through the glacier drainage system for a given moulin input and proglacial discharge which is achieved using a lumped element model (Clarke, 1996) combined with a water flow speed calculation. We envisage that the traced water enters a moulin which connects to a Röthlisberger-type of channel (R channel, Röthlisberger, 1972), through which the bulk of proglacial discharge is routed (Fig. 4.2). The moulin element has a cone-like geometry and is fed by Q_m. The water level in the moulin element is equal to the hydraulic head h at the upper end of the R channel element and thus the amount of water contained in the moulin changes according to the pressure conditions in the R channel element. A turbulent flow resistor of resistance R is used for the R channel element, carrying a given

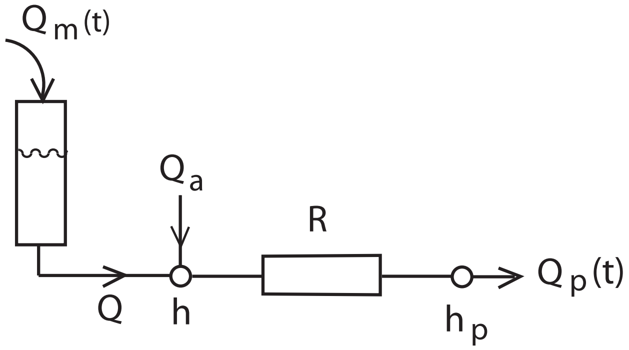

Figure 4.2: *The lumped element model consisting of a moulin element (left) and a channel element (right). It is driven by the measured discharge into the moulin Q_m and the proglacial discharge Q_p. Note that the additional discharge Q_a, required for conservation of water mass, is not of interest for our purposes and is not calculated.*

proglacial discharge Q_p. This model is governed by the equations

$$\frac{dh}{dt} = \begin{cases} 0 & \text{if } h \geq h_\mathrm{max},\, Q_\mathrm{m} \geq Q \\ \dfrac{Q_\mathrm{m} - Q}{A(h)} & \text{otherwise} \end{cases} \tag{4.2}$$

$$\Delta h = R Q_\mathrm{p}^2 \tag{4.3}$$

$$\frac{dS}{dt} = C_1 \frac{Q_\mathrm{p} \Delta h}{l} - C_2 (h_\mathrm{ob} - \bar{h})^n S, \tag{4.4}$$

which are solved for the hydraulic head h, the discharge exiting the moulin Q and the cross-sectional area of the R channel S. $C_1 = (1 - \rho_\mathrm{w} c_\mathrm{p} c_\mathrm{t}) \frac{\rho_\mathrm{w} g}{\rho_\mathrm{i} L}$ and $C_2 = 2B \left(\frac{\rho_\mathrm{w} g}{n}\right)^n$ are constants (c.f. Table 4.1), h_max is the maximal possible filling height of the moulin, $A(h)$ is the cross-sectional area of the moulin as a function of height, h_p is the hydraulic head at the glacier terminus, $\Delta h = h - h_\mathrm{p}$ is the head drop in the R channel, l is the R channel flow path length, $h_\mathrm{ob} = \rho_\mathrm{ice} h_\mathrm{ice} / \rho_\mathrm{w}$ is the hydraulic head corresponding to flotation pressure of the ice above the channel and $\bar{h} = \frac{1}{2}(h + h_\mathrm{p})$ is the mean hydraulic head in the R channel. Equation (4.2) assumes that the input discharge into the moulin reaches the water level in the moulin without delay. Table 4.2 summarises the model parameters and constants. The resistance R for a channel of circular cross-section is given by

$$R = 2^{4/3} \pi^{2/3} n_\mathrm{man}^2 \, l \, S^{-8/3}, \tag{4.5}$$

where n_man is the friction factor used in the Gauckler-Manning-Strickler formulation (Chow et al., 1998).

Using Eq. (4.3), the hydraulic head h can be calculated that is required to drive the given discharge Q_p through the R channel element. This hydraulic heads defines the water level in the moulin. Thus in this model, the R channel is independent of the moulin but not vice versa.

Exploiting our finding that model performance is not compromised by assuming a static R channel (thus now referred to as channel), Eqs. (4.2–4.4) can be simplified further. The steady-state value of the channel cross section (S_c) is related to R,l and the mean proglacial discharge $\bar{Q}_\mathrm{p}$ by setting $\mathrm{d}S/\mathrm{d}t = 0$ in Eq. (4.4). Furthermore, the case distinction in Eq. (4.2) is removed and

Table 4.1: *Physical constants*

Physical constant	Variable	Value
Constant 1	C_1	$2.2 \times 10^{-5}\mathrm{m}^{-1}$
Constant 2	C_2	$3.7 \times 10^{-13}\mathrm{m}^{-\mathrm{n}}\,\mathrm{s}^{-1}$
Density of water	ρ_{w}	$1000\,\mathrm{kg\,m}^{-3}$
Density of ice	ρ_{ice}	$900\,\mathrm{kg\,m}^{-3}$
Gravitational acceleration	g	$9.8\,\mathrm{m\,s}^{-2}$
Ice flow constant	B	$5.3 \times 10^{-24}\mathrm{Pa}^{-\mathrm{n}}\,\mathrm{s}^{-1}$
Ice flow exponent	n	3
Latent heat of fusion	L	$333.5\mathrm{k\,J\,kg}^{-1}$
Pressure melting coefficient	c_{t}	$7.5 \times 10^{-8}\mathrm{K\,Pa}^{-1}$
Specific heat capacity of water	c_{p}	$4180\mathrm{J\,kg}^{-1}\,\mathrm{K}^{-1}$

h_{p} is set to atmospheric pressure ($\approx 0\,\mathrm{m}$). The system thus simplifies to

$$\frac{dh}{dt} = \frac{Q_{\mathrm{m}} - Q}{A(h)} \tag{4.6}$$

$$h = R{Q_{\mathrm{p}}}^2. \tag{4.7}$$

Equation (4.6) can be solved for Q

$$Q = Q_{\mathrm{m}} - A(h)\frac{dh}{dt}, \tag{4.8}$$

where $\frac{dh}{dt}$ is determined by differentiating Eq. (4.7).

Transit speed calculation

To compute the transit speed, for comparison with the observations, we first determine the residence time of a parcel of water. Tracer diffusion and storage-release processes are neglected. The exit time of the tracer t_j^{out} from a lumped element j obeys

$$\int_{t_j^{\mathrm{in}}}^{t_j^{\mathrm{out}}} Q_j(t)dt = V_j(t_j^{\mathrm{out}}), \tag{4.9}$$

where Q_j is the discharge into the element, V_j is the water volume in the element and t_j^{in} is the tracer entry time. Thus, the volume of water flowing into the element between entry and exit of the tracer is equal to the volume of water in the element at the exit time. The total tracer residence time Δt for an injection at time t_1^{in} is then given by the sum of the residence times of each element Δt_j

$$\Delta t = \sum_j \Delta t_j, \tag{4.10}$$

where $\Delta t_j = t_j^{\mathrm{out}} - t_j^{\mathrm{in}}$.

In the moulin, pressurised flow conditions prevail only below its filling height h, and the model (Eqs. 4.2-4.5) assumes that injected water reaches h instantaneously. Thus, the volume of water in the moulin at the exit time (t_{m}) of the water parcel can be obtained by integrating the moulin

Table 4.2: *Model constants and fitting parameters*

Model parameter	Variable	Units
Channel cross-sectional area	S	m^2
Channel flow path length	l	m
Channel roughness	n_{man}	$\mathrm{m}^{-1/3}\,\mathrm{s}$
Channel sinuosity	σ	
Coordinate height	z	m
Coordinate time	t	s
Discharge into moulin	Q_{m}	$\mathrm{m}^3\,\mathrm{s}^{-1}$
Discharge out of moulin	Q	$\mathrm{m}^3\,\mathrm{s}^{-1}$
Discharge proglacial	Q_{p}	$\mathrm{m}^3\,\mathrm{s}^{-1}$
Discharge, mean proglacial	$\bar{Q}_{\mathrm{p}}$	$\mathrm{m}^3\,\mathrm{s}^{-1}$
Element j discharge	Q_j	$\mathrm{m}^3\,\mathrm{s}^{-1}$
Element j cross-sectional area	A_j	m^2
Element j volume	V_j	m^3
Element j entry time	t_j^{in}	s
Element j exit time	t_j^{out}	s
Exit time channel	t_{p}	s
Exit time moulin	t_{m}	s
Injection time	t_{inj}	s
Lake hypsometry	A_{lake}	m^2
Lake level height	h_{lake}	m
Meltwater input into lake	Q_{melt}	$\mathrm{m}^3\,\mathrm{s}^{-1}$
Moulin cross-sectional area	A	m^2
Pressure head in moulin	h	m
Pressure head difference in channel	Δh	m
Pressure head average in channel	$\bar{h}$	m
Residence time moulin	Δt_{m}	s
Residence time channel	Δt_{c}	s
Synthetic Q_{m} mean	q_{m}	$\mathrm{m}^3\,\mathrm{s}^{-1}$
Total residence time	Δt	s
Transit distance	$\hat{l}$	m
Transit speed	$\hat{v}$	$\mathrm{m}\,\mathrm{s}^{-1}$
Model constants	**Variable**	**Value**
Mean ice overburden pressure head	h_{ob}	270 m
Mean ice thickness	h_{ice}	300 m
Moulin bottom	h_{min}	0 m
Moulin top	h_{max}	300 m
Proglacial water pressure head	h_{p}	0 m
Synthetic Q_{p} amplitude	q_{p}^*	$9.16\,\mathrm{m}^3\,\mathrm{s}^{-1}$
Synthetic Q_{p} frequency	ω	$2\pi\mathrm{d}^{-1}$
Synthetic Q_{p} mean	$\bar{q}_{\mathrm{p}}$	$25.3\,\mathrm{m}^3\,\mathrm{s}^{-1}$
Synthetic Q_{p} phase	ϕ	3.13
Model tuning parameters	**Variable**	**Units**
Channel resistance	R	$\mathrm{s}^2\,\mathrm{m}^{-5}$
Moulin cross-sectional area top	A_{t}	m^2
Moulin cross-sectional area bottom	A_{b}	m^2

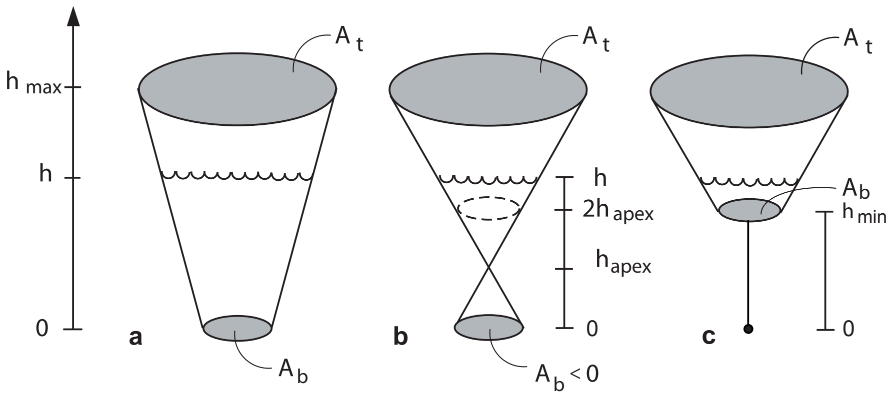

Figure 4.3: *The geometry of the moulin element, with water filling height h, top (A_t) and bottom (A_b) cross-sectional area. (a) $A_\mathrm{b} > 0$; (b) $A_\mathrm{b} < 0$, in which case the apex of the cone has height h_apex and the volume below the apex is negative; (c) equivalent moulin geometry to (b) provided h does not fall below $h_\mathrm{min} = 2h_\mathrm{apex}$.*

cross-sectional area A from the bottom to $h(t_\mathrm{m})$. We prescribe A as a linear function of height above the bed z (Fig. 4.3)

$$A(x) = \frac{A_\mathrm{t} - A_\mathrm{b}}{h_\mathrm{max}}\, z + A_\mathrm{b}, \tag{4.11}$$

where A_t is the cross-sectional area at the glacier surface and A_b is the cross-sectional area at the glacier bed. Integrating Eq. (4.11) from 0 to $h(t_\mathrm{m})$ and substituting it into Eq. (4.9) gives

$$\int_{t_\mathrm{inj}}^{t_\mathrm{m}} Q_\mathrm{m}(t) dt = \frac{A_\mathrm{t} - A_\mathrm{b}}{2\, h_\mathrm{max}} h(t_\mathrm{m})^2 + A_\mathrm{b} h(t_\mathrm{m}), \tag{4.12}$$

where t_inj is the injection time. This equation can be solved for t_m once Q_m is specified and then gives the moulin residence time $\Delta t_\mathrm{m} = t_\mathrm{m} - t_\mathrm{inj}$.

The channel cross-sectional area S and its flow path length l are constant, hence the water volume in the channel is equal to Sl, assuming fully pressurised flow. Equation (4.9) becomes

$$\int_{t_\mathrm{m}}^{t_\mathrm{c}} Q_\mathrm{p}(t)\, dt = Sl \tag{4.13}$$

and can be solved for the channel exit time t_c once Q_p is specified. The (static) channel volume Sl is obtained by solving Eq. (4.4) with $\frac{\mathrm{d}S}{\mathrm{d}t} = 0$:

$$Sl = \frac{C_1 R \bar{Q}_\mathrm{p}^3}{C_2\, (h_\mathrm{ob} - \frac{1}{2} R \bar{Q}_\mathrm{p}^2)^n}. \tag{4.14}$$

Thus by specifying R and $\bar{Q}_\mathrm{p}$, the channel volume is fixed without prescribing either S or l. It follows that the equations for channel cross-sectional area S, channel flow path length l and channel roughness n_man comprise an under-determined system given by Eq. (4.5) and Eq. (4.14). With $\Delta t_\mathrm{c} = t_\mathrm{c} - t_\mathrm{m}$, the (total) residence time Δt is given by

$$\Delta t = \Delta t_\mathrm{m} + \Delta t_\mathrm{c}, \tag{4.15}$$

which is a function of t_inj. The solutions of Eqs. (4.12) for t_m and t_c and (4.13) will have to be determined numerically for general Q_m and Q_p. Finally, the transit speed is given by

$$\hat{v} = \frac{\hat{l}}{\Delta t}, \tag{4.16}$$

where $\hat{l}$ is the transit distance (Fig. 4.1).

Model configuration

The lumped element model is driven by the discharge into the moulin Q_{m} and the proglacial discharge Q_{p}, and uses atmospheric pressure at the terminus as the lower boundary condition. Defined in this way, three free parameters remain: A_{t} and A_{b} describing the geometry of the moulin and the channel resistance R. As the channel parameters S, l and n_{man} are non-unique, we will present the range of n_{man} and S corresponding to a range of sinuosities σ between 1 and 2.

To compare the model results to the measurements from Gornergletscher and Unteraargletscher (Schuler et al., 2004), the model was run with the measured proglacial discharge, the measured discharge into the moulin for Unteraargletscher and the derived (Eq. 4.1) discharge into the moulin for Gornergletscher. The measured data was interpolated using a piecewise cubic Hermite polynomial to obtain a continuous discharge function. These piecewise polynomial representations of the discharge were then integrated numerically for use in Eqs. (4.12) and (4.13). On Gornergletscher, the transit distance was $\hat{l} = 5250\,\mathrm{m}$, the mean proglacial discharge $\bar{Q}_{\mathrm{p}}$ was 25.3 $\mathrm{m^3\,s^{-1}}$ and we ran the model from 10:00 on 18 July to 23:59 on 20 July 2006. On Unteraargletscher, $\hat{l}$ was 4450 m, the two model run time intervals were 27 h long starting at 9:00 on 2 August 2000 and 8 September 2000 and the corresponding $\bar{Q}_{\mathrm{p}}$ were equal to 10.9 and 14.0 $\mathrm{m^3\,s^{-1}}$. In the Appendix, further results are presented exploring the model behaviour with synthetic data.

Fitting procedure and error estimates

The tuning parameters (A_{t}, A_{b}, R) were fitted by minimising the least square differences between modelled and measured transit speed. For the experiments on Unteraargletscher we found that using different A_{t} and A_{b} did not improve the fit and thus we set $A_{\mathrm{t}} = A_{\mathrm{b}}$. On Gornergletscher however, it was essential to have different A_{t} and A_{b}. For Unteraargletscher, model runs denoted U1 and U2 correspond to the experiment performed in August and September, respectively. For Gornergletscher, we employed two fitting strategies. First, we fitted the model using all available tracer experiments (model run G1) and second, we used only the tracer experiments during the first 24 h and also excluding the experiment which was conducted at 17:00 18 July, just before an iceberg was blocking the spillway (model run G2).

The errors on the measured transit speed are small (1% for Unteraargletscher and 4% for Gornergletscher experiments) and were thus ignored in our estimation of the errors of the fitting parameters. However, the errors on the discharge data are larger. For the discharge measurements by salt dilution at Unteraargletscher, Schuler et al. (2004) estimate an error of 5%. The proglacial discharge on Gornergletscher was measured by the hydroelectric power company for which we estimate an error of 10%. The discharge into the moulin was derived from lake level measurements and a modelled meltwater inflow (Eq. 4.1) and has estimated errors of up to 20%, which are probably systematic. In addition, the interpolation gives rise to further errors.

A simple scheme was employed to estimate the influence of these errors on the model estimate of $\hat{v}$. The moulin input and proglacial discharge data were modified by increasing and decreasing their mean and amplitude by the errors given above. For the moulin discharge on Gornergletscher, we also used a $\pm 2.5\,\mathrm{h}$ phase shift of the modelled water input into the lake Q_{melt} (Eq. 4.1) to account for inaccuracies in the linear-reservoir model. The model was then fitted to the transit speed using the modified discharges. Thus, for Unteraargletscher the model was fitted to 3^4 different combinations of discharges and for Gornergletscher to 3^5 different combinations of discharges. The range of $\hat{v}$ obtained by this procedure we take as the error bounds and are presented as bands in the figures.

4.4 Results

We first present the tracer experiments and related measurements conducted on Gornergletscher and we give a short summary of the tracer experiments conducted by Schuler et al. (2004), then the results of applying the model to the experiment series are given.

4.4.1 Observations

The results of the tracer experiments and other related measurements are presented in Fig. 4.4. During the observation period (18 to 20 July 2006), the weather conditions were stable with no precipitation and air temperature in the range 6–15°C (Fig. 4.4g) and the drainage system was well established in its summer configuration (Chapter 2). At this time, the lake had been draining into the moulin for two weeks and hence the moulin had adjusted to the greatly enhanced input. Due to the stable weather, the hydraulic conditions in the glacier drainage system were also stable, as can be inferred from the regularly varying proglacial discharge (Fig. 4.4a) and englacial water pressure (Fig. 4.4f). The water pressure head in the borehole fluctuated between $315\,\mathrm{m}$ in the morning and $345\,\mathrm{m}$ in the late afternoon. Proglacial discharge varied between 15 and $35\,\mathrm{m}^3\,\mathrm{s}^{-1}$ and was in phase with the water pressure fluctuations in the borehole. The lake discharge varied between 1.8 and $4\,\mathrm{m}^3\,\mathrm{s}^{-1}$, except on 18 July in the afternoon, when it suddenly dropped to $1\,\mathrm{m}^3\,\mathrm{s}^{-1}$ followed by a subsequent rise to $5\,\mathrm{m}^3\,\mathrm{s}^{-1}$. This erratic fluctuation was caused by an iceberg collapsing (17:00) at the lake outlet and blocking the spillway. The iceberg obstructed the discharge out of the lake for about four hours, and therefore was also responsible for the enhanced discharge once the lake outlet was cleared. Figure 4.4b shows that the tracer transit speed varied between 0.49 and $0.76\,\mathrm{m\,s}^{-1}$. The lowest tracer transit speed was measured in the 17:00 experiment on the first day when the tracer was injected two minutes before the blockage of the lake spillway. This unanticipated blockage led us to conduct more experiments on the following days to fill the gap left by this unrepresentative experiment. The injection done on the third day at 17:00 yielded a transit speed of $0.65\,\mathrm{m\,s}^{-1}$ compared to $0.49\,\mathrm{m\,s}^{-1}$ after the blockage. Thus, the highest transit speed of $0.75\,\mathrm{m\,s}^{-1}$ was attained at 11:00 when the subglacial water pressure started to rise; the speed then dropped to $0.65\,\mathrm{m\,s}^{-1}$ in the afternoon (neglecting the transit speed during the blockage), rose again to $0.75\,\mathrm{m\,s}^{-1}$ during the night and lowered again to $0.68\,\mathrm{m\,s}^{-1}$ in the morning. Dispersion was between 2.5 and $4.5\,\mathrm{m}^2\,\mathrm{s}^{-1}$ apart from the outlier on the second day with $6.5\,\mathrm{m}^2\,\mathrm{s}^{-1}$ (Fig. 4.4c). It was in phase with moulin and proglacial discharge with its highest value at 20:00. The fraction of mobile water was generally very close to 1 except during the afternoon (Fig. 4.4d). The fraction of returned tracer mass averaged around 0.8, was lower (0.6) in the afternoon and higher (1.0) in the early morning (Fig. 4.4e).

Summary of observations on Unteraargletscher

Schuler et al. (2004) conducted two series of tracer injections (to which we will apply our model too), each over a diurnal cycle in August and September 2000 on Unteraargletscher, a temperate

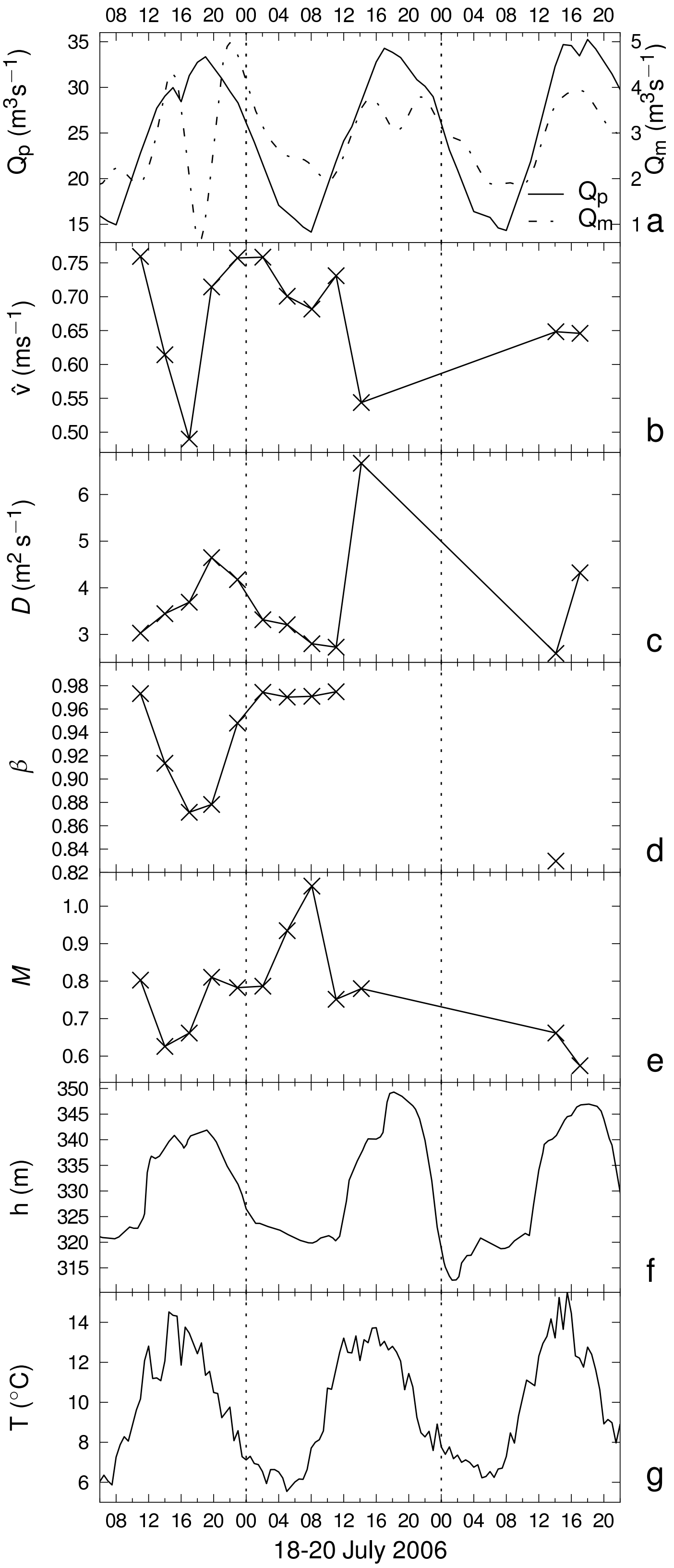

Figure 4.4: *Tracer and other hydraulic measurements. (a) proglacial discharge (solid line, left scale) and inferred discharge into the moulin (dashed line, right scale, c.f. Eq. (4.1)), (b) tracer transit speed, (c) tracer dispersion, (d) fraction of mobile water, (e) fraction of returned tracer mass, (f) water pressure head in borehole, (g) ventilated air temperature off-ice. The vertical dotted lines demarcate the days.*

valley glacier in the Bernese Alps, Switzerland. Their main finding was that transit speed covaried with supraglacial discharge input into the moulin but not with proglacial discharge. The measured transit speed varied between $0.75\,\mathrm{m\,s^{-1}}$ in the afternoon and $0.15\,\mathrm{m\,s^{-1}}$ in the early morning. The discharge input into the moulin varied over an order of magnitude between $0.3\,\mathrm{m^3\,s^{-1}}$ in the afternoon and $0.01\,\mathrm{m^3\,s^{-1}}$ in the early morning.

4.4.2 Model applied to Gornergletscher

Figure 4.5 shows input data, measurements and the results of fitting the model to all measured transit speeds (model run G1). The discharges Q_m and Q_p, which were used as model input, are shown in Fig. 4.5a. Note the signature of the iceberg blockage event on the first day at 17:00 and the higher day-to-day variability of Q_m compared to that of Q_p. The observed transit speeds (Fig. 4.5b, diamonds) lie within the error bounds of the modelled values, except for those on the third day. The model reproduces the observed twice-daily maxima and minima on all three modelled days. However, the error bounds are fairly large, on average $\pm 0.1\,\mathrm{m\,s^{-1}}$ and in places up to $\pm 0.3\,\mathrm{m\,s^{-1}}$. The large error bounds on the first day, during the iceberg blockage event, arise because Q_melt (Eq. 4.1) was shifted by up to $\pm 2.5\,\mathrm{h}$ for the error estimate, which is also the cause of the large error bounds on the last day. The hydraulic variables (Q_p, h and Q, Fig. 4.5c–e) do not change considerably during the passage of the tracer, apart for injections conducted during the blockage event when Q drops to almost zero. Q_p and thus h are almost periodic functions during the three days considered. The moulin residence time Δt_m varies between $5\,\mathrm{min}$ and $105\,\mathrm{min}$, its minimum is at $6\,\mathrm{h}$ and its maximum at around $16\,\mathrm{h}$ (Fig. 4.5f solid and dashed line, respectively); during the iceberg blockage Δt_m reaches $200\,\mathrm{min}$. The channel residence time Δt_c varies between 60 and $130\,\mathrm{min}$, its maximum coincides with the minimum of Δt_m and vice versa. The total residence time Δt displays two maxima, one at each maximum of its components Δt_m and Δt_c. The range of Δt is between 115 and $160\,\mathrm{min}$, and is smaller than the ranges of Δt_m and Δt_c.

Table 4.3 summarises the fitting parameters and derived quantities for both model runs G1 and G2. The confidence intervals for R are smaller than 10% and the estimates of R from the two model runs lie within 2% of each other. The moulin cross-sectional areas show a large confidence interval for G1 and G2 of $\pm 30\,\mathrm{m^2}$. A_t is between 35 and $110\,\mathrm{m^2}$ and A_b between -40 and $50\,\mathrm{m^2}$. Note that the negative area of A_b does not cause unphysical effects because the total volume of water contained in the moulin is always larger than zero (i.e. $h > h_\mathrm{min}$ at all times, c.f. Fig. 4.3).

The root mean squared error (RMSE) of $\hat{v}$ in G1 is $0.1\,\mathrm{m\,s^{-1}}$ and $0.07\,\mathrm{m\,s^{-1}}$ in G2. Values for channel cross-sectional area are $22 > S > 11\,\mathrm{m^2}$ and those for roughness $0.24 > n_\mathrm{man} > 0.062\,\mathrm{m^{-1/3}\,s}$ for a given channel sinuosity $1 < \sigma < 2$. Table 4.4 summarises the ranges and means of the fitting parameters when the uncertainties related to Q_m and Q_p are taken into account. It shows that the parameters are constrained better for G1 than for G2. However, even in G1, the range of values of the moulin cross-sectional area is large. R is similar for G1 and G2 and better constrained than A_t and A_b.

4.4.3 Model applied to Unteraargletscher

Figure 4.6 shows the input data, measurements and the results of the model fitted to the data from tracer experiments performed at Unteraargletscher in August 2000 (U1, Fig. 4.6a–g) and

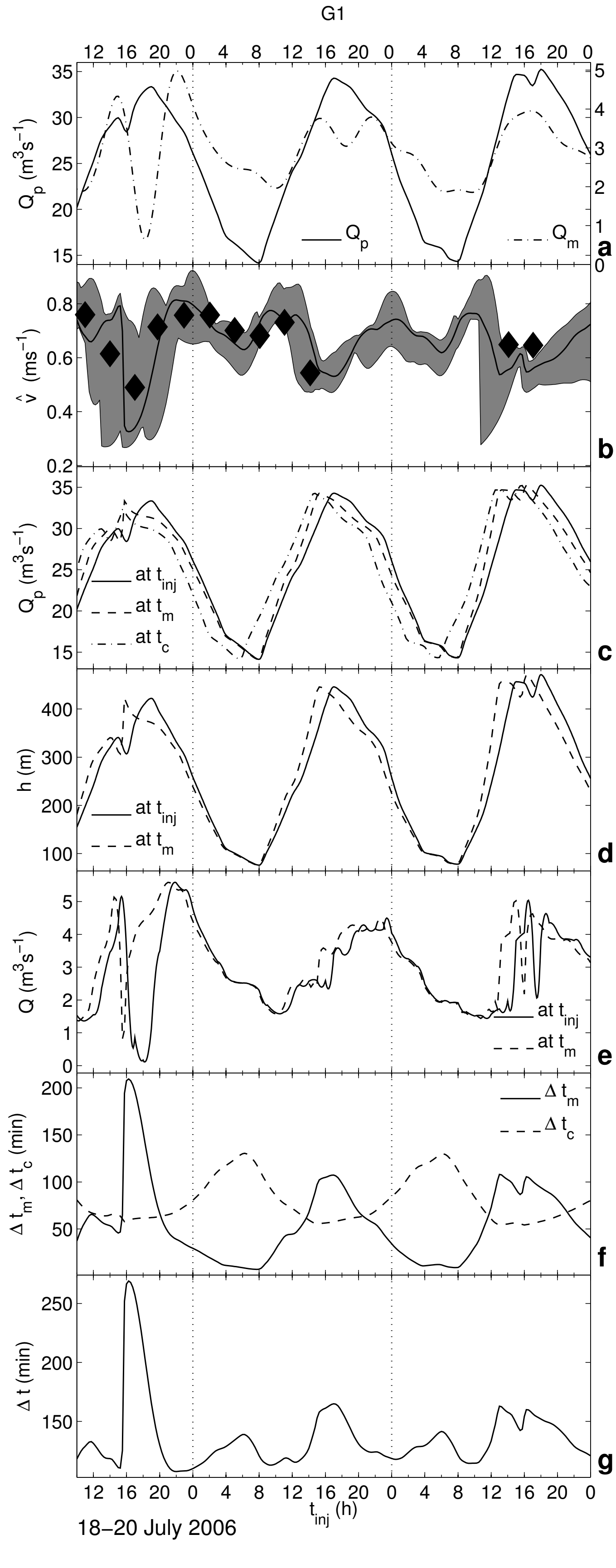

Figure 4.5: *Model inputs, outputs and comparison with measurements from fitting the model to all the transit speed data from the Gornergletscher experiments (model run G1). (a) Proglacial discharge Q_p (left scale) and moulin input Q_m (right scale); (b) measurements of transit speed are indicated by diamond symbols, the model output $\hat{v}$ by the solid line and the error bounds of $\hat{v}$ in grey; (c) proglacial discharge at injection time t_inj (solid), at moulin exit time t_m (dashed) and channel exit time t_c (dashed-dotted); (d) hydraulic head h (line style as in c); (e) discharge from the moulin Q (line style as in c), the dotted line marks zero discharge; (f) moulin residence time Δt_m (solid) and channel residence time Δt_c (dashed); (g) total residence time Δt. The vertical dotted lines demarcate the days.*

Table 4.3: *Parameters from fitting the model to measurements from Gornergletscher (G1 & G2) and Unteraargletscher (U1 & U2). The fitting parameters and their 95% confidence intervals: A_t and A_b are moulin cross-sectional area at top and bottom, respectively, and R is channel resistance. The root mean squared error (RMSE) of the fit of $\hat{v}$. Derived parameters for a sinuosity σ of the channel between 1 and 2: Manning roughness n_man and channel cross-sectional area S*

Model run	Experiment	A_t (m^2)	A_b (m^2)	R ($\mathrm{s}^2\mathrm{m}^{-5}$)	RMSE (ms^{-1})	n_man ($\mathrm{m}^{-1/3}\mathrm{s}$)	S (m^2)
G1	Gorner all	65±30	5±43	0.38±0.03	0.100	0.22–0.062	22–11
G2	Gorner first day	85±25	-13±31	0.39±0.03	0.072	0.24–0.067	23–11
U1	Unteraar August	1.15±0.24	-	2.11±0.05	0.036	0.27–0.077	13–6
U2	Unteraar September	1.53±0.45	-	1.40±0.04	0.039	0.48–0.135	22–11

Table 4.4: *Parameters from the error estimate taking uncertainties of Q_m and Q_p into account: Range of A_t, mean $\bar{A}_\mathrm{t}$ with mean 95% confidence interval, similarly for A_b, $\bar{A}_\mathrm{b}$, R, $\bar{R}$. Range of RMSE and mean $\overline{\mathrm{RMSE}}$*

Model run	A_t (m^2)	$\bar{A}_\mathrm{t}$ (m^2)	A_b (m^2)	$\bar{A}_\mathrm{b}$ (m^2)	R ($\mathrm{s}^2\mathrm{m}^{-5}$)	$\bar{R}$ ($\mathrm{s}^2\mathrm{m}^{-5}$)	RMSE (ms^{-1})	$\overline{\mathrm{RMSE}}$ (ms^{-1})
G1	18–125	63±38	-35–159	18±62	0.29–0.42	0.37±0.05	0.07–0.17	0.12
G2	-71–204	76±70	-38–207	13±79	0.26–0.42	0.37±0.06	0.07–0.18	0.12
U1	0.9–1.7	1.3±0.3	-	-	2.05–2.15	2.10±0.06	0.04–0.04	0.04
U2	1.0–2.7	1.7±0.6	-	-	1.33–1.43	1.38±0.05	0.03–0.06	0.04

in September 2000 (U2, Fig. 4.6h–n). In U1, the model input Q_p displays a maximum at $0\,\mathrm{h}$ and a minimum at $8\,\mathrm{h}$. Q_m has its maximum at $14\,\mathrm{h}$ and minimum between 3 and $6\,\mathrm{h}$. The measured variation of transit speed has two maxima ($0.75\,\mathrm{m\,s^{-1}}$) at 12 and $16\,\mathrm{h}$ and its global minimum at $3\,\mathrm{h}$ ($0.34\,\mathrm{m\,s^{-1}}$, Fig. 4.6b). For U1, our model reproduces the measured transit speeds well using the fitting parameters presented in Table 4.3. The largest discrepancies are for the injections conducted at $0\,\mathrm{h}$ and at $10\,\mathrm{h}$ on the second day, where the model underestimates the observed $\hat{v}$. The error bounds on $\hat{v}$ are generally below $\pm 0.025\,\mathrm{m\,s^{-1}}$ except for the time of low moulin discharge when they reach $\pm 0.05\,\mathrm{m\,s^{-1}}$. Apart from the outliers mentioned above, all measured transit speeds are within or very close to the error bounds. The hydraulic conditions change considerably during the passage of the tracer (Fig. 4.6c–e). Δt_c stays fairly constant between 70 and $100\,\mathrm{min}$, whereas Δt_m varies between 20 and $100\,\mathrm{min}$ (Fig. 4.6f). Thus, most of the variation of Δt stems from Δt_m (Fig. 4.6g), although the small maximum (and corresponding dip in $\hat{v}$) at $14\,\mathrm{h}$ is caused by changes in Δt_c.

In U2, the model input Q_m has its maximum at $14\,\mathrm{h}$ and minimum between 22 and $8\,\mathrm{h}$, and its amplitude is larger than in U1 (Fig. 4.6h). Q_p increases between 9 and $18\,\mathrm{h}$, stays at an almost constant level overnight and continues to rise again after $10\,\mathrm{h}$ on the next day which is quite different to Q_p of U1. The measured transit speed has its maximum at $12\,\mathrm{h}$ ($0.55\,\mathrm{m\,s^{-1}}$) and its minimum at $0\,\mathrm{h}$ ($0.15\,\mathrm{m\,s^{-1}}$), thus they are both lower than the respective extrema in August but their amplitude is the same (Fig. 4.6i). U2 overestimates the transit speed of the first tracer experiment and underestimates the transit speed of those conducted during the night as well as that of the last one. The error bounds on $\hat{v}$ are generally smaller than $\pm 0.025\,\mathrm{m\,s^{-1}}$ except at 20 and $22\,\mathrm{h}$. U2 fits the measured transit speed slightly better than U1 (Table 4.3). The difference in hydraulic conditions at t_inj and t_m between U1 and U2 is most apparent in Q (Fig. 4.6e,l). For

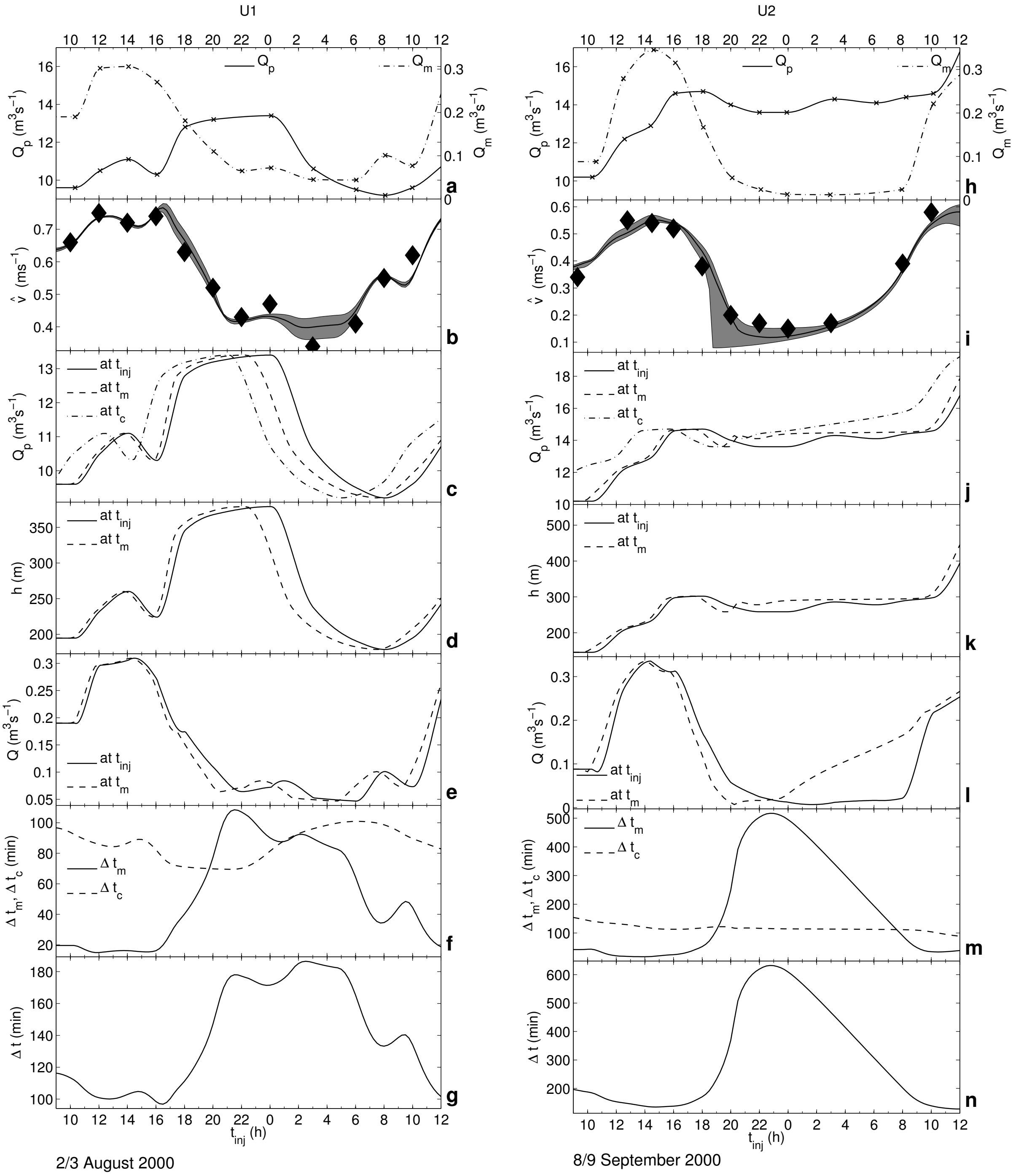

Figure 4.6: *Input, results and comparison to transit speed of the model fitted to the data from Unteraargletscher experiments in August (left, U1) and September 2000 (right, U2). The layout is identical to Fig. 4.5. (a) Q_p and Q_m, crosses mark the measurements, the line is the interpolation. (b) measured transit speeds (diamonds), modelled $\hat{v}$ and the error bounds of $\hat{v}$ (grey).*

U2, only tracer injected between 20 and 23 h actually exits the moulin during the time of low Q_m. Tracer injected later does not exit the moulin before 8 h after Q_m has increased again. Δt_c stays fairly constant between 150 and 100 min, whereas Δt_m varies between 20 and 500 min, thus the variation Δt is dominated by Δt_m (Fig. 4.6m,n).

Table 4.3 lists the fitting parameters and their ranges for U1 and U2. The estimated moulin cross-sectional areas are 1.2 and $1.5\,\mathrm{m}^2$ for U1 and U2 respectively, with an error of about $\pm 0.35\,\mathrm{m}^2$ for both. The values for resistance are 2.1 and $1.4\,\mathrm{s}^2\,\mathrm{m}^{-5}$ for U1 and U2, respectively, both with an error of about $\pm 0.05\,\mathrm{s}^2\,\mathrm{m}^{-5}$. Thus, even though the moulin size is similar for U1 and U2, the channel resistance is quite different. The RMSE for both is smaller than $0.04\,\mathrm{m\,s}^{-1}$. Assuming a channel sinuosity $1 < \sigma < 2$, the Manning roughness for U1 is $0.27 > n_{\mathrm{man}} > 0.076\,\mathrm{m}^{-1/3}\,\mathrm{s}$ and the cross-sectional area of the channel is $12 > S > 6\,\mathrm{m}^2$. For U2, the corresponding ranges are $0.48 > n_{\mathrm{man}} > 0.13\,\mathrm{m}^{-1/3}\,\mathrm{s}$ and $22 > S > 11\,\mathrm{m}^2$. Thus the channel properties differ significantly between August and September. Table 4.4 summarises the ranges and mean of the fitting parameters when uncertainties related to Q_{m} and Q_{p} are taken into account. The fitting parameters and RMSE for both U1 and U2 are stable within the error estimate.

4.4.4 Implications for experiment design

To infer the flow conditions and evolution of the channelised component of the drainage system with tracer experiments, the effects of all the system's constituents must be accounted for. Here we investigate how many tracer experiments and discharge measurements are actually needed to estimate the model parameters (A_{t}, R) accurately. We fitted the model to all combinations of three or more tracer experiments chosen from one of the two injection series of Unteraargletscher (with 12 and 11 injections, for a total of 6142 combinations), (a) using discharge data collected only at the injection time of the chosen experiments and (b) using all the available discharge data. For (a) we find a wide range of RMSE for the predicted $\hat{v}$ when using less than ten experiments, accompanied by a wide distribution of estimated model parameters. For (b), the range of RMSE for $\hat{v}$ is much reduced compared to (a) and the distribution of estimated parameters is much narrower. With eight tracer experiments in (b), the fit becomes almost as good as with all 11 or 12 experiments: the standard deviation of the distribution of A_{t} is $0.1\,\mathrm{m}^2$, of R is $0.01\,\mathrm{s}^2\,\mathrm{m}^{-5}$ and of the RMSE for $\hat{v}$ is $0.002\,\mathrm{m\,s}^{-1}$ (c.f. Table 4.3). Furthermore, for three suitably chosen experiments (e.g., at $10\,\mathrm{h}$, $16\,\mathrm{h}$ and $20\,\mathrm{h}$) the model parameters are well estimated, but only when using all discharge data available (b).

4.5 Discussion

4.5.1 Model

An observation we made during the model development is that for a given channel resistance R of an R channel in steady state, the sinuosity σ, the channel cross section S and the Manning roughness n_{man} are not independent. This follows from Eq. (4.14), which shows that for a given R and $\bar{Q}_{\mathrm{p}}$ the channel volume (needed to calculate the residence time, Eq. 4.9) is fixed, irrespective of σ, S and n_{man}. This arises because channel enlargement is proportional to l^{-1} (Eq. 4.4, first term on right hand side) and channel closure is proportional to S (second term on right hand side). All other variables only depend on R or $\bar{Q}_{\mathrm{p}}$. Channel residence times thus only depend on R and $\bar{Q}_{\mathrm{p}}$, hence we fitted R and not σ and n_{man}. But this also means that σ and n_{man} cannot be unambiguously inferred from tracer experiments. Even in time dependent situations, this distinction is not clear as shown in Chapter 6 and by Schuler and Fischer (2009). The latter found similar responses of modelled transit speeds to perturbations applied to roughness, sinuosity and parameters controlling the channel geometry.

The model presented here is similar to that of Kohler (1995) which was used to interpret tracer experiments conducted on Storglaciären. Kohler (1995) also used a static channel and a cylindrical moulin, but includes an open channel flow section and assumes a constant discharge along the tracer flow path. Kohler's (1995) primary aim was to determine the extent of open channel flow within the glacier.

4.5.2 Observations

The transit speeds measured on Gornergletscher and Unteraargletscher show both quantitative and qualitative differences. For the Unteraargletscher experiments, the transit speed correlates well with supraglacial discharge into the moulin, exhibiting one maximum in the afternoon and one minimum in the early morning. In contrast, the Gornergletscher transit speeds display two maxima and two minima, the latter coinciding with both maximal and minimal lake and proglacial discharge. We interpret these observations as follows. High discharge in the main drainage system causes high englacial water pressures, and correspondingly, a high filling level of the moulin. Therefore, the injected tracer has a longer residence time in the moulin, that more than compensates the faster flow in the main drainage system. At low discharge the situation is reversed: the passage through the moulin is faster as its filling level is lower, however the flow speed in the main drainage system is low, which more than compensates the fast flow in the moulin. Maxima in transit speed occur when flow is moderately fast in both components. The pronounced decrease in moulin discharge, caused by the blockage event, lead to lower transit speeds as the passage through the moulin was prolonged. The range of measured transit speeds on Unteraargletscher was 0.1–0.75 $\mathrm{m\,s^{-1}}$ compared to only 0.5–0.75 $\mathrm{m\,s^{-1}}$ on Gornergletscher. The smaller observed range of transit speeds on Gornergletscher is caused by the relatively smaller range of moulin discharge and is further aggravated by the opposing processes described above.

There are other processes influencing the passage of the tracer through the glacier. Both the fraction of mobile water β and the fraction of returned tracer mass M are lower during the afternoon when high subglacial water pressure prevails and higher during other times with a maximum of M in the morning. This suggests that during high subglacial water pressure, water is pushed into storage areas, i.e. water spreads laterally from the R channel and thus M and β are decreased (c.f. Chapter 5).

4.5.3 Model applied to Gornergletscher

The model reproduces the observed transit speeds within the error bounds (Fig. 4.5b). The characteristic occurrence of two diurnal maxima and minima in transit speed $\hat{v}$ is robust against the large errors in Q_m. This is due to a combination of two factors. First, this type of behaviour is already possible with a constant Q_m as is seen in the model S1 (c.f. Appendix, Fig. 4.7a–g). Second, the conical shape of the moulin makes the maximum of Δt_m narrower and the minimum broader (Fig. 4.7f). Without this the two maxima and minima per day in Δt would vanish due to negative interference of Δt_m and Δt_c. The variation of subglacial water pressure head $100 < h < 400\,\mathrm{m}$ (Fig. 4.5d) is larger than that observed in BH1: $310 < h < 350\,\mathrm{m}$ (Fig. 4.4c). However, subglacial water pressure measurements from the same borehole in the previous year produced a range of $280 < h < 350\,\mathrm{m}$ (Chapter 6), suggesting that BH1 was not well connected during the course of the tracer experiments presented here. Nevertheless, the calculated range of h is still too large, demonstrating that the predicted channel resistance R is too high. The iceberg blockage event produced a visible reduction in both measured and modelled $\hat{v}$, clearly demonstrating that the water flux into the moulin is a key determinant of $\hat{v}$.

The fitted moulin cross-sectional areas (A_t, A_b) are large but A_t matches the observed cross-sectional area of $\sim 80\,\mathrm{m}^2$ at the glacier surface. The water draining into the moulin from the lake had a temperature of $\sim 1°\mathrm{C}$ (Chapter 6); thus a large moulin cross-sectional area at depth seems plausible. For a sinuosity $\sigma = 1$, the Manning roughness $n_\mathrm{man} = 0.24\,\mathrm{m}^{-1/3}\,\mathrm{s}$ is improbably high and thus the channel is likely to be sinuous or to have a low and broad cross section. For a channel with a semi-circular cross section, n_man is reduced by a factor of 1.1 compared to a channel with a circular cross section, and more for a low and broad geometry (Hooke et al. (1990) and Chapter 6).

The error ranges and the confidence intervals of A_t and A_b are large (Table 4.4). This poorly constrained moulin geometry in turn affects the estimates of R. Therefore, the estimated range of R is much larger than for U1 and U2. However, even though the errors on the input data are large, we submit that the model captures the major processes determining the variation of $\hat{v}$ because it reproduces many of the observed features. Nevertheless, it is possible that there are other important processes influencing the passage of the tracer. Furthermore, this large error shows that the discharge into the moulin is an important parameter to measure accurately when performing tracer experiments.

4.5.4 Model applied to Unteraargletscher

The model is successful in explaining the variation of transit speed $\hat{v}$ obtained from tracer experiments at Unteraargletscher. It produces reasonable values for the fitted parameters and hydraulic variables, and even succeeds in reproducing minor features in the transit speed variations. For example, in U1 (Fig. 4.6a–g), we modelled two maxima of $\hat{v}$ in quick succession, interrupted by a small local minimum at $14\,\mathrm{h}$, as was observed. This minimum is one of the few qualitative features caused during the passage of the tracer through the channel: at the time the tracer of the $14\,\mathrm{h}$ injection passes through the channel (Fig. 4.6c, dash-dotted line), Q_p drops from 11 to $10\,\mathrm{m}^3\,\mathrm{s}^{-1}$ causing channel residence time to increase. This shows that although the variation of $\hat{v}$ is largely dominated during the tracer passage through the moulin, the model also captures small features caused by the channel.

The lower error bound on $\hat{v}$ in U2 (Fig. 4.6i) has a large jump at $19\,\mathrm{h}$ due to the same process that causes the discontinuity in S2 model presented in the Appendix (Fig. 4.7h–n). The lower error bound is produced by lowering Q_m by 5%, which is low enough to allow upwelling of subglacial water into the moulin. The variation of Δt_m is much larger for U2 than U1 due to the larger variation in Q_m and, in particular, due to the very low discharges during the night.

The fitted values of A_t are reasonable (Table 4.3) and their 95% confidence intervals are small. In September, A_t is larger which can be attributed to the seasonal evolution of the moulin. However, R is quite different for U1 and U2 which suggests that the channel system either had a different morphology or that different subglacial discharge conditions prevailed. The weather before the September experiments was cold and discharge was low (Schuler et al., 2004); the temperature and associated meltwater production then increased just prior to the experiments and discharge steadily increased (Fig. 4.6h). The channel was therefore not in steady state but increasing in size as suggested by Schuler and Fischer (2009). This limits the applicability of our static channel element and leads to exceedingly high modelled water pressure head h at the end of the period considered in U2 (Fig. 4.6k). A large h leads to increased retardation in the moulin and therefore an underestimated $\hat{v}$ for the two last experiments.

For the Unteraargletscher experiment, the moulin has a greater influence on the variation of the residence time than the channel. However, it is important to note that the mean of Δt_c is comparable to the mean of Δt_m but the variation of Δt_c is not as large. Thus, the variation in $\hat{v}$ arises during the passage through the moulin but its mean value is determined during both the passage through the channel and the moulin.

Schuler and Fischer (2009) also modelled the transit speeds of the measurements from Unteraargletscher with a model consisting of a moulin element as used in our model but coupled to an R channel described by partial differential equations. They found different values for the moulin diameter: 4 and $5\,\mathrm{m}^2$ for the August and September experiments, respectively, compared to 1.2 and $1.5\,\mathrm{m}^2$ found here. This mismatch arises for two reasons: first, their modelled subglacial water pressure is lower, leading to a lower filling level of the moulin and shorter moulin residence time; second, their channel residence time is shorter than ours. These two effects need to be compensated to fit the measured total transit time, which they achieved with a larger moulin cross-sectional area.

The subglacial water pressure produced by our model is too high, especially for the September experiments where it reaches 1.5 times the overburden pressure. In this respect, the model of Schuler and Fischer (2009) is more accurate and, for that reason, our model underestimates the moulin cross-sectional area. Conversely, there is evidence that the channel residence time in our model is more accurate: the double maxima of transit speed observed at $14\,\mathrm{h}$ in the August experiments are produced during the flow through the channel (Fig. 4.6b). Our model run U1 reproduces this feature whereas Schuler and Fischer's (2009) model does not. One cause for the discrepancy between the model results could be that Schuler and Fischer (2009) tuned their model manually and, consequently, their results might not be close to the best fit. Another factor could be that our model does not capture all the relevant physical processes occurring in the drainage system. Hence, these differences merit further investigation.

Nienow et al. (1996) also conducted high frequency tracer injections over diurnal discharge cycles on Haut Glacier d'Arolla (Switzerland). They also found covariations between tracer transit speed and moulin discharge, similar to the observations of Schuler et al. (2004). Tentatively, we fitted our model to two of their experiment series, one on 13 August 1991 using moulin m2Ec and one on 26 August using moulin m5Wf. The model fit the former experiments well and the latter reasonably, demonstrating the applicability of our model to that situation as well.

4.5.5 Implications for experiment design

The fitting of the model to all possible combinations of three or more tracer injections chosen from one of the Unteraargletscher datasets showed that a near continuous record of both the moulin and proglacial stream discharge is a prerequisite for running the model, whereas tracer experiments do not need to be as frequent once it has been shown that the presented model can be applied. These insights allow to formulate a measurement strategy tailored to probe the evolution of the drainage system over several days to weeks: first, determine if the model is applicable to a specific experimental situation with a series of at least eight injections over a diurnal discharge cycle to which the model is fitted; second, once the applicability of the model is established, three injections per day at rising, high and low discharge are then sufficient to monitor the evolution of the drainage pathway. The model should be validated again by conducting another high frequency series injections after a time span of days to weeks or after an event with a high impact on the drainage system. For longer study periods, it would be necessary either to use this model with an evolving R channel, and possibly also with a dynamic moulin cross section, or to fit the model independently for each day.

4.6 Conclusion

Tracer experiments were conducted to investigate the diurnal variability of the glacier drainage system under different conditions at Gornergletscher and previously Unteraargletscher (Schuler et al., 2004). The supraglacial input to the injection moulin at Unteraargletscher displayed a pronounced diurnal cyclicity. In contrast, the experiments at Gornergletscher were performed using a moulin into which an ice-dammed lake drained, providing input with a much smaller relative diurnal variability. The transit speed of water flow through a moulin–channel system is affected by discharge variations in each of the subsystems. Hence, on Gornergletscher, having a reduced variability in input discharge, we expected that the experiments would provide more direct information about the subglacial component. Instead, the observed transit speeds vary in a complex fashion, displaying two maxima and minima over one diurnal discharge cycle. The influence of the moulin and channel were found to be equally important with the flow speed variations in the two subsystems in antiphase, leading to the complex observed behaviour. Conversely, on Unteraargletscher, the transit speed correlated with discharge into the moulin and displayed only one daily maximum and minimum.

Our simple two-component model of the glacier drainage system simulates water flow through a moulin and a channel. Both the moulin and the channel element share the characteristic that water flow speed is proportional to the discharge and inversely proportional to the water volume they contain. The water volume in the channel element is constant whereas, in the moulin element, it changes with the filling level of the moulin governed by the subglacial water pressure, which is, in turn, proportional to the squared discharge of the channel element (Q_{p}). Thus, with increasing proglacial discharge, flow speed increases in the channel element but decreases in the moulin element. The interplay of these two opposing processes leads to the complex variation of observed transit speed in tracer experiments. The qualitative differences in the Gornergletscher and Unteraargletscher experiments are captured by our model, suggesting that the interaction between inflow modulation and channel flow are indeed responsible for the observed behaviour.

The input discharge into the moulin is a key parameter for modelling the tracer transit speed. This is demonstrated by two findings: (a) the uncertainty related to the input discharge on Gornergletscher substantially reduces the performance of the model, and (b) fitting the model to only a selection of observations from Unteraargletscher showed that frequent discharge measurements are more important than frequent tracer injections. These findings emphasise the importance to record the moulin discharge with a high frequency during the tracer experiments and we propose a measurement strategy that permits to infer the evolution of the drainage system over time scales of days to weeks. Furthermore, our results demonstrated that the sinuosity and roughness of the channel are not independently constrained by measurements of transit speed and thus other experiments are required to discriminate between them.

Appendix A

Model runs with synthetic data

The behaviour of the model was also explored with synthetic data. For the proglacial discharge the following function was used $Q_\mathrm{p} = q_\mathrm{p}^* \sin(\omega t + \phi) + \bar{q}_\mathrm{p}$, with amplitude $q_\mathrm{p}^* = 9.16\,\mathrm{m^3\,s^{-1}}$, radial frequency $\omega = 2\pi\mathrm{d}^{-1}$, mean discharge $\bar{q}_\mathrm{p} = 25.3\mathrm{m^3\,s^{-1}}$ and phase shift $\phi = 3.13$. The parameters were chosen such that this function fits the proglacial discharge of Gornergletscher during the presented tracer experiments. The discharge into the moulin was set to be constant $Q_\mathrm{m} = q_\mathrm{m}$. The resistance was taken as $R = 0.25\,\mathrm{s^2\,m^{-5}}$ which corresponds to, for example, $l = 5000\mathrm{m}$, $S = 6.9\mathrm{m}^2$ and $n_\mathrm{man} = 0.04\,\mathrm{m^{-1/3}\,s}$ and for the moulin, we set $A_\mathrm{t} = A_\mathrm{b} = 1\,\mathrm{m}^2$. To explore the model response, we performed model runs using different constant input discharges q_m in the range between 0.005 and $1\,\mathrm{m^3\,s^{-1}}$, including two detailed model runs with input discharge $q_\mathrm{m} = 0.2\,\mathrm{m^3\,s^{-1}}$ and $q_\mathrm{m} = 0.008\,\mathrm{m^3\,s^{-1}}$ to which we refer to as S1 and S2, respectively.

In S1, the variation of $\hat{v}$ displays two minima of similar size, coinciding with maximal and minimal Q_p (Fig. 4.7b). The hydraulic variables Q_p, h and Q at t_inj, t_m and t_c are almost identical (Fig. 4.7c–e), thus the passage of the tracer is fast compared to the change of the hydraulic variables. Note that even though Q_m is constant, the discharge out of the moulin Q varies with time (Eq. 4.8, Fig. 4.7e). The moulin residence time Δt_m varies between 5 and $25\,\mathrm{min}$ and is in phase with Q_p (Fig. 4.7f). The channel residence time Δt_c varies between 17 and $35\,\mathrm{min}$ but is in antiphase with Q_p (Fig. 4.7f). Since the amplitudes of Δt_m and Δt_c are similar but vary in antiphase, the resulting variation of their sum (Δt) and, consequently, $\hat{v}$ display two maxima and minima each. It should be noted that it is essential that Δt_m and Δt_c are not quite sinusoidal, because otherwise their superposition would produce a constant function. The results of model run S2 are displayed in Fig. 4.7 (right). The resulting variation of transit speed $\hat{v}$ shows only one maximum and one minimum, both occurring in the morning (Fig. 4.7i). There is a discontinuity in $\hat{v}$ at 6.5 h. The mean $\hat{v}$ is about one order of magnitude smaller in S2 than in S1; however the amplitudes in both model runs are of similar absolute size. Since the total residence time Δt is up to $10\,\mathrm{h}$ long, the hydraulic variables Q_p, h and Q differ substantially during the passage of the tracer (Fig. 4.7j–l). Q_p at t_c (dashed-dotted line in Fig. 4.7j) is similar to Q_p at t_m (dashed line), as in S1, since the passage through the channel is not affected by the choice for Q_m. Conversely, the hydraulic variables change greatly between t_inj (solid line) and t_m (dashed line) because the moulin residence time (Δt_m) is long. Q varies between -1×10^{-3} and $17 \times 10^{-3}\,\mathrm{m^3\,s^{-1}}$ (Fig. 4.7l) and Q at t_inj and at t_m differ qualitatively as the latter has a kink at 6.5 h. Both the mean and amplitude of Δt_m in S2 are much larger than those of Δt_c, thus Δt is almost exclusively determined by Δt_m (Fig. 4.7n).

Varying the input discharge Q_m affects only Δt_m but not Δt_c, and accordingly, the influence of the moulin on the total residence time Δt changes. Figure 4.8a shows t_inj against $\hat{v}$ for different values of Q_m. The transit speed $\hat{v}$ is fastest for the largest $Q_\mathrm{m} = 1\,\mathrm{m^3\,s^{-1}}$ and has its maximum and minimum at $18\,\mathrm{h}$ and $6\,\mathrm{h}$, respectively, coinciding with the maximum and minimum of Q_p. For $Q_\mathrm{m} = 0.5\,\mathrm{m^3\,s^{-1}}$ a second minimum appears at $19\,\mathrm{h}$. Both maxima and minima become comparable in size for $Q_\mathrm{m} = 0.2\,\mathrm{m^3\,s^{-1}}$ (c.f. S1, Fig. 4.7a–g). The minimum at $6\,\mathrm{h}$ disappears for $Q_\mathrm{m} = 0.08\,\mathrm{m^3\,s^{-1}}$ and $\hat{v}$ is in antiphase with respect to Q_p. For even smaller $Q_\mathrm{m} = 0.008\,\mathrm{m^3\,s^{-1}}$, a discontinuity in $\hat{v}$ (c.f. S2, Fig. 4.7h–n) appears. Figure 4.8b shows a phase portrait of the timings of the extrema of $\hat{v}$ in the t_inj–Q_m space. At low moulin discharge Q_m, there is one maxima and minima occurring in the morning. As Q_m increases both extrema

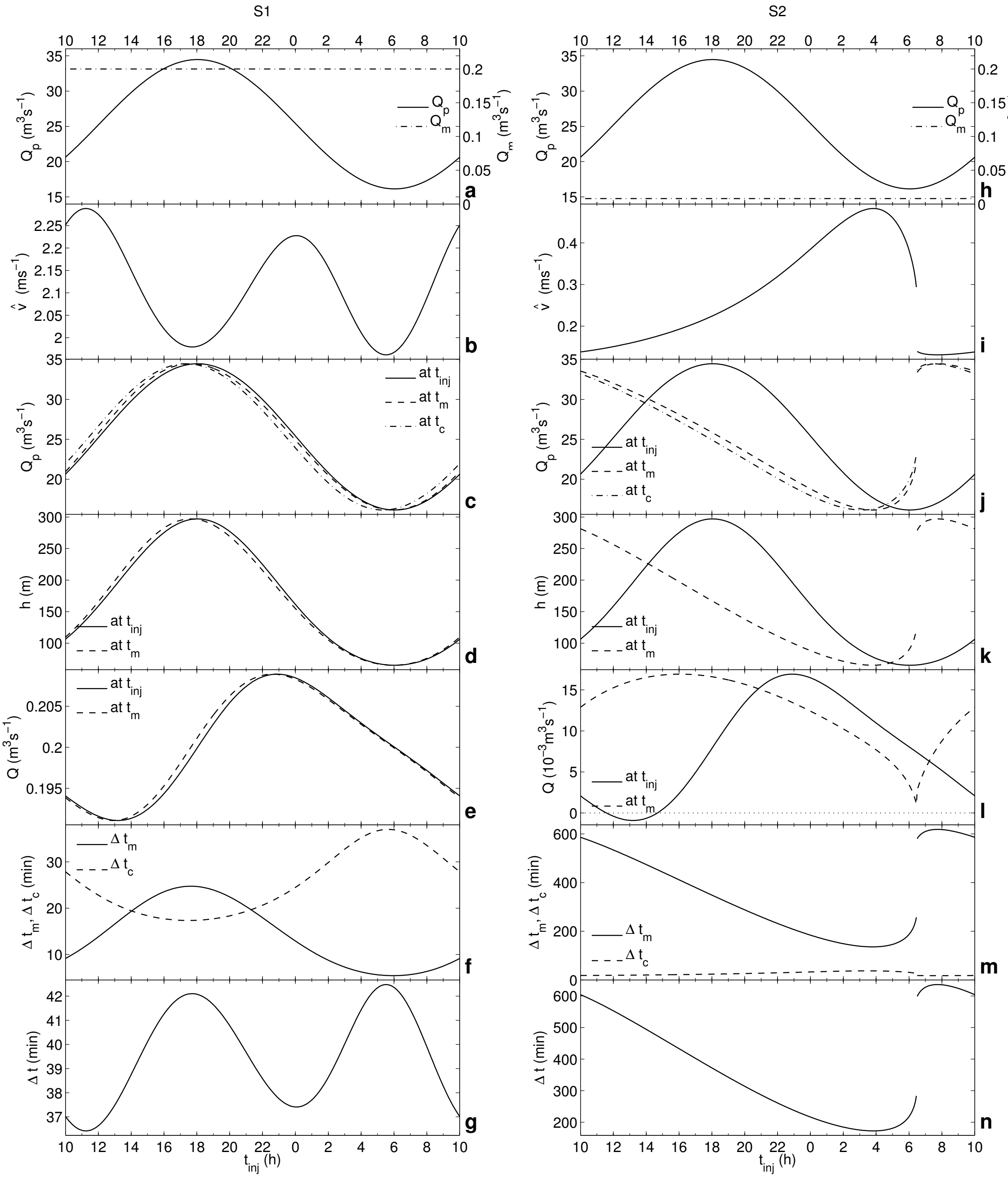

Figure 4.7: *The model input and output variables against injection time t_{inj} from running the model with synthetic data: left panels (a–g), model run S1 with Q_{m}=0.2 $\mathrm{m}^3\,\mathrm{s}^{-1}$ and right panels (h–n) model run S2 with $Q_{\mathrm{m}} = 0.008\,\mathrm{m}^3\,\mathrm{s}^{-1}$. The layout is identical to Fig. 4.5.*

migrate towards later times in the day. At $Q_{\mathrm{m}} = 0.08\,\mathrm{m}^3\,\mathrm{s}^{-1}$ a new pair of extrema arises at 4 h. At $Q_{\mathrm{m}} = 0.5\,\mathrm{m}^3\,\mathrm{s}^{-1}$ the original $t^{\downarrow}_{\mathrm{inj}}$ branch annihilates with the new $t^{\uparrow}_{\mathrm{inj}}$ branch (the graph is periodic in t_{inj}).

Even using simple and idealised input data, the model exhibits complex behaviour, thereby providing insights into several observed characteristics of the drainage system. The qualitative behaviour of the modelled transit speed (Fig. 4.8) can be understood in terms of the moulin Δt_{m}

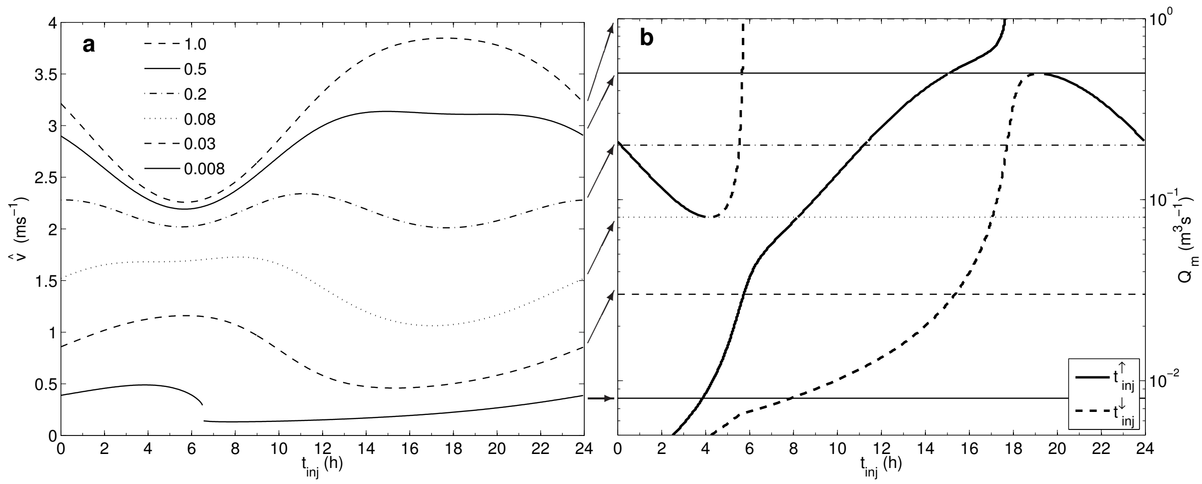

Figure 4.8: *(a)* t_{inj} *versus* $\hat{v}$ *for* $Q_{\mathrm{m}} = \{1, 0.5, 0.2, 0.08, 0.03, 0.008\}\,\mathrm{m^3\,s^{-1}}$. *(b) phase portrait of the timing of extrema in* $\hat{v}$ *in* t_{inj}*-*Q_{m} *space.* $t^{\uparrow}_{\mathrm{inj}}$ *and* $t^{\downarrow}_{\mathrm{inj}}$*, denote the timing of maximum and minimum* $\hat{v}$*, respectively. The dashed horizontal lines indicate the discharge which corresponds to the model runs shown in (a).*

and channel Δt_{c} residence time whose superposition gives the total residence time $\Delta t = \Delta t_{\mathrm{m}} + \Delta t_{\mathrm{c}}$. They both vary nearly sinusoidally, at least for $Q_{\mathrm{m}} > 0.01\,\mathrm{m^3\,s^{-1}}$, and are in antiphase. At low $Q_{\mathrm{m}} \sim 0.03\,\mathrm{m^3\,s^{-1}}$, the total residence time Δt is dominated by Δt_{m} and the transit speed $\hat{v}$ has its maximum in the morning when Δt_{m} is short. At intermediate $Q_{\mathrm{m}} \sim 0.2\,\mathrm{m^3\,s^{-1}}$ (Fig. 4.7a-g), Δt_{m} and Δt_{c} are of similar magnitude and $\hat{v}$ has two maxima and minima, the latter coinciding with the maxima of Δt_{m} and Δt_{c}. The resulting variation of $\hat{v}$ is comparable to the observations on Gornergletscher with the timing of transit speed extrema reproduced correctly. At even higher Q_{m}, Δt_{m} becomes negligible, as if tracer was injected directly into the main channel and $\hat{v}$ has a single maximum in the afternoon. The model behaves qualitatively differently at very low $Q_{\mathrm{m}} < 0.01\,\mathrm{m^3\,s^{-1}}$ when a discontinuity appears in most of the model variables (e.g. S2, Fig. 4.7h–n). It can be seen in the results of S2 that this discontinuity is related to the negative Q between 12 h and 15 h, i.e., water is flowing from the subglacial drainage system into the moulin which is caused by the quickly increasing subglacial water pressure head h. During such periods of upwelling, the tracer cannot exit the moulin and a discontinuity is produced in Δt_{m} (Fig. 4.7m) which is propagated to the other variables. If such a situation was encountered during a tracer experiment, it would produce a double peaked return curve; part of the tracer cloud exits the moulin but the rest is pushed back up and exits later. However, only one tracer experiment, non-overlapping with others, could yield double peaks by this mechanism.

Chapter 5

Dye tracing a jökulhlaup: Subglacial water transit speed and water storage mechanism

Abstract We present results of an investigation of two jökulhlaups (glacial lake outburst floods) at Gornergletscher, Switzerland, using dye tracer experiments and complementary hydrological measurements. Repeated dye injections into moulins showed that tracer transit speeds were larger after the lake had emptied, but when proglacial discharge was still high, than during the main phase of the jökulhlaup. This counterintuitive finding was modelled by tracer retardation inside the injection moulin. This model, together with an estimate of the maximum time the tracer takes to transit the injection moulin, allowed to calculate bounds on the transit speed in the main drainage channel where the lake water flows. These results indicate that the main drainage channel transit speeds are indeed highest during the peak of the flood. Moreover, it is known from a previous study that water amounting to half of the lake volume is temporarily stored within the glacier during a Gornergletscher jökulhlaup. Our observations suggest that this process occurred via lateral spreading of water at the glacier bed.

5.1 Introduction

Jökulhlaups, also known as glacier lake outburst floods, commonly occur in glaciated regions around the world and present one of the greatest glacier related hazards. Ice dammed lakes have a tendency to drain rapidly once an initial drainage pathway has been established. The jökulhlaup starts and proceeds either by melt enlargement of the drainage channel or by flotation of the ice dam (Roberts, 2005; Tweed and Russell, 1999). Jökulhlaups represent a unique test piece for theories of the evolution of the subglacial drainage system (e.g. Nye, 1976; Spring and Hutter, 1982; Clarke, 2003). They allow the study of the response of the glacial drainage system and also of the entire glacier to a large basal perturbation (e.g. Björnsson, 1998; Sugiyama et al., 2007; Bartholomaus et al., 2008; Stearns et al., 2008). Many aspects of jökulhlaups are still poorly understood, and two large field campaigns were conducted recently to produce more experimental data. Anderson et al. (2003) studied the jökulhlaups of Kennicott Glacier, Alaska, and our group studied the jökulhlaups of Gornergletscher, Switzerland (Huss et al., 2007; Sugiyama et al., 2007, 2008; Walter et al., 2008, 2009).

The glacial drainage system changes on spatial and temporal scales which are far smaller than those of most other relevant glaciological processes. This fact and the general inaccessibility of the glacial drainage system make its experimental investigation a formidable task. Tracer experiments offer one of the few experimental methods to probe the sub- and englacial drainage system. Others methods include measurements of subglacial water pressure in boreholes, slug tests, discharge into and out of the glacier, and geophysical methods such as radar and seismology. Dye tracer investigations on glaciers range from studies of the aquifer in the firn (e.g. Lang et al., 1979) to studies resolving the highly dynamic nature of the drainage system on an hourly time scale (e.g. Schuler et al., 2004). However, only two other dye tracer studies on aspects of jökulhlaups have been published, namely Aschwanden and Leibundgut (1982), which investigates also a Gornergletscher jökulhlaup, and Fisher (1973). Tracer experiments yield information integrated over the entire flow path of the water on its passage through the glacier. This makes their quantitative evaluation difficult, as most established theories of the glacial drainage system describe only a part of the tracer flow path. In particular, models of jökulhlaups describe the flow of the lake water in the R channel connecting the lake to the proglacial stream (Fowler, 1999; Clarke, 2003), ignore the rest of the glacial drainage system and thus neglect the influence of the outburst on the drainage of the supraglacial meltwater. However, it is this meltwater which is usually traced and its whole flow path needs to be taken into account to interpret tracer experiments correctly.

From 2005 to 2007, we conducted more than 200 tracer experiments to study the yearly jökulhlaups on Gornergletscher. The aim was to investigate the reaction of the glacial drainage system to the large perturbation caused by the jökulhlaups. The results and interpretation of some of these tracer experiments are presented in this paper and in its companion paper (Chapter 6). The present paper focuses on the influence of the jökulhlaup on the whole glacial drainage system in the years 2005 and 2007 when the lake was drained as an intense subglacial jökulhlaup. We first define our terminology and give a brief overview of the field site, the experimental methods and the techniques used for data processing. We introduce a simple lumped element model to estimate the influence of englacial water flow on the tracer passage before it meets up with the lake water in the main subglacial drainage channel. Measurements of subglacial water pressure head, lake and proglacial discharge are presented to complement the results of tracer experiments conducted before, during and after the jökulhlaups using moulins situated downglacier of the lake. From the measured transit speeds we derive a range of lake main drainage channel transit speeds during the jökulhlaup using the lumped element model. The companion paper (Chapter 6) focuses, not on the whole drainage system, but on the development of the lake drainage channel during the onset of the jökulhlaup in 2006. On the first 1.5 days of this jökulhlaup, we were able to inject tracer into the lake outlet, thus measure the transit speed of the lake water and thereby allowing, for the first time, to test a jökulhlaup model (Clarke, 2003) not only against lake discharge but also against flow speeds inferred from measurements.

5.2 Terminology

In order to describe and discuss the tracer experiments and the accompanying model, a few concepts need to be elucidated and terms defined. We assume that both the tracer and the water travel at the same velocity and thus in the following definitions apply equally to both.

The time interval between the passage of the maximum concentration of the tracer cloud at two locations is the *residence time* (t, sometimes called dominant residence time). The shortest possible horizontal distance between those two locations is the *transit distance* ($\hat{l}$), leading to the *transit speed* as the ratio of the transit distance and residence time ($\hat{v} = \hat{l}/t$). If not specified further, the two locations are implied to be injection and detection site. The actual distance travelled by the tracer is the *flow path length* (l). Of course, the time to traverse the *flow path* is also the residence time. Note that the flow path length will, in general, be larger than the transit distance due to the additional vertical distance covered and due to the geometry and sinuosity of the flow path. This means that the transit speed is a lower bound on the mean, channel cross-section averaged *flow speed* ($v = l/t$).

Note that hydraulic models, like the one presented in this paper, use the flow path length and calculate flow speed, not transit distance and speed, thus care must be taken when comparing experimental and model results. The reason to introduce the transit speed and not exclusively use the residence time is that it makes a comparison of results from experiments using different injections sites having different transit distances possible. Our definition of transit speed is identical to the sometimes used term "dominant effective flow velocity" (Käss, 1998); however, we decided to introduce the new terms transit distance and speed to make their close association clear and distinguish them from the flow path length and flow speed. Furthermore, note that the *mean* residence time is the time interval between injection until half the tracer cloud has passed the detection site, and will be longer than the residence time, as we defined it, in the (usual) situation when storage-release processes occur.

5.3 Field site

Gornergletscher, Switzerland, is the second largest glacier in the Alps with an area of $\sim$60 km^2. It covers an altitude range from 4600 m a.s.l. down to 2200 m a.s.l. and has a maximum length of 14 km (Huss et al., 2007). Gornersee is an ice marginal lake located in the confluence area of the two main tributaries Gorner- and Grenzgletscher (Fig. 5.1). The lake has an elevation of 2530 m a.s.l. and lies 5.25 km upglacier from the terminus. The maximum ice thickness of 450 m is found 1 km downglacier of the lake (Sugiyama et al., 2008). Gornersee fills every spring and drains in summer, normally as a subglacial jökulhlaup, but supraglacial overspill has also been observed. In the past years the maximum volume of the lake basin was estimated to be $\sim 4.5\times10^6$ m^3. However, the lake does not always fill up completely. Peak discharge from the lake is $\sim$20 m^3 s^{-1} and in the proglacial stream it is $\sim$40 m^3 s^{-1}, of which about half is meltwater and the rest is from the lake. Peak inflow of meltwater into the lake is $\sim$5 m^3 s^{-1}. The jökulhlaup lasts for about two to seven days, depending on the lake volume and the exact outburst mechanism (Huss et al., 2007). The lake takes about three weeks to empty if it drains by supraglacial overspill into a moulin. Two features which set Gornersee jökulhlaups apart from most others studied so far is that the lake is small compared to the glacier damming it, and that peak proglacial discharge during the jökulhlaup is only about twice the discharge due to melt.

5.4 Methods

We used the two fluorescent dyes Uranine (UR) and Rhodamine WT (RWT) for tracer injections. Both are suited to glacial environments and can be used simultaneously. Injections were

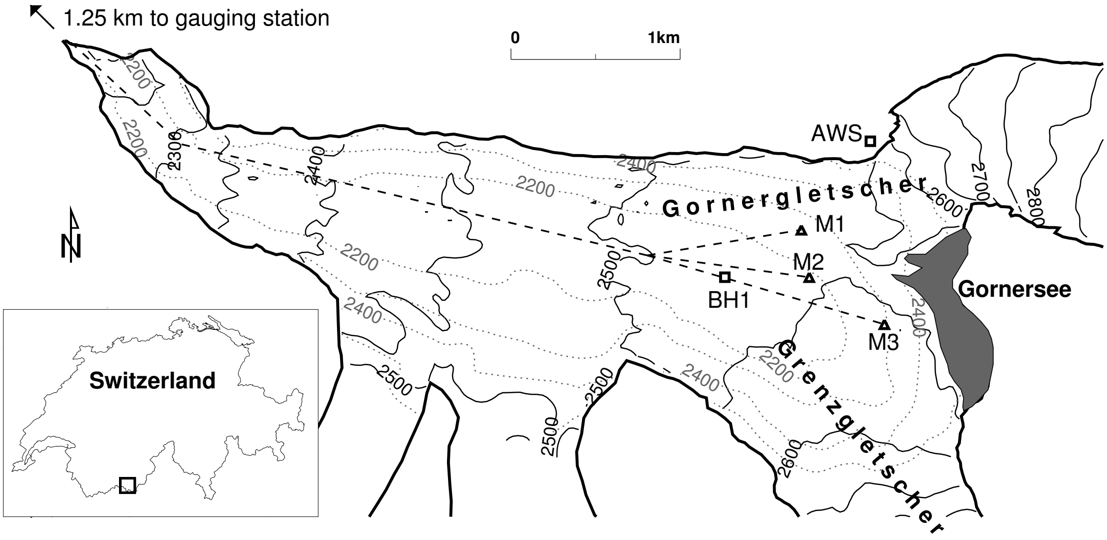

Figure 5.1: *Map of the tongue of Gornergletscher with solid contours of surface elevation and dotted contours of bed elevation. The location of the moulins used for the tracer injections are marked by triangles and labelled M1, M2 and M3. The dashed lines indicate the path used to compute the transit distance of each moulin. The subglacial water pressure was measured in a borehole (BH1). The position of automatic weather station is marked (AWS).*

done by hand into selected meltwater streams just before they entered into a moulin. The time required for the injection was always short compared to the residence time so, for data evaluation, we can assume instantaneous injections. All injections were carried out at 14:00 local daylight savings time (CEST, UTC+2) to keep the boundary conditions as constant as possible. We present results of 24 of a total of 101 injections conducted at a daily interval in 2005 year and less frequently in 2007.

Tracer injections were performed using three moulins (M1, M2, M3); their positions are marked in Figure 5.1. M1, used in 2005, was located 600 m downglacier of the lake. During the measurement period, the daily discharge maximum of M1 was around 0.5 $m^3\,s^{-1}$. M2, used in 2007, was situated 500 m downglacier of the lake, probably closer to the main subglacial drainage channel (where the bulk of the glacier discharge flows) than M1 (see Chapter 6 for a discussion of the location of the main subglacial drainage channel). M2 carried a discharge comparable to M1. M3, also used in 2007, was located 200 m from the lake, just on the downglacier edge of the lake dam on the Grenzgletscher side. It was substantially smaller than M1 and M2, attaining an estimated daily discharge maximum of around 0.05 $m^3\,s^{-1}$ during the measurement period. M1 and M2 have each a transit distance of 6 km and M3 of 6.5 km. The corresponding paths are shown as a dashed line in Figure 5.1 for each moulin.

The dye was detected about 1.25 km downstream of the terminus at the water gauging station of Grande Dixence SA. RWT concentration was measured using a Turner 10-AU flow-through fluorometer that allows continuous measurements. Water was fed through the fluorometer by a pump submerged in the pool of the gauging station. The UR concentration was measured using a BackScat submersible fluorometer, at the same location, also allowing continuous dye detection. Both fluorometers were calibrated using the water of the proglacial stream. The detection limit for the two dyes was around 0.3 ppb, but for good signal-to-noise ratio a peak concentration above 3 ppb was desirable. The conducted experiments had an average fraction of recovered dye mass of around 0.5 and thus a considerable amount of dye was lost somewhere in the glacial drainage system which could interfere with subsequent experiments. However, the main concentration peaks of the presented experiments are high and narrow enough that dye released from previous experiments is unlikely to modify them significantly. Furthermore, on days when no tracer experiments were conducted, the fluorometers continued to run and never registered any release events which were clearly above the background noise.

The proglacial discharge was measured by Grande Dixence SA at the gauging station with an error of 10%. The lake discharge was derived from the measured lake level and water input into the lake which was calculated by a melt model driven by temperature data from the automatic weather station (marked AWS in Fig. 5.1, see Huss et al. (2007) for details). The error in the lake discharge was estimated to be 20%. For 2005, we present subglacial water pressure head data measured in a borehole drilled to the bed (marked BH1 in Fig. 5.1). Subglacial water pressure data are not available for 2007.

5.4.1 Data processing

Mostly, the processing of the tracer data follows Schuler et al. (2004). The continuous time series recorded by the fluorometers were segmented into pieces corresponding to the individual injections. No breakthrough curves of the presented experiments were overlapping. To characterise the breakthrough curves, an advection-dispersion model with storage term (ADSM) was fitted to them (van Genuchten and Wierenga, 1976; Smedt et al., 2005). The equations for this model in a glaciological setting are given in Schuler et al. (2004). The fitting was performed using the CXTFIT2.0 program which is available from the U.S. Salinity Laboratory (Toride et al., 1999). The program requires as input the tracer concentration time series, transit distance and initial guesses for the fitting parameters. The ADSM returns four parameters estimating the mean transit speed, the hydrodynamic dispersion (D), the fraction of mobile water (β) and the exchange rate between mobile and immobile water (ω). We present the transit speed and not the mean transit speed as returned by the ADSM as the former is more readily compared to results from our hydraulic model. Figure 5.2 illustrates the different parameters characterising a breakthrough curve. D is a measure of the width of the rising part of the breakthrough curve (see Fountain, 1993; Schuler and Fischer, 2003). D depends mostly on the intensity of turbulent mixing: a boulder-strewn riverbed leads to more dispersion than a smooth bed. The two storage-release terms β and ω are both measures of the size of the tail of a breakthrough curve. In the case of a bad fit of the ADSM to the breakthrough curve, we omitted the estimated parameters in the figures. The fraction of returned tracer mass M was obtained by integrating the tracer concentration multiplied by the proglacial discharge divided by the injected tracer mass. Our interpretation rests on the transit speed, D, β and M, thus the presentation of ω is omitted.

5.4.2 Lumped element model

We envisage that surface water entering a moulin will first have to flow englacially and possibly also subglacially through a tributary flow path before it reaches the main drainage channel, where the bulk of the meltwater and also the lake water flows. This main drainage channel is likely located at the glacier bed (Fountain and Walder, 1998) and consists of a semi-circular channel incised into the ice, a so-called R channel (Röthlisberger, 1972). Here we set up a model to simulate the flow of the water through a moulin and a subsequent tributary R channel

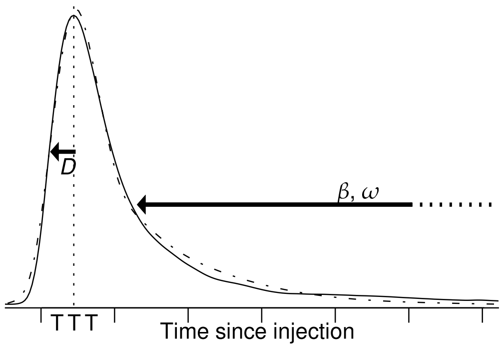

Figure 5.2: *Illustration of a tracer breakthrough curve (solid line) and ADSM fit (dashed line). The residence time is the time interval between injection and peak concentration, indicated by the vertical dashed line. Dispersion D characterises the width of the rising part of the curve, β and ω the length and size of the tail.*

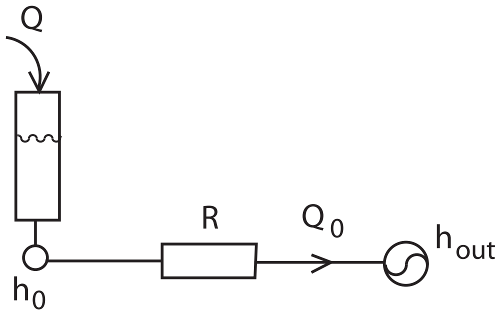

Figure 5.3: *Diagram of the lumped element model used to simulate transit speed. The moulin element (left) is fed by the input discharge Q and has a filling height h_0. The R channel element (middle) has resistance R and discharge Q_0. The lower boundary condition (right) is prescribed by the time varying pressure head h_{out}.*

before it reaches the main drainage channel. The ratio of the water volume to the discharge of a moulin is large and thus water flow speed in the moulin is slow. The water volume contained in the moulin is dictated by the filling height of the moulin which is equal to the subglacial water pressure head. This leads to water flow speed inside the moulin which is inversely proportional to subglacial water pressure. This is very different to water flow in R channels where flow speed increases with increasing subglacial water pressure gradient. This process of water retardation inside a moulin is called inflow modulation (Kohler, 1995; Nienow et al., 1996; Schuler et al., 2004). We model the inflow modulation by using the simple and elegant lumped element approach (Clarke, 1996). This model will then be used to interpret the measured transit speeds of the experiments conducted using M1.

The model is schematised in Figure 5.3 and consists of a moulin element connected to a R channel element. The moulin element has a constant cross-sectional area S_{m}, a filling height h_0 and is fed by a time-varying input discharge Q. The moulin element is connected via a R channel element to the main drainage channel. The R channel has circular cross-section, a resistance R and carries a discharge Q_0. We did not simulate the main drainage channel, instead we used measured subglacial water pressure head as the boundary condition h_{out} at the lower end of the R channel element.

Table 5.1: *Constants used in lumped element model*

Constant	Variable	Value
Ice flow exponent	n	3
Latent heat of fusion	L	$333.5\,\mathrm{kJ\,kg^{-1}}$
Pressure melting coefficient	c_{t}	$7.5 \times 10^{-8}\,\mathrm{K\,Pa^{-1}}$
Specific heat capacity of water	c_{p}	$4180\,\mathrm{J\,kg^{-1}\,K^{-1}}$
Gravitational acceleration	g	$9.8\,\mathrm{m\,s^{-2}}$
Density of water	ρ_{w}	$1000\,\mathrm{kg\,m^{-3}}$
Density of ice	ρ_{i}	$900\,\mathrm{kg\,m^{-3}}$
Ice flow constant	B	$5.3 \times 10^{-24}\,\mathrm{Pa^{-n}\,s^{-1}}$

Following Clarke (1996), the model is described by the system of equations

$$\frac{\mathrm{d}h_0}{\mathrm{d}t} = \begin{cases} 0 & \text{if } h_0 \geq h_{\max}, Q \geq Q_0 \\ \frac{Q-Q_0}{S_{\mathrm{m}}} & \text{otherwise} \end{cases} \tag{5.1}$$

$$h_0 - h_{\mathrm{out}} = RQ_0^2 \tag{5.2}$$

$$\frac{\mathrm{d}S_{\mathrm{c}}}{\mathrm{d}t} = C_1 Q_0 (h_0 - h_{\mathrm{out}})/l_{\mathrm{c}} - C_2 (h^* - \bar{h})^n S_{\mathrm{c}}. \tag{5.3}$$

where $C_1 = (1 - \rho_{\mathrm{w}} c_{\mathrm{p}} c_{\mathrm{t}}) \frac{\rho_{\mathrm{w}} g}{\rho_{\mathrm{i}} L}$ and $C_2 = 2B \left(\frac{\rho_{\mathrm{w}} g}{n}\right)^n$ are constants, $h_{\max}$ is the maximum filling height of the moulin, S_{c} is the channel cross section, $h^* = \rho_{\mathrm{i}} h_{\mathrm{i}} / \rho_{\mathrm{w}}$ is the pressure head corresponding to flotation pressure above the channel, $\bar{h} = \frac{1}{2}(h_0 + h_{\mathrm{out}})$ is the mean pressure head in the channel and l_{c} is the channel (flow path) length. The values used for the physical constants are given in Table 5.1.

Equation (5.1) relates the time evolution of the filling height of the moulin to input and output discharge. Note that this assumes that water entering the moulin reaches the filling level h_0 immediately. This is a good approximation as flow speed is fast in the very steep shaft. The R channel is modelled as a turbulent flow resistor (Eqn. 5.2). The time evolution of the cross-sectional area of the R channel is given by Equation (5.3), where the first term describes channel enlargement through dissipation of potential energy and the second term channel closure by ice creep. The resistance R is calculated from S_{c}, assuming a circular cross-section, with

$$R = 2^{4/3} \pi^{2/3} \, n_{\mathrm{man}}^2 \, l_{\mathrm{c}} \, S_{\mathrm{c}}^{-8/3}, \tag{5.4}$$

using the Gauckler-Manning-Strickler formulation with Manning roughness n_{man} (Chow et al., 1998). This system of differential algebraic equations was solved with Matlab's ode15s solver.

The modelled residence time in the moulin element is approximated by

$$t_{\mathrm{m}} = \frac{S_{\mathrm{m}}}{Q_0} h_0, \tag{5.5}$$

assuming constant discharge conditions during the passage of the tracer. Similarly, the modelled residence time in the R channel element is approximated by

$$t_{\mathrm{c}} = \frac{S_{\mathrm{c}}}{Q_0} l_{\mathrm{c}} \tag{5.6}$$

and the sum

$$t = t_{\mathrm{m}} + t_{\mathrm{c}} \tag{5.7}$$

Table 5.2: *Comparison of the key observations on the lake drainages in the years 2005 and 2007*

Year	Lake drainage character	Date of onset	Duration (d)	Peak lake disch. ($m^3\,s^{-1}$)	Peak progl. disch. ($m^3\,s^{-1}$)	Lake Vol. ($10^6\,m^3$)
2005	Subglacial	10 June	6	10	20	1.5
2007	Sub- & Supraglacial	4 July	8	15	27	3.7

is the modelled residence time of moulin and tributary channel, i.e. the time it takes the tracer to reach the main drainage channel. Assuming correctness of the model, the transit speed in the main drainage channel $\hat{v}_{\mathrm{main}}$ can be calculated by

$$\hat{v}_{\mathrm{main}} = \frac{\hat{l}_{\mathrm{main}}}{t_{\mathrm{tot}} - t}, \tag{5.8}$$

where t_{tot} is the measured residence time and $\hat{l}_{\mathrm{main}}$ is the transit distance of the main drainage channel.

5.5 Results

For both years 2005 and 2007, we first outline the general course of events during the jökulhlaup (Table 5.2) and then we focus on the results of the tracer experiments. To help the presentation, we divided the time span of both jökulhlaups into three phases: (I) the onset phase when the proglacial discharge had not increased yet; (II) the main phase when lake and proglacial discharge was high, and (III) the terminating phase when the lake had emptied but proglacial discharge was still high. In the figures displaying the results, these three phases are shaded with different levels of grey (Figs. 5.4–5.7). In the last part of this section, we present results of running the lumped element model with data from 2005 to establish bounds on water transit speed in the main drainage channel.

5.5.1 Observations in 2005

The lake was filled to one-third of its potential volume when the jökulhlaup began (10 June). The lake discharge increased progressively until the lake was empty on 15 June (Fig. 5.4e, Phases I and II). Hydrograph separation (Huss et al., 2007) showed that lake water was exiting the glacier between 13 and 15 June (Phases II and III). In Phase I, the daily minima of the subglacial water pressure head (Fig. 5.4f) increased until, during Phase II, the water pressure remained at flotation level throughout the day. In Phase III the pressure dropped abruptly and diurnal fluctuations recommenced the day after, albeit with a larger amplitude than before the jökulhlaup. The transit speed from the experiments conducted using M1 increased evenly throughout the measurement period (Fig. 5.4a) apart from a local maximum on 15 June during Phase III. The corresponding residence time of the injection on 15 June was 30 min shorter than the residence time of the one on 14 June. The injection on 12 June (Phase I) during the onset of the jökulhlaup produced a high dispersion D combined with a low fraction of mobile water β. The fraction of returned tracer mass M peaked at 0.8 during Phase II and was otherwise around 0.4.

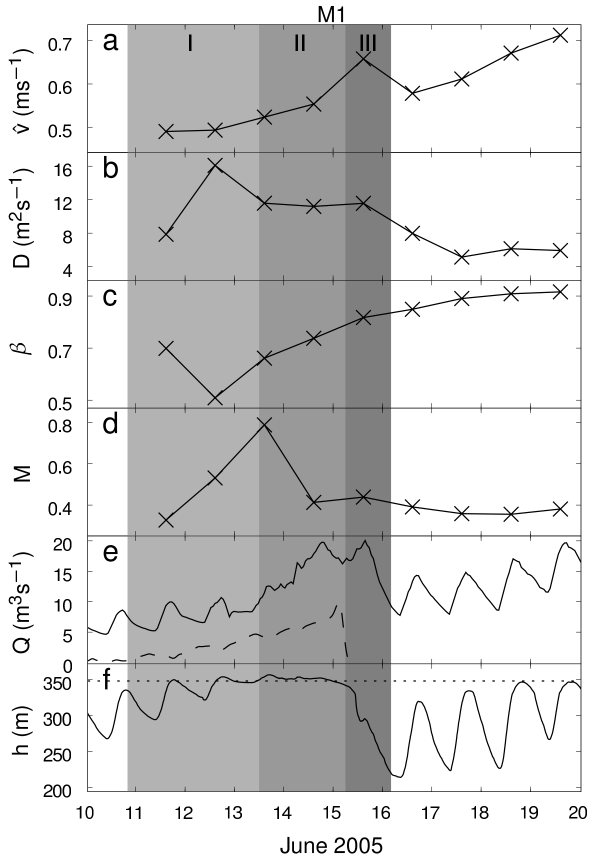

Figure 5.4: *Results from daily injections into moulin M1, hydrographs and subglacial water pressure head during and after the jökulhlaup in 2005. The crosses are plotted at the time of injection. (a) transit speed $\hat{v}$; (b) dispersion D, (c) fraction of mobile water β; (d) fraction of returned tracer mass M; (e) lake (dashed) and proglacial discharge (solid) and (f) subglacial water pressure head in borehole BH1 (dotted line corresponds to flotation level). The three Phases (I–III) into which the jökulhlaup was divided are shaded in grey.*

5.5.2 Observations in 2007

The lake was filled to its maximum volume when its shore reached a moulin on 4 July. It spilled over into this moulin and discharge stayed low until subglacial lake drainage initiated on 7 July. The main outburst happened during the next two days when the bulk of the lake water drained into a crevasse which had opened at around mid-height of the lake basin. During the main outburst the peak lake discharge of $15\,\mathrm{m^3\,s^{-1}}$ was attained. On 9 July, the lake level had dropped to the height of this crevasse and drainage occured again by supraglacial overspill. During the next five days subglacial drainage and supraglacial overspill alternated twice again until the lake was empty on 15 July. This caused the lake discharge to fluctuate considerably (Fig. 5.5e,j). The proglacial discharge rose to $27\,\mathrm{m^3\,s^{-1}}$ at the end of the main outburst and less during the subsequent subglacial drainage periods.

Figure 5.5 (a–d) shows the results from injections using M2. Before and during Phases I and II of the jökulhlaup, the transit speed was around $0.8\,\mathrm{m\,s^{-1}}$. The injection on 13 July (Phase III) produced the maximum transit speed of $1.3\,\mathrm{m\,s^{-1}}$. The transit speed of the injection after the jökulhlaup was slightly lower at $1.2\,\mathrm{m\,s^{-1}}$. The experiments yielded a decreased D during the later stage of Phase II and during Phase III, and an increased D after the jökulhlaup. β was high throughout and M peaked in Phase II.

Prior to the jökulhlaup in 2007, the injection using M3 on 2 July resulted in a transit speed of $0.6\,\mathrm{m\,s^{-1}}$ (Fig. 5.5f–i). In Phase II, there was a local maximum of transit speed ($0.8\,\mathrm{m\,s^{-1}}$) obtained from the injection on 10 July. The global maximum of the measured transit speed of $1.1\,\mathrm{m\,s^{-1}}$ was attained two days after Phase III on 15 July. One week later, the transit speed dropped back to $0.7\,\mathrm{m\,s^{-1}}$. D had a maximum on 10 July coinciding with the local maximum of the transit speed and the minimum of β (Phase II). M was 0.7 before and dropped to 0.1–0.4 during the jökulhlaup. Figure 5.6 shows the breakthrough curves from experiments using M3. The experiment on 9 July (Phase II) returned the lowest M of 0.1 and its breakthrough curve was very spread out and could not be fitted by the ADSM.

5.5.3 Model results

We ran the lumped element model (Fig. 5.3) to investigate the influence of inflow modulation on the results of injections into M1 from 7 to 17 June 2005. The model calculates the time to reach the main drainage channel t (Eqn. 5.7) and the transit speed in the main drainage channel $\hat{v}_{\mathrm{main}}$ (Eqn. 5.8). For the lower boundary condition (h_{out}) we used the subglacial water pressure head data from BH1 (Fig. 5.4f). The lack of corresponding pressure data for 2007 was the reason why this model was only applied to 2005. For the upper boundary condition, we assumed a sinusoidally varying discharge Q into the moulin element having an amplitude $0.26\,\mathrm{m^3\,s^{-1}}$, a mean value $0.30\,\mathrm{m^3\,s^{-1}}$ and its maximum at 14:00. Table 5.3 summarises the used model parameters. The length of the connection channel $l_{\mathrm{c}} = 500\,\mathrm{m}$ was chosen equal to the horizontal distance between M1 and BH1. This is the shortest conceivable connection channel length. The only data available to fit the model were the observed decrease of the residence time of 30 min from 14 to 15 June. For the first model run (Mod1), we chose the cross-sectional area of the moulin $S_{\mathrm{m}} = 15.5\,\mathrm{m^2}$ such that t also decreased by 30 min from 14 to 15 June (Fig. 5.7a,b). The 30 min residence time difference is a likely a lower bound as elucidated in the Discussion and thus, we performed a second model run (Mod2) with a 1.5 times larger cross-sectional area of the moulin $S_{\mathrm{m}} = 23\,\mathrm{m^2}$ (Fig. 5.7c,d) which resulted in a t decrease of 43 min from 14 to 15

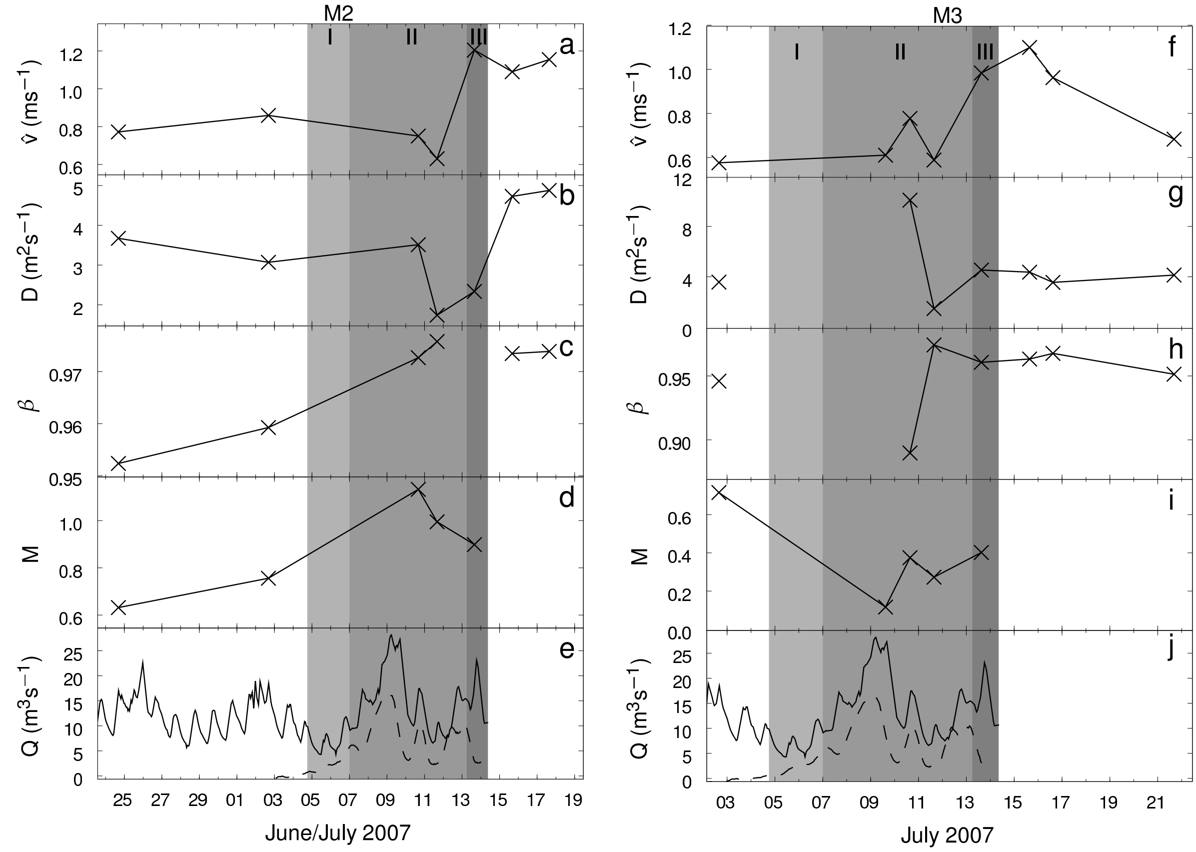

Figure 5.5: *Results from injections into moulin M2 (left) and into moulin M3 (right) and hydrographs for the jökulhlaup in 2007. The crosses are plotted at the time of injection. (a,f) transit speed $\hat{v}$; (b,g) dispersion D, (c,h) fraction of mobile water β; (d,i) fraction of returned tracer mass M; (e,j) lake (dashed) and proglacial discharge (solid). The three Phases (I–III) into which the jökulhlaup was divided are shaded in grey. Missing points indicate that the ADSM could not be fitted (c,g,h) or that the proglacial discharge measurement was broken (d,e,i,j).*

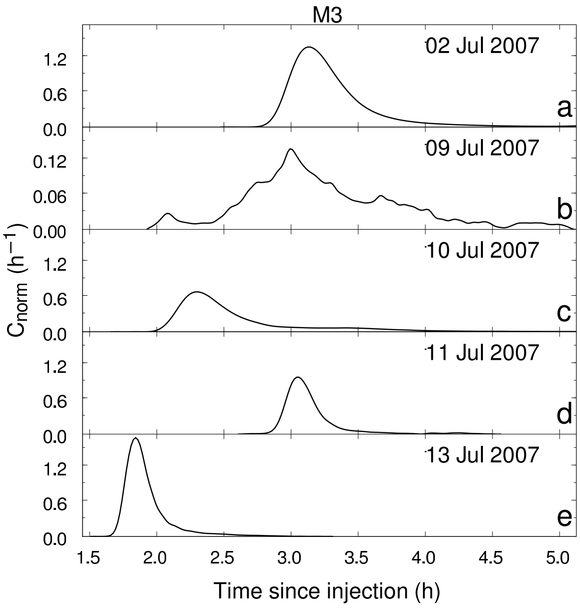

Figure 5.6: *Breakthrough curves from injections into M3 (c.f. Fig. 5.5) normalised by dividing the tracer mass flux through the injected mass. The label gives the injection date. All the plots have the same y-axis scale except (b) having a 10 times smaller one.*

June. The model has other free parameters (l_c and n_{man}) but there were not enough field data available to constrain these and thus they are set to physically reasonable values. This means that the calculated time to reach the main drainage channel t are only relative values, i.e. the whole time series of the t could be shifted by a constant offset (c.f. Fig. 5.7a,c). Bounds of the minimum and maximum value of t can be obtained by the following argument. The calculated residence time in the connection channel (t_c, Eqn. 5.6) stayed fairly constant at ~7 min and we assumed that the residence time in the moulin (t_m, Eqn. 5.5) was at least as long (the moulin was 400 m deep), thus the minimum t was at least 14 min (i.e. $\min(t) > 14\,\text{min}$). The experiment on 24 June 2005 yielded the shortest measured residence time of 113 min, thus we assumed that the maximum t is smaller than 113 min (i.e. $\max(t) < 113\,\text{min}$). The two time series $t_{\min}$ and $t_{\max}$ we defined as the ones containing the smallest and largest possible t, respectively

$$\min(t_{\min}) = 14\,\text{min} \tag{5.9}$$
$$\max(t_{\max}) = 113\,\text{min}. \tag{5.10}$$

For Mod1 this resulted in a shift of 69 min with respect to each other (Fig. 5.7a), and of 54 min for Mod2 (Fig. 5.7c). The minimum and maximum transit speed in the main drainage channel, $\min(\hat{v}_{\text{main}})$ and $\max(\hat{v}_{\text{main}})$ in Figures 5.7b and 5.7d, could now be calculated using Equation (5.8) by substituting $t_{\min}$ and $t_{\max}$ for t.

In the model run Mod1, the minimum/maximum time to reach the main drainage channel $t_{\min/\max}$ (Fig. 5.7a) increased by 20 min in Phases I and II and then dropped by 30 min by Phase III (as required by our fitting procedure). The transit speed in the main drainage channel $\max/\min(\hat{v}_{\text{main}})$ (Fig. 5.7b), calculated from $t_{\min/\max}$ and the measurements (Eqn. 5.8), increased during Phases I and II, stayed level in Phase III and decreased the day after. In the model run Mod2, $t_{\min/\max}$ (Fig. 5.7c) increased by 30 min during Phases I and II (10 min more than in Mod1) and dropped by 43 min by Phase III (13 min more than in Mod1). $\hat{v}_{\text{main}}$ (Fig. 5.7d) increased throughout Phases I and II and peaked at the end of Phase II, decreased in

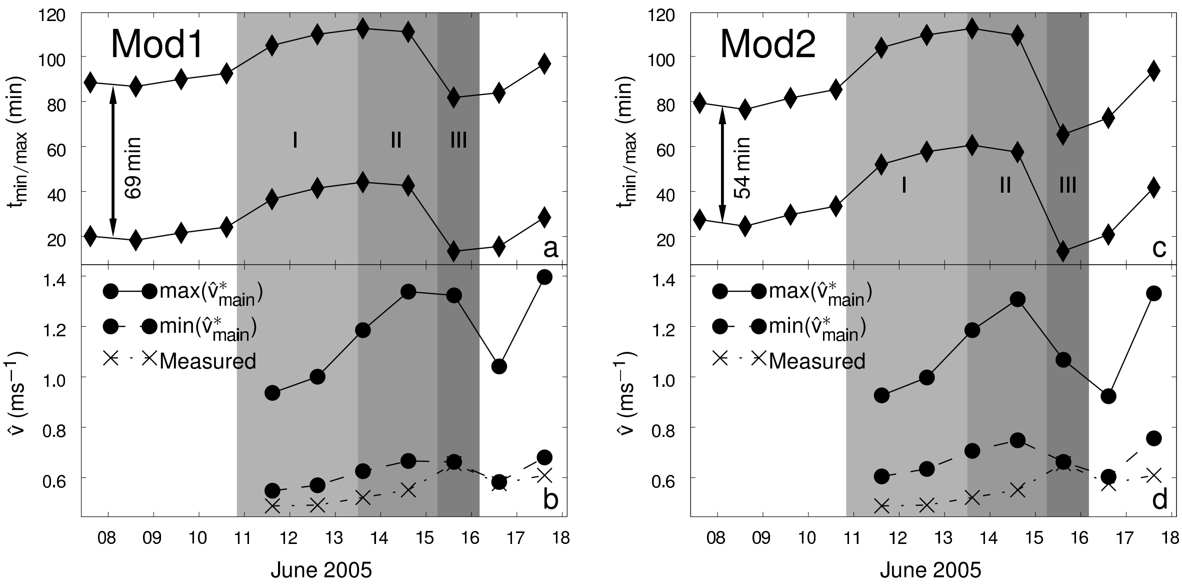

Figure 5.7: *Results of model run Mod1 ($S_\mathrm{m} = 15.5\,\mathrm{m}^2$, a, b) and Mod2 ($S_\mathrm{m} = 23\,\mathrm{m}^2$, c, d): (a,c) Minimum and maximum modelled time ($t_{\mathrm{min/max}}$) to reach the main drainage channel at 14:00 and (b,d) measured (total) transit speed $\hat{v}$ and the derived bounds on the transit speed in the main drainage channel ($\hat{v}_\mathrm{main}$, Eqns. 5.8–5.10). The three Phases (I–III) of the jökulhlaup are shaded in grey, identical to Figure 5.4.*

Table 5.3: *Parameters of the lumped element model*

Parameter	Variable	Value
Channel flow path length	l_c	500 m
Transit distance of main drainage channel	$\hat{l}_\mathrm{main}$	5500 m
Moulin cross-sectional area	S_m	15.5 & 23.0 m^2
Ice thickness	h_ice	400 m
Max. filling height	h_max	400 m
Manning roughness factor	n_man	0.033 $\mathrm{m}^{-1/3}\mathrm{s}$

Phase III and had its minimum the day after. The maximum $\hat{v}_\mathrm{main}$ was 1.34 m s^{-1} for both models as dictated by Equation (5.10) and (5.8). The measured transit speed (i.e. between injection and detection) was lower than the calculated transit speed in the main drainage channel ($\hat{v}_\mathrm{main}$) in both models as the minimum time spent to reach the main drainage channel was greater than zero (14 min, Eqn. 5.9).

5.6 Discussion

We infer from the steadily increasing transit speeds resulting from injections using M1 (Fig. 5.4a) that during the jökulhlaup in 2005, the glacial drainage system was in its transition phase from the winter to the summer regime (Chapter 2). This transition is a gradual process and progresses upglacier as temperatures rise (Hubbard and Nienow, 1997). Superimposed on the steady increase of transit speed was a maximum on 15 June 2005 in Phase III of the jökulhlaup. The transit speed of this maximum is 0.1 m s^{-1} larger than what would be expected from an uninterrupted steady increase of the transit speed. The maximum occured not at the time of highest lake discharge (Phase II), but when the lake had already drained (Phase III).

In 2007 the jökulhlaup had a greater impact on the results of the tracer experiments than in 2005. The injection into M2 on 13 July yielded a transit speed of $1.2\,\mathrm{m\,s^{-1}}$, twofold the transit speed of the injection two days before. Similarly, an increase from 0.6 to $1.1\,\mathrm{m\,s^{-1}}$ was observed in the experiments using M3. This greater influence is probably due to three factors. Firstly, the moulins M2 and M3 were situated closer to the likely drainage path of the lake than M1. Secondly, the jökulhlaup was larger in 2007 ($15\,\mathrm{m^3\,s^{-1}}$ peak outflow) than in 2005 ($10\,\mathrm{m^3\,s^{-1}}$). Thirdly, during the jökulhlaup in 2007 the drainage system was in a steady summer configuration, whereas the ongoing winter–summer transition of the drainage system in 2005 possibly masked the effects of the jökulhlaup. The timing of the maximum transit speed recorded from injections using M2 and M3 was similar to 2005; the maxima did not occur during peak lake discharge but afterwards. The transit speeds resulting from injections into M3 showed two maxima, the first one after the main lake discharge event and the second, larger one after the lake had drained completely.

In both 2005 and 2007, the maximum transit speed occurred after the lake has emptied (Phase III) and not during the peak of the jökulhlaup (Phase II). We explain this counterintuitive behaviour with tracer retardation inside the injection moulin. The effects of this so-called inflow modulation on the results of the experiment conducted using M1 (2005) were simulated with model runs Mod1 and Mod2 (Fig. 5.7). In both model runs, the calculated time to reach the main drainage channel t (Eqn. 5.7) was longer during Phases I and II of the jökulhlaup than before and after them (Fig. 5.7a,c), because the tracer was delayed due to the higher filling level of the moulin caused by the high subglacial water pressure. t increases enough during Phases I and II to mask the effects of the jökulhlaup on the measured transit speed, however, the calculated transit speed in the main drainage channel ($\hat{v}_{\mathrm{main}}$, Eqn. 5.8), increases during Phase I and in particular Phase II as would be expected (Fig. 5.7b,d). Note that for Mod1, $\hat{v}_{\mathrm{main}}$ at the end of Phase II and in Phase III were identical due to our fitting procedure in which we adjusted S_{m} such that the measured residence time difference between the 14 and 15 of June was attained. In reality, it is likely that the actual $\hat{v}_{\mathrm{main}}$ was lower on 15 June by following argument: The subglacial water pressure head in BH1 was 350 m on 14 June and 290 m on 15 June at 14:00. On both days, roughly the same discharge ($20\,\mathrm{m^3\,s^{-1}}$) was flowing at 14:00 in the main drainage channel, but on 15 June with a lower pressure differential. Hence, the main channel cross-sectional area must have been larger on 15 June to reduce frictional losses and this means that the flow speed in the main channel was lower on 15 June. Thus, our estimated S_{m} of Mod1 represents a lower bound on the moulin cross-sectional area. With Mod2 we investigated the influence of a 1.5 times larger S_{m} on $\hat{v}_{\mathrm{main}}$, showing a pronounced maximum of $\hat{v}_{\mathrm{main}}$ during the peak of the flood in Phase II (14 June, Fig. 5.7d) which is, according to above argument, more realistic. S_{m} used in Mod1 and Mod2 are reasonable estimates for a moulin operating over several years (like M1) and are comparable to the cross-sectional area at the top of the moulin Piccini et al. (2002) explored on Gornergletscher.

We do not have enough data to fit the other free parameters (l_{c} and n_{man}) of the model nor constrain the geometry of the moulin better. For this, injections over the whole diurnal discharge cycle (Schuler et al., 2004) and in particular during periods of low subglacial water pressure would be needed which would then give better bounds on $\hat{v}_{\mathrm{main}}$. Fitting l_{c} and n_{man} can pose additional problems, as is shown in the companion paper (Chapter 6).

The maximum $\hat{v}_{\mathrm{main}}$ was obtained by estimating the maximum t (Eqn. 5.10). Even this maximum transit speed $\hat{v}_{\mathrm{main}}$=$1.34\,\mathrm{m\,s^{-1}}$ is low compared to predictions of a jökulhlaup model applied to Gornergletscher. In the companion paper (Chapter 6), we ran Clarke's (2003) jökulhlaup model for the first 3 days of the 2006 outburst. At discharges of $18\,\mathrm{m^3\,s^{-1}}$ (the proglacial discharge measured at maximum $\hat{v}_{\mathrm{main}}$ on 14 June 2005 at the time of injection) the calculated flow speed is in the range of 2.0 to $3.5\,\mathrm{m\,s^{-1}}$, depending on the model parameters used. And even for discharges of $7\,\mathrm{m^3\,s^{-1}}$, corresponding to the lake discharge at the injection time, the range of calculated water flow speed was 1.6–$2.6\,\mathrm{m\,s^{-1}}$. The comparison, albeit rather crude as the model is not set up for the 2005 jökulhlaup, shows that the simulated flow speed is larger than the measured transit speed, concurring with the findings of the companion paper. This discrepancy can be due to a sinuous channel, an erroneous estimate of maximum t (Eqn. 5.10), or shortcomings of the jökulhlaup model.

Schuler et al. (2004) showed that the diurnal variability of transit speed (0.3–$0.8\,\mathrm{m\,s^{-1}}$) is due to changes in meltwater flux and can be as great as the variability we found during the jökulhlaups. Chapter 4 shows that most of this diurnal variability is due to the changing moulin discharge but that some is also due to the changing subglacial water pressure conditions. By injecting the dye always at the same time of the day, these conditions were kept as constant as possible for different injections, given the changing environment and boundary conditions inherent in all field experiments. This procedure made the results from different injections comparable to each other, however, some of the observed changes could also be due to these other factors and not the jökulhlaup. In 2005, during the presented injections using M1, the weather conditions were stable, apart from a colder 14 June and thus we think that our interpretation of the results is valid. In 2007, the weather was not as stable, however the doubling of transit speed is a very strong signal and thus it is likely that the jökulhlaup contributed significantly to this. Furthermore, only tracer experiments conducted using the same moulin should be directly compared to one another, as other tracer experiments (not presented here) showed that injections done at the same time of the day using different moulins can yield varying transit speeds of almost an order of magnitude Chapter 2. Aschwanden and Leibundgut (1982) conducted a tracer study during the jökulhlaup of Gornersee in 1979. They performed three injections: one before the jökulhlaup, one when the proglacial discharge reached its maximum and one just after. However, they injected at different times of the day using two different moulins and thus their results cannot be compared to ours.

During the jökulhlaup, an amount of water equal to half of the lake volume is temporarily stored within the glacier. It can be calculated by integrating the lake discharge minus the additional proglacial discharge due to the lake drainage (Huss et al., 2007). We have clear evidence for water storage processes from tracer experiments in both 2005 and 2007. On 12 June 2005, in Phase I of the jökulhlaup, the maximum dispersion D and the minimum fraction of mobile water β (Fig. 5.4b,c) was recorded. On this day very turbid water exited at the glacier terminus and Huss et al. (2007) report the onset of storage of lake water within the glacier. This concurrence of maximum D and minimum β was also observed in 2007 (injection into M3 on 10 July, Fig. 5.5g,h) during one of the intermittent subglacial discharge events in Phase II. Also in 2007, the injection into M3 on 9 July (Fig. 5.6b) resulted in a M of 0.1 compared to 0.35 throughout the rest of the jökulhlaup (Fig. 5.5i). The breakthrough curve of that experiment (Fig. 5.6) could not be fitted by the ASDM model but it was very broad and thus D was high. These observations suggest that water is stored at the glacier bed by spreading laterally from the channel outwards. This increases turbulent mixing, leading to a higher D, and large amounts of water can access regions which otherwise conduct little discharge and mobilise the sediment there, leading to turbid water. The water which is spread out laterally will flow slower and thus causes parts of the tracer to be delayed (lower β) and to be diluted to concentrations too low to detect (lower M).

5.7 Conclusions

To estimate water transit speed in the main subglacial drainage channel from tracer experiments, the whole flow path of the tracer must be taken into account. We showed that tracer retardation in the injection moulin can explain the low measured tracer transit speeds during the peak of the jökulhlaup. To arrive at main drainage channel transit speed estimates, it was necessary to make some assumptions on the moulin residence time of the tracer. These assumptions could be better constrained if tracer were injected more often, in particular at times of low subglacial water pressure. Our estimates of the main drainage channel transit speeds, where also the lake water flows, show that they are low compared to flow speed predictions of a jökulhlaup model. Water storage processes during jökulhlaups are important and our observations suggest that they are caused by lateral spreading of the water at the bed.

Part II

Modelling jökulhlaups

Chapter 6

Testing a jökulhlaup model against flow speeds inferred from measurements

Abstract Observational data allowing the validation of jökulhlaup models are sparse. We were able to inject dye tracer directly into the drainage channel of a glacial lake during the onset of its outburst. This made it possible to test an established jökulhlaup model, not only against discharge measurements, but for the first time also against water flow speeds inferred from measurements. We drive the jökulhlaup model, based on the Spring-Hutter equations, with measured subglacial water pressure, lake water temperature and lake level. The model is fitted to the measured lake discharge and inferred flow speeds using the initial channel size, the channel roughness and sinuosity. Our calculations show that an ingenuous application of the model, fitting it to the lake discharge only, overestimates water flow speeds. For the second day of the outburst, this can be remedied by fitting the model to the inferred flow speeds as well, requiring that either the heat transfer or the sinuosity of the channel be increased. However, the low inferred flow speeds on the first day of the outburst cannot be fitted with any parameter combination showing that, initially, the water does not flow through an R channel. Hence, the early stages of this jökulhlaup cannot be simulated by a R channel model.

6.1 Introduction

The simulation of jökulhlaups, also known as glacial lake outburst floods, has become a standard test case for channel flow models (e.g. Nye, 1976; Spring and Hutter, 1982; Clarke, 2003). Empirical results for validating the model outputs are often sparse consisting, for example, of the discharge data from the proglacial stream and the lake, sometimes the lake and outlet temperature are also measured. However, these measurements are not sufficient to constrain all the free parameters of jökulhlaup models. Recently, efforts have been made to collect more accurate and comprehensive data on glacial lake outburst floods: Anderson et al. (2003) on Kennicott Glacier, Alaska, and this study on Gornergletscher, Switzerland (Huss et al., 2007; Sugiyama et al., 2007, 2008; Walter et al., 2008, 2009).

The data we present were collected in 2006, when the ice marginal lake Gornersee drained via supraglacial overspill. However, the first 1.5 days of the drainage were very similar to an onset of a subglacial outburst flood: the drainage moulin was filled to its top because its capacity was not sufficient to carry all the supplied lake water. Thus pressurised flow conditions prevailed in the entire lake outlet channel during these 1.5 days. This *onset period* is the focus of the present investigation, during which we measured the flow speed of the lake water by means of direct tracer injections into the lake outlet. And thus, for the first time it is possible to compare water flow speeds simulated with a jökulhlaup model to direct measurements.

We present measurements of tracer transit speeds, subglacial water pressure head, lake and proglacial discharge, lake temperature and meteorological conditions. From the measured transit speeds we infer water flow speeds in the connection channel between the lake and the main subglacial drainage channel. These inferred speeds are compared to modelled ones calculated using Clarke's (2003) jökulhlaup model which is based on the Spring-Hutter equations (Spring and Hutter, 1982). The model is driven by the measured water pressure at both ends of the channel connecting the lake to the main drainage channel and calibrated against lake discharge and inferred water flow speeds. To fit the model to the inferred flow speeds, simulations are performed using a sinuous channel or an increased heat transfer.

In the accompanying Part I of this publication (Chapter 5), the focus lies on the influence of the jöklulhaups in 2005 and 2007 on the glacial drainage system as a whole, also using tracer experiments as the main tool of investigation. The outbursts in those two years proceeded subglacially and thus were shorter and more intense. In those years, we were not able to trace the lake water directly. Instead, moulins downglacier of the lake were used for injections giving us the opportunity to study the overall reaction of the glacial drainage system to a large perturbation.

6.2 Terminology

We need to elucidate a few concepts and define terms to make the description and discussion of the tracer experiments, the accompanying model and their comparison possible. We assume that tracer and water travel at the same velocity and thus the following definitions apply to both. We include a generic variable name in brackets, if it is used later. The definitions here are a slight generalisation of the ones used in the companion paper (Chapter 5).

The *flow path* is the path traversed by the tracer with the associated *flow path length* (l). The *residence time* (t) between two locations on the flow path is the time interval between the passage of the maximal tracer concentration at those locations. The *flow speed* (v) between those two locations is $v = l/t$, i.e. the flow path cross-section averaged speed. The *transit distance* is the shortest possible horizontal travel distance of the tracer between two locations and has an associated *transit path* (Fig. 5.1). The ratio of the residence time and transit distance gives the corresponding *transit speed* ($\hat{v}$).

This careful distinction is necessary as, with the presented field experiments, only the residence time, transit distance and speed can be determined, whereas theories of glacial hydraulics work with the flow path length and speed. Solely the residence time is applicable to both and thus care must be taken when comparing measurements to model results: in general, the transit distance is shorter than the flow path length due to the geometry and sinuosity of flow path and to the vertical distance covered, meaning that the transit speed is a lower bound on the average flow speed.

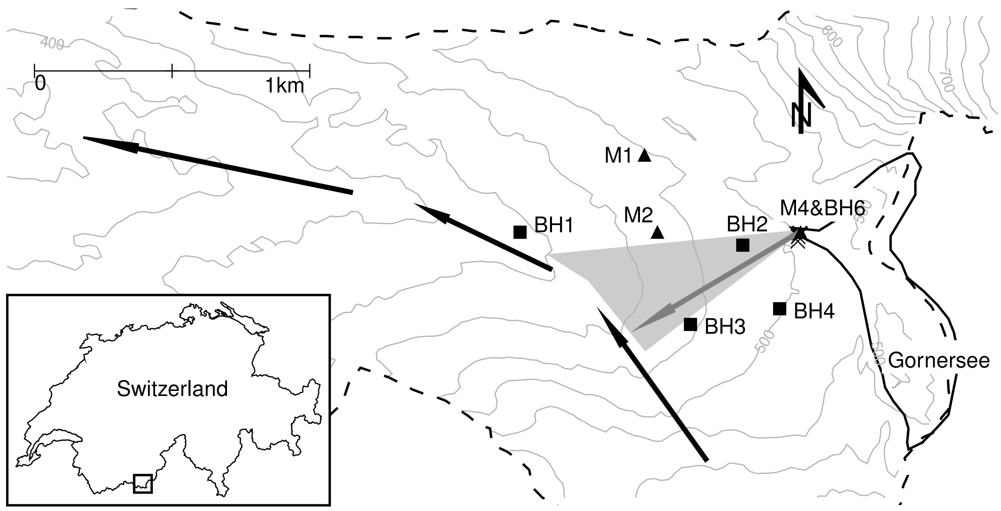

Figure 6.1: *Overview map of Gornergletscher. Contours of the hydraulic potential* $\phi = z_\mathrm{b} + f_\mathrm{float}\,\rho_\mathrm{i}/\rho_\mathrm{w}(z_\mathrm{s} - z_\mathrm{b})$ *are plotted, where* z_b *and* z_s *are the bed and surface elevation, respectively,* ρ_i *and* ρ_w *the densities of ice and water, and* f_float *the fraction of the water to ice overburden pressure, set to 0.9 (Flowers and Clarke, 1999).* z_s *was obtained from photogrammtery and* z_b *from radar measurements (Sugiyama et al., 2008). The black arrows indicate a likely location for the main drainage channel. The grey arrow shows a possible location of the connection channel from the lake to the main channel, and the grey shaded area indicates the range of possible connection channel locations considered. Moulins (triangles), boreholes (squares), lake border (solid line), glacier border (dashed line), maximal lake extent (dashed line) and active seismics shots (crosses) are also marked.*

6.3 Field site and methods

Intensive field measurements on Gornergletscher were conducted in the years 2004 to 2008 in order to investigate the jökulhlaups of Gornersee. Gornergletscher, Switzerland, is the second largest glacier in the Alps ($\sim$60 km^2, 4600–2200 m a.s.l., 14 km long). Gornersee is an ice marginal lake situated in the confluence area of the two main tributaries of Gornergletscher (Fig. 6.1). Gornersee has a volume of about 4×10^6 m^3 and usually drains as a subglacial outburst flood over the course of 2–7 days at the beginning of summer. The lake is located at an elevation of 2530 m a.s.l. and lies 6.5 km upglacier from the terminus. The maximal ice thickness of 450 m is found 1 km downglacier of the lake. The field site is described in more detail in Chapter 5 and Huss et al. (2007).

6.3.1 Field methods and data processing

The fluorescent dyes Uranine and Rhodamine WT were used for the injections. The detection was performed at the gauging station of Grande Dixence SA, 1.25 km below the terminus of the glacier where proglacial discharge was measured. The dye was monitored continuously with a flow-through and a submersible fluorometer. We present a total of eleven dye injections which were conducted into the lake drainage moulin in the morning (8:30, CEST, UTC+2), early afternoon (14:00) and evening (21:00) between 28 June and 18 July 2006. The diurnal variability of tracer experiments conducted using the same moulin can be large (Schuler et al., 2004) to minimise the influence of such effects only experiments conducted during the same time of the day were compared directly.

We present the tracer transit speed and to characterise the breakthrough curves, an advection-dispersion model with storage (ADSM) was fitted to them (Toride et al., 1999). See Schuler et al. (2004) for a glaciological application of this model. The ADSM takes as input the concentration time series and the transit distance. The ADSM returns estimates of the mean tracer transit speed (not presented), the dispersion D, the fraction of mobile water β and the exchange coefficient between mobile and immobile water (not presented). All the breakthrough curves considered in this paper were fitted accurately by the ADSM, and are thus fully described by these parameters. Furthermore, the fraction of returned tracer mass M is obtained by integrating the tracer concentration multiplied by the proglacial discharge and divided by the injected tracer mass.

In this paper we are interested in the time the tracer spends within the glacier, the *glacial residence time*. Hence it is important to estimate the *proglacial residence time*, i.e., the time spent in the proglacial stream. Eighteen injections were conducted in the proglacial stream at different discharge levels throughout the field campaign. To the resulting proglacial transit speeds we fitted the expression

$$\hat{v}_{\mathrm{pro}} = k(Q - Q_0)^e, \tag{6.1}$$

with a least-square regression. The parameters were estimated to be $k = 0.66\,\mathrm{m}^{1-3e}\,\mathrm{s}^{e-1}$, $Q_0 = 6.4\,\mathrm{m}^3\,\mathrm{s}^{-1}$, $e = 0.34$ with a coefficient of determination (R^2) of 0.8. The zero proglacial transit speed limit as $Q \to 6.4\,m^3\,s^{-1}$ is unphysical but the proglacial discharges relevant here are all above $Q = 10\,m^3\,s^{-1}$. From the fit of Equation (6.1) to the data we estimated the error in the calculated proglacial residence time to about 30%. The measurement error on the (total) residence time was $<1\%$. This led to a 4% error in the calculated glacial residence time because the proglacial residence time was around ten times shorter than the total residence time. The ADSM parameters were not corrected for possible influences of the proglacial stream.

Subglacial water pressure data were obtained from pressure transducers (Gekon 4500) installed in boreholes drilled to the bed (labelled BH1–BH4 and BH6 in Fig. 6.1). The lake level was monitored with a pressure transducer (Keller DX series). Lake discharge was determined from measurements of the channel cross section and of the water flow speed (with a current meter Schiltknecht MiniWater20) and the error was estimated to be 10%. The measured discharge agreed well with the independent estimate derived from lake level, bathymetry and water input into the lake calculated with a melt model (using the method of Huss et al., 2007). A thermistor was immersed into the lake water directly at M4 to measure the temperature. The air temperature and precipitation were measured at an automatic weather station located off-ice at the northern glacier margin (Fig. 5.1). . To determine the geometry of the moulin shaft of M4, active source seismology was conducted two weeks after the presented tracer experiments by lowering explosives into M4. The detonations were detected on the seismic network (Walter et al., 2008) installed in the vicinity, on the glacier (personal communication, Fabian Walter, 2008).

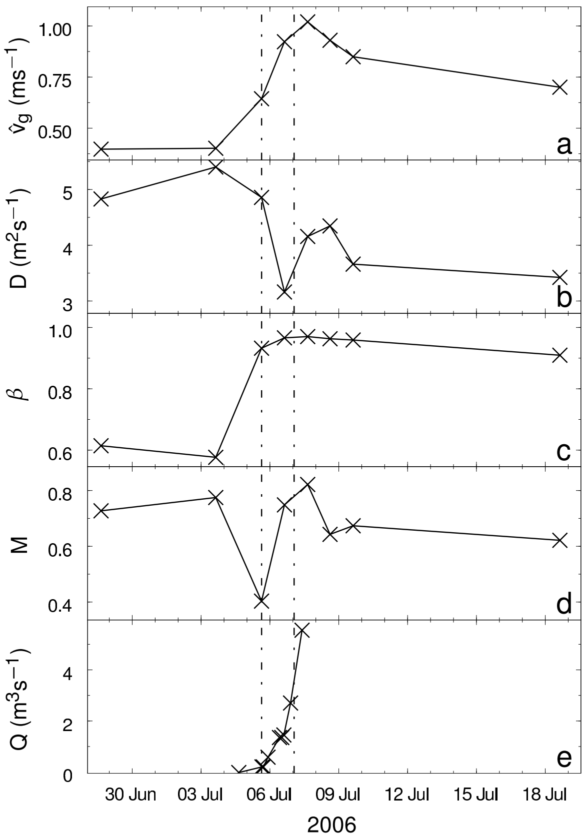

Figure 6.2: *(a) Glacial transit speed $\hat{v}_{\rm g}$, (b) ADSM parameters dispersion D, (c) the fraction of mobile water β, and (d) the fraction of recovered tracer mass M from injections done at 14:00 into M4; (e) lake discharge into M4. The two vertical lines delimit the* onset period *(of the lake drainage, 5 July 14:00–6 July 24:00): the 1.5 days during which pressurised channel flow conditions prevailed in the moulin.*

6.4 Observations

In 2006, Gornersee filled until its shore reached the moulin M4 (Fig. 6.1). Prior to the lake drainage, M4 had a diameter of 0.5 m and carried a maximal discharge of $<0.1\,\mathrm{m^3\,s^{-1}}$. Once the lake shore reached M4, the lake started draining into the moulin. The water level in M4 was equal to the lake level during the first 1.5 days of the lake drainage (henceforth called *onset period*), which lasted from 5 July 14:00 to 6 July 24:00. During the onset period, the lake discharge into the moulin increased from around $0.1\,\mathrm{m^3\,s^{-1}}$ to $3.5\,\mathrm{m^3\,s^{-1}}$ (Fig. 6.2e). At the end of the onset period, M4 had adjusted its capacity and its water level dropped, thus the lake discharge became limited by the height of the spillway. This terminated the onset period, the time during which the lake outlet was fully pressurised. Subsequently, the lake lowered its level by incising a canyon into the ice (Raymond and Nolan, 2000), it subsided slightly more than $1\,\mathrm{m\,d^{-1}}$ and lake discharge was in the range of 2–5 $\mathrm{m^3\,s^{-1}}$. It took about three weeks to empty the lake which initially contained about $4\times10^6\mathrm{m^3}$ of water. At the end of the lake drainage, the canyon was ∼200 m long, ∼5 m wide and up to 50 m deep; the diameter of M4 reached ∼10 m.

In contrast to a subglacial lake drainage, the lake outlet (M4) was accessible and we used it for tracer injections and direct discharge measurements; the results are shown in Figure 6.2. The

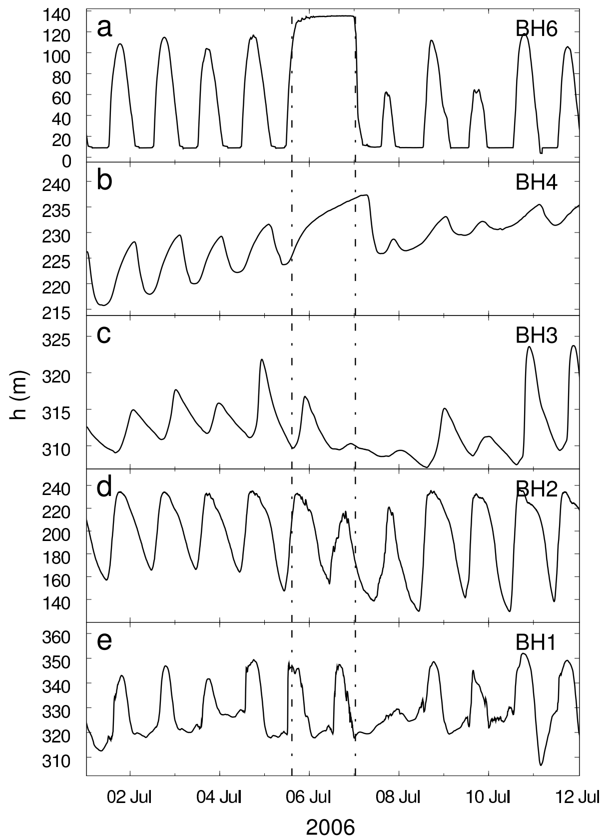

Figure 6.3: *Subglacial water pressure head measured in boreholes in the vicinity of the lake and connection channel. The two vertical lines delimit the onset period.*

glacial transit speed was steady at 0.4 m s^{-1} for a week before the onset period and, during that time, the other ADSM parameters and M did not fluctuate significantly either. At the beginning of the onset period, glacial transit speed increased to 0.65 m s^{-1} and the fraction of mobile water β increased, whereas the fraction of returned tracer mass M dropped from 0.8 to 0.4. Towards the end of the onset period, lake discharge had increased to 3 m^3 s^{-1} and glacial transit speed to 0.95 m s^{-1}, accompanied by a sharp drop in dispersion D. The lake discharge reached $\sim$5.5 m^3 s^{-1} the day after the onset period. At the same time the glacial transit speed reached its maximum of 1.05 m s^{-1} and then decreased to values in the range of 0.9-0.7 m s^{-1}, typical for a well-developed moulin on Gornergletscher (Chapter 2).

Figure 6.3 shows the subglacial water pressure heads of five boreholes. BH6, located 50 m from M4, responded strongly to the lake drainage: its water level stayed high throughout the onset period, and afterwards it fluctuated again diurnally. BH4 is 400 m south and upstream of M4 and also responded strongly. Note that the decrease in water pressure was delayed by 8 hours as compared to BH6. The water pressure in boreholes BH1, BH2 and BH3 did not react to the lake drainage. In contrast, when the lake drained as a subglacial outburst flood a response could be seen for several days in all these boreholes (Chapter 5 and Huss et al. (2007)).

Figure 6.4 presents complementary measurements around the onset period. The water exiting the lake was 2°C on the first day of the onset period, then dropped to 0.8°C during the night and rose to 1°C on the second day of the onset period (Fig. 6.4b). Figure 6.4d shows subglacial

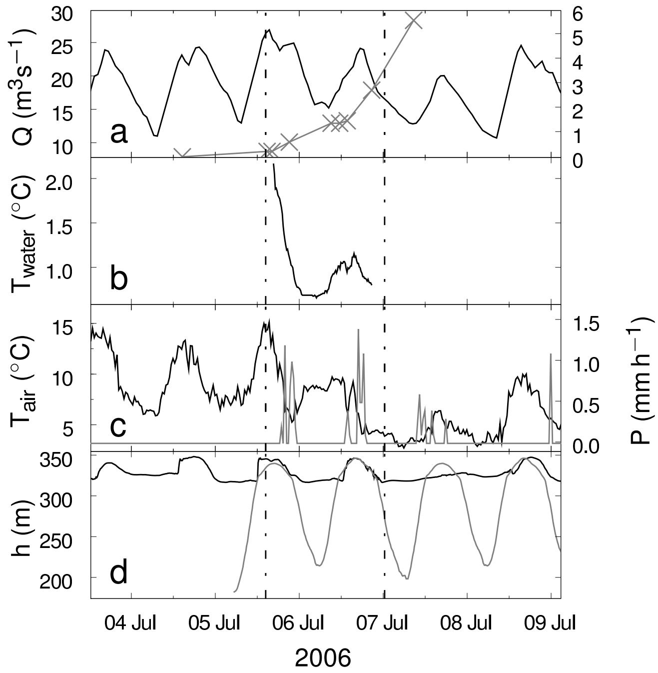

Figure 6.4: *a) Proglacial discharge (black, left scale), lake discharge (grey, right scale) b) temperature of water entering M4 c) air temperature (black) and precipitation (grey) d) pressure head in borehole BH1: (black line are the data from 2006, grey line are data from 2005). The two vertical lines delimit the onset period.*

water pressure head data from BH1 in 2006 (black line, also shown in Fig. 6.3e) and data, also from BH1 (grey line), but from the year 2005. The peak-to-peak amplitude of the diurnal water pressure head fluctuations in BH1 were 25 m in 2006 and 150 m in 2005. Note that the water pressure head in 2006 stayed level at about 325 m during the time of low pressure and then increased during the day. The rain events on 5 and 6 July (Fig. 6.4c) can be recognised in the proglacial discharge and in BH1 and BH2. The colder temperature on 7 July led to lower proglacial discharge and a drop in water pressure in BH1 and BH3.

6.5 Jökulhlaup model

We compare flow speeds inferred from tracer experiments with water flow speeds calculated with Clarke's (2003) model. So far this model has been calibrated only using lake and proglacial discharge hydrographs. Thus this study presents the first chance to test this model more stringently by comparing it to inferred water flow speeds and not only to the lake discharge.

6.5.1 Model formulation

Clarke's (2003) jökulhlaup model integrates a modified version of the Spring-Hutter equations (Spring and Hutter, 1982) which describe water flow through R channels (c.f. next Section). These R channels (Röthlisberger, 1972) are en- or subglacial circular or semi-circular channels incised into the ice. These equations describe the time evolution of water pressure, channel cross section, water flow speed and water temperature. The Spring-Hutter equations contain several empirical relations, two of which are of interest here, firstly, the relation between pressure gradient and water flow speed and secondly, the heat transfer relation.

The Manning–Gauckler–Strickler formula relates water flow speed v to hydraulic head gradient $\frac{\mathrm{d}H}{\mathrm{d}s}$

$$v = \frac{1}{n_{\mathrm{man}}} R_{\mathrm{h}}^{\frac{2}{3}} \sqrt{\frac{\mathrm{d}H}{\mathrm{d}s}}, \tag{6.2}$$

where n_{man} is the Manning roughness, s is the along channel coordinate and R_{h} is the hydraulic radius defined by

$$R_{\mathrm{h}} = S P_{\mathrm{w}}^{-1} \tag{6.3}$$

where S is the cross-sectional area of the channel and P_{w} is the wetted perimeter (see Section 2.3.2 for an in-depth description of the channel geometry). The Manning roughness is one of the tuning parameters of the model. The same average roughness is used for englacial and subglacial channels. Reasonable values of n_{man} lie in the range $0.02\,\mathrm{m}^{-1/3}\,\mathrm{s} < n_{\mathrm{man}} < 0.08\,\mathrm{m}^{-1/3}\,\mathrm{s}$. (e.g. Clarke, 2003).

The amount of melted ice m at the conduit walls per unit length is proportional to the temperature difference between ice and water ΔT

$$U_{\mathrm{h}} \Delta T = mL, \tag{6.4}$$

where L is the latent heat of fusion and U_{h} is the heat transfer coefficient. The model uses the following empirical relation (McAdams, 1951)

$$U_{\mathrm{h}} = 0.023\,\kappa\, Re^{\frac{4}{5}}\, Pr^{\frac{2}{5}} \frac{P_{\mathrm{m}}}{4R_{\mathrm{h}}}, \tag{6.5}$$

where Re is the Reynolds number, Pr is the Prandtl number, κ is the thermal conductivity of water and P_{m} is the ice-walled perimeter of the conduit. For a list of alternative heat transfer relations see Bird et al. (1960).

As input the model needs the geometry of the connection channel and the thickness of the overlying ice. Channels of different sinuosities σ are implemented in the model by stretching the along channel coordinate s by σ. The boundary conditions at the inlet are the water level and the water temperature. At the outlet the water pressure is needed as a boundary condition. Clarke's (2003) code has been modified such that the water level at the outlet (normally used to simulate a jökulhlaup which terminates underwater) can be a function of time. The fitting parameters are the initial cross-sectional area of the connection channel c_0, its sinuosity σ and its roughness n_{man}. The model was fitted to the lake discharge and for some runs also to the inferred water flow speeds using first a grid search on the tuning parameters (n_{man}, σ, c_0) and a subsequent steepest descent method.

6.5.2 Governing equations

The governing equations of the model are summarised here, for a more in-depth presentation refer to Clarke (2003). The equations describe the time evolution of the water pressure p_{w}, the channel cross section S, the water flow speed v and water temperature T_{w}. The spatial coordinate s is the along flow path length of the channel.

$$\frac{\partial p_{\mathrm{w}}}{\partial t} = -\frac{1}{\beta S}\left(\frac{\partial S}{\partial t} + \frac{\partial}{\partial s}(vS) - \frac{m}{\rho_{\mathrm{w}}}\right) \tag{6.6}$$

$$\frac{\partial S}{\partial t} = \frac{m}{\rho_{\mathrm{i}}} - 2\,\mathrm{sgn}(p_{\mathrm{e}})\left(\frac{|p_{\mathrm{e}}|}{nB}\right)^{n} S \tag{6.7}$$

$$\frac{\partial v}{\partial t} = -\frac{\partial}{\partial s}\left(\frac{1}{2}v^2 + \frac{p_{\mathrm{w}}}{\rho_{\mathrm{w}}} + gZ_{\mathrm{k}}\right) - \frac{1}{\rho_{\mathrm{w}} S}(mv + P_{\mathrm{w}}\tau_0) \tag{6.8}$$

$$\frac{\partial T_{\mathrm{w}}}{\partial t} = -v\,\frac{\partial T_{\mathrm{w}}}{\partial s} + \frac{1}{\rho_{\mathrm{w}} c_{\mathrm{w}} S}\left(P_{\mathrm{w}}\tau_0 v - m\left(L + c_{\mathrm{w}}(T_{\mathrm{w}} - T_{\mathrm{i}}) - \frac{v^2}{2}\right)\right) \tag{6.9}$$

where

$$p_{\mathrm{i}} = \rho_{\mathrm{i}} g(Z_{\mathrm{i}} - Z_{\mathrm{k}}) \tag{6.10}$$

$$p_{\mathrm{e}} = p_{\mathrm{i}} - p_{\mathrm{w}} \tag{6.11}$$

$$T_{\mathrm{i}} = -c_{\mathrm{T}} p_{\mathrm{w}} \tag{6.12}$$

$$Q = vS \tag{6.13}$$

$$\tau_0 = g\, {n_{\mathrm{man}}}^2 R_{\mathrm{H}}^{-1/3} \rho_{\mathrm{w}}\, v|v| \tag{6.14}$$

$$\mathrm{Re} = 4\rho_{\mathrm{w}}|v|R_{\mathrm{H}}/\mu_{\mathrm{w}} \tag{6.15}$$

$$\mathrm{Pr} = \mu_{\mathrm{w}} c_{\mathrm{w}}/\kappa \tag{6.16}$$

$$\mathrm{Nu} = 0.023\,\mathrm{Re}^{4/5}\mathrm{Pr}^{2/5} \tag{6.17}$$

$$m = P_{\mathrm{m}}\kappa \mathrm{Nu}(T_{\mathrm{w}} - T_{\mathrm{i}})/4LR_{\mathrm{H}} = P_{\mathrm{m}} U_{\mathrm{h}}(T_{\mathrm{w}} - T_{\mathrm{i}})/4LR_{\mathrm{H}} \tag{6.18}$$

Refer to Table 6.1 for a compilation of model parameters. Note that Equation (6.2) is equivalent to Equations (6.8) and (6.14) if the acceleration and kinetic energy terms are neglected in Equation (6.8).

The channel has either a circular or semi-circular geometry which leads to the following relations for the wetted perimeter P_{w}

$$P_{\mathrm{w}} = \begin{cases} 2\pi R & \text{circle} \\ (\pi + 2)R & \text{semi-circle} \end{cases} \tag{6.19}$$

and cross-sectional area

$$S = \begin{cases} \pi R^2 & \text{circle} \\ \frac{1}{2}\pi R^2 & \text{semi-circle} \end{cases} \tag{6.20}$$

Furthermore, the melting perimeter P_{m} of the conduit is defined as the part of the conduit perimeter that is ice-walled and subject to melting

$$P_{\mathrm{m}} = \begin{cases} 2\pi R & \text{ice-walled circular conduit} \\ \pi R & \text{rock-floored semi-circular conduit.} \end{cases} \tag{6.21}$$

The boundary conditions are the water pressure at the channel inlet and outlet and the water temperature at the inlet as discussed in Section 6.5.5.

6.5.3 Connection channel location

Only the *connection channel*, connecting the lake to the main drainage channel of the glacier, is subjected to a jökulhlaup-like evolution (grey arrow in Figure 6.1) and hence can be simulated using Clarke's (2003) model. We consider a connection channel transit path lying in the

Table 6.1: *Model parameters and constants*

Parameter	Description, value and units
B	coefficient in Glen's flow law (5.28×10^7 Pa s$^{1/n}$)
c_T	pressure melting coefficent for ice (7.5×10^{-8} K Pa^{-1})
c_w	specific heat capacity of water (4217.7 J kg^{-1} K^{-1})
g	gravity acceleration (9.80 m s^{-2})
H	hydraulic head, $H = p_\mathrm{w}/(\rho_\mathrm{w} g) + z$ (m)
L	latent heat of melting for ice (3.335×10^5 J kg^{-1})
m	mass rate of melting per unit length of conduit (kg m^{-1} s^{-1})
Nu	Nusselt number
n	exponent of Glen's flow law (3)
n_man	Manning roughness (m$^{-1/3}$ s)
P_m	melting perimeter of conduit (m)
P_w	wetted perimeter of conduit (m)
Pr	Prandtl number
p_e	effective pressure (Pa)
p_i	ice overburden pressure (Pa)
p_w	water pressure (Pa)
Q	discharge through the conduit (m^3 s^{-1})
q	heat flux (W m^{-2})
R	conduit radius (m)
R_H	hydraulic radius of conduit (m)
Re	Reynolds number
S	cross-sectional area of drainage conduit (m^2)
s	downflow distance measured from conduit inlet (m) (flow path length)
T_i	ice temperature (C)
T_lake	lake temperature (C)
T_w	water temperature (C)
t	time (s)
U_h	empirical heat transfer coefficient (W m^{-2} K^{-1})
v	cross-sectionally averaged water velocity (m s^{-1})
Z_b	elevation of bed surface above datum (m)
Z_i	elevation of ice surface above datum (m)
Z_k	elevation of conduit above datum (m)
z	elevation above datum (m)
β	fluid compressibility (Pa^{-1})
κ	thermal conductivity of water (0.558 W m^{-1} K^{-1})
μ_w	viscosity of water (1.787×10^{-3} Pa s)
ρ_i	density of ice (900 kg m^{-3})
ρ_w	density of water (1000 kg m^{-3})
τ_0	wall stress exerted by turbulent flow (Pa)

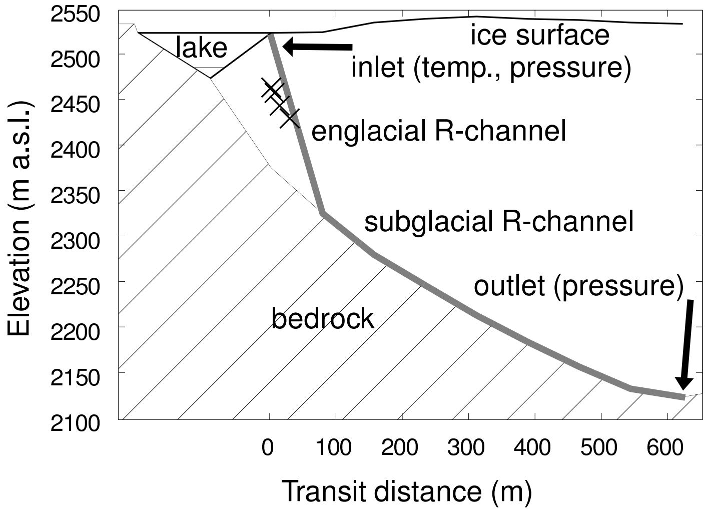

Figure 6.5: *A cross section of the glacier with the assumed connection channel in grey. The crosses indicate locations of active seismic shots conducted inside M4. The boundary conditions needed at the inlet and outlet are given in brackets.*

region of the grey shaded area in Figure 6.1. The reasons to restrict it to this area are: Tracer experiments from both M2 and M1 (Fig. 6.1) showed only a modest response to the subglacial outburst floods in 2005 and 2007 (Chapter 5), hence connection channels lying north of M2 are not considered. The response of BH4 during the onset period can be explained by a flow direction in the lake dam area parallel to the crevasse orientation, as was also determined by tracer experiments (Chapter 3). The direction of the crevasses is north-south and BH4 lies upstream of M4. Borehole BH3 did not show a response either, so connection channels south of BH3 are not considered either, which would also grossly disagree with the direction of steepest descent of the hydraulic potential. Borehole BH2 also does not show a response, which is puzzling as it lies in the middle of the region of possible transit paths. The active source seismology (conducted by lowering explosives into M4) showed that the moulin/channel shaft drops very steeply (crosses on Figures 6.1 and 6.5 mark shot locations) and is orientated slightly southwards, suggesting that the connection channel lies south of BH2. A connection channel lying in the grey shaded area (Fig. 6.1) has a transit distance of $625\,\mathrm{m} < \hat{l}_{\mathrm{con}} < 1000\,\mathrm{m}$.

The geometry of the channel in the vertical is depicted in Figure 6.5 which shows a cross section of the glacier along the connection channel. We assume that the channel drops steeply englacially, as supported by the active source seismology, to reach the bed and then follows it. The length along the connection channel, having a transit distance $\hat{l}_{\mathrm{con}} = 625\,\mathrm{m}$, is $l_{\mathrm{con}} = 790\,\mathrm{m}$. The vertical geometry of channels lying in the grey shaded area is very similar and thus their geometry can be adjusted to different transit distances by stretching it in the horizontal. This leads to a range of $790\,\mathrm{m} < l_{\mathrm{con}} < 1120\,\mathrm{m}$. To finally arrive at the channel flow path length, we assume the connection channel sinuosity to be constrained by $1 \leq \sigma < 2$. We absorb above range of l_{con} into the sinuosity, fix $l_{\mathrm{con}} = 790\,\mathrm{m}$ and vary the $1 < \sigma < 2.8$, of which a factor of up to 1.4 can be due to different connection channel transit paths.

6.5.4 Flow speed estimate

An estimate must be made of the tracer flow speed in the connection channel in order to be able to compare the water flow speeds from the model with the experimental data. We divide the total residence time t^i_{tot}, i.e. the time the tracer took in experiment i to reach the detection station, into the sum of three parts: the proglacial residence time (t^i_{pro}), the main channel residence time (t^i_{main}) and the connection channel residence time (t^i_{con}):

$$t^i_{\mathrm{con}} = t^i_{\mathrm{tot}} - t^i_{\mathrm{pro}} - t^i_{\mathrm{main}}, \tag{6.22}$$

where t^i_{tot} was measured and t^i_{pro} can be determined from Equation (6.1). t^i_{main} is unknown but must be greater than 0 to assure a finite flow speed in the main channel. To get an upper bound on t^i_{main}, we assume that t^i_{main} does not change much due to the additional lake water influx and due to changing meltwater discharge conditions from day to day, as suggested by the constant amplitude and mean of the proglacial discharge (Fig. 6.4a). Hence an upper bound for t^i_{main} is the shortest measured glacial residence time

$$t^i_{\mathrm{shortest}} = \min(t^i_{\mathrm{tot}} - t^i_{\mathrm{pro}}), \tag{6.23}$$

where the experiments conducted in the morning, early afternoon and evening are treated separately, i.e., a different t_{shortest} is obtained for each time of the day. All of them achieved the shortest glacial residence time on 7 July, the day after the onset period. The t_{shortest} for morning, early afternoon and evening correspond to main channel transit speeds of 0.65, 0.86 and 0.79 $\mathrm{m\,s^{-1}}$, respectively.

The inequality on t^i_{main}

$$0 < t^i_{\mathrm{main}} < t^i_{\mathrm{shortest}} \tag{6.24}$$

together with Equation (6.22) leads to upper and lower bounds for t^i_{con}

$$t^i_{\mathrm{tot}} - t^i_{\mathrm{pro}} - t_{\mathrm{shortest}} < t^i_{\mathrm{con}} < t^i_{\mathrm{tot}} - t^i_{\mathrm{pro}} - 0. \tag{6.25}$$

These bounds on t^i_{con} rest only on the assumption that t^i_{main} does not exceed t_{shortest}. To translate this into flow speed bounds which can be compared to Clarke's (2003) model, an assumption on the connection channel flow path length needs to be made as discussed in the previous section

$$\frac{\sigma\, l_{\mathrm{con}}}{t^i_{\mathrm{tot}} - t^i_{\mathrm{pro}} - t_{\mathrm{shortest}}} > v^i_{\mathrm{con}} > \frac{\sigma\, l_{\mathrm{con}}}{t^i_{\mathrm{tot}} - t^i_{\mathrm{pro}}}. \tag{6.26}$$

The v^i_{con} will be referred to as *inferred flow speeds* or *flow speed bounds*. Note that the flow speed bounds depend on the sinuosity σ.

6.5.5 Model setup

The model is run with the channel geometry discussed above (Fig. 6.5). The channel cross section is set to circular for the englacial part and to semi-circular for the subglacial part. To have fewer free parameters, we use an average Manning roughness and do not distinguish between the roughness of the ice walls and the glacier bed. The boundary conditions at the channel inlet are the measured water temperature (Fig. 6.4b) and lake level, which was constant during the onset period. At the channel outlet we use the water pressure measured in borehole BH1 and also data from the same borehole but from the previous year 2005, as the borehole was not so well connected in 2006 (Fig. 6.4c).

Four different model runs (Mod1–Mod4) are used to investigate the influence of different boundary conditions, physics and fitting procedures. We tune the model Mod1 to the lake

Table 6.2: *Summary of the settings and results (n_{man}, σ and c_0) for the model runs Mod1–Mod4.*

Model run	Fitting parameters	Fitting to	BH data year	Enhanced heat transfer	n_{man} ($\mathrm{m}^{-1/3}\,\mathrm{s}$)	σ ()	c_0 (m^2)
Mod1	n_{man}, c_0	Q	2006	no	0.071	1.00	0.38
Mod2	n_{man}, c_0, σ	Q, v_{con}	2006	no	0.049	1.43	0.37
Mod3	n_{man}, c_0, σ	Q, v_{con}	2005	no	0.046	1.86	0.39
Mod4	n_{man}, c_0, σ	Q, v_{con}	2006	yes	0.105	1.00	0.61

discharge only and Mod2–Mod4 also to the inferred flow speeds. The tuning parameters are the Manning roughness n_{man}, the initial channel size c_0 and for Mod2–Mod4 also the sinuosity σ.

It is found that the modelled flow speeds in Mod1 are higher than the inferred ones. If the sinuosity is increased, the inferred flow speed also increases, which is simulated in Mod2 and Mod3. Another possibility is to lower the modelled flow speeds. For pressurised channel flow the discharge is equal to the flow speed times the channel cross-sectional area. Hence, to decrease the flow speed for a given discharge the cross-sectional area needs to be larger. This can be achieved by increasing melt of the channel walls (i.e., the heat transfer) or by reducing creep closure. It turns out that creep closure can be neglected in these settings as the high water pressure prevents it. This leaves the heat transfer, which is increased by a factor of 2 in Mod4. Table 6.2 gives a summary of the four model runs performed.

6.6 Model results

Mod1 (Fig. 6.6a,b) is fitted to the lake discharge using n_{man} and c_0 as tuning parameters and setting $\sigma = 1$. The roughness is high at $n_{\mathrm{man}} = 0.071\,\mathrm{m}^{-1/3}\,\mathrm{s}$. The lake discharge fits the measurements well but the model speeds are about 0.55 and 0.25 $\mathrm{m\,s}^{-1}$ too high on the first and second day of the onset period, respectively.

Mod2 (Fig. 6.6c,d) is fitted to both Q and v_{con} using all three tuning parameters (n_{man}, c_0 and σ). The model fits the inferred flow speeds of the second day well, but not the ones of the first day (0.5 $\mathrm{m\,s}^{-1}$ difference). Mod2 has, compared to Mod1, a larger sinuosity and roughness of 1.43 and $0.049\,\mathrm{m}^{-1/3}$ s, respectively. Note that, due to the larger sinuosity, the upper flow speed bounds estimated by Equation (6.26) become greater than for Mod1.

Mod3 (Fig. 6.6e,f) is fitted like Mod2 but uses 2005 subglacial water pressure data as a lower boundary condition. The modelled discharge has larger diurnal fluctuations and fits less well, in particular, its increase at the end of the onset period is far steeper than that of the measurements. Also, the pronounced modelled flow speed peak in the morning of the second day cannot be seen in the inferred flow speeds. The modelled flow speeds are $0.4\,\mathrm{m\,s}^{-1}$ too high on the first day and lie within the flow speed bounds on the second day. The roughness is comparable to Mod2 whereas the sinuosity is greater (1.86).

Mod4 (Fig. 6.6g,h) is run with a two fold increased heat transfer. It is fitted to both Q and v_{con} using n_{man}, σ and c_0. The modelled flow speeds are lower than in the other models and fit well on the second day but are still $0.3\,\mathrm{m\,s}^{-1}$ too high on the first day. The Manning roughness $n_{\mathrm{man}} = 0.105\,\mathrm{m}^{-1/3}$ s is large and the sinuosity is fitted to 1.00.

The time evolution to 1.5 days beyond the onset period of the modelled discharges, flow speeds and outlet water temperatures is shown in Figure 6.7. The modelled discharges Q diverge and

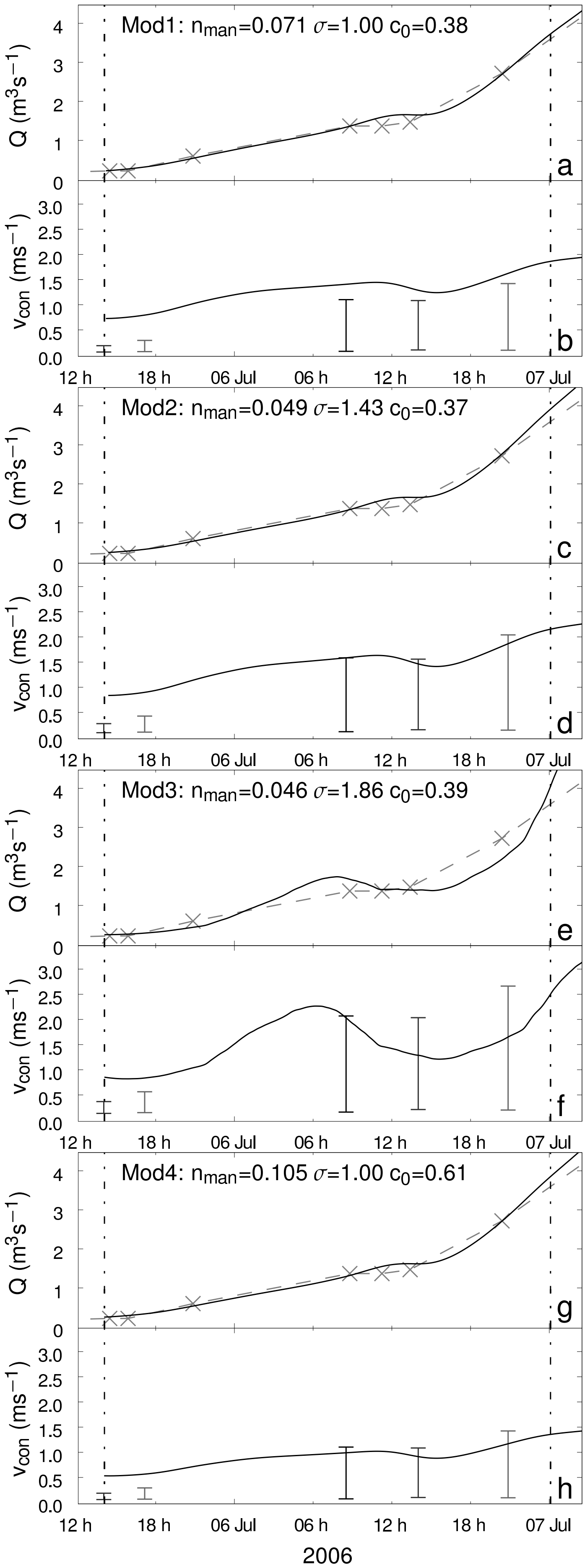

Figure 6.6: *Results of model runs Mod1–Mod4, top panels show the modelled discharge Q (solid line) and measured discharge (crosses); bottom panels show modelled flow speeds v_{con} (solid lines) and inferred flow speeds bounds (bars). The legend gives the model name, the Manning roughness n_{man}, the sinuosity σ and the initial channel cross section c_0 of each model run. The dashed lines delimit the onset period. a,b) Mod1 fitting only the discharge; c,d) Mod2 also fitting the inferred flow speeds; e,f) Mod3 using subglacial water pressure data from 2005 with higher diurnal variations; g,h) Mod4 using enhanced heat transfer (c.f. Table 6.2).*

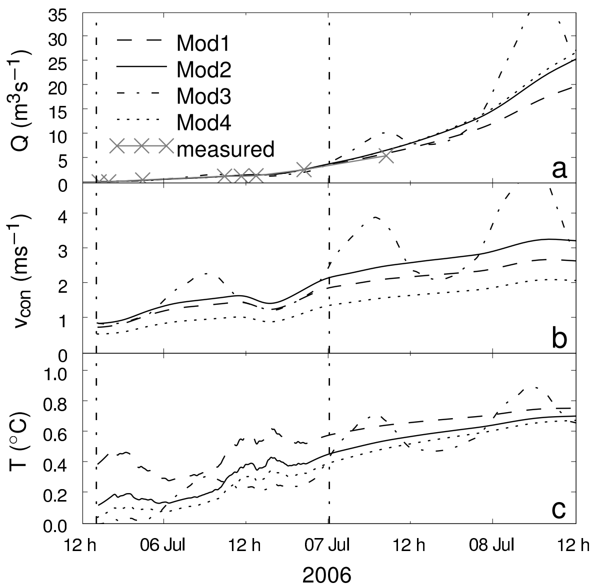

Figure 6.7: *The simulated jökulhlaup evolution up to 1.5 days beyond the onset period of Mod1–Mod4. a) lake discharge Q (measured discharges are marked with crosses); b) flow speed v_{con}; c) water temperature at the connection channel outlet T.*

reach 20–28 $\mathrm{m^3\,s^{-1}}$ in the end. The modelled flow speeds v_{con} are between 2.2 (Mod4) and 3.4 $\mathrm{m\,s^{-1}}$ (Mod2). The connection channel outlet water temperature are all within 0.1°C of each other. The output of Mod3 exhibits much larger fluctuations due to the larger pressure fluctuation at its outlet. Note that these model results cannot be compared to measurements, as the lake drainage was spillway limited after the onset period. This means that the water flow inside the moulin was partly open channel flow whereas the model only works for fully pressurised flow conditions.

The comparison of measured lake discharge data and inferred tracer flow speeds to results obtained with Clarke's (2003) model shows that:

- Fitting the model only to the lake discharge using the shortest possible connection channel yields model speeds that are too large and a high Manning roughness (Mod1).
- The model can be fitted to the inferred flow speeds on the second day with a higher sinuosity (or a longer connection channel).
- Alternatively, the model speeds can be fitted to the inferred ones by enhancing the heat transfer. This leads to a very high Manning roughness (Mod4).
- It is not possible to discriminate between Mod2 and Mod4 on the basis of the presented experimental data.
- The low inferred flow speeds on the first day cannot be modelled by any parameter combination that would give a reasonable fit on the second day.
- All the modelled flow speeds are either higher than or near the upper end of the experimental bounds.
- Mod3, using the subglacial water pressure recorded in 2005 as lower boundary condition, results in a poorer fit than Mod2 or Mod4.

6.7 Discussion

6.7.1 Observations

The tracer experiments show a pronounced evolution of the drainage path of M4 during the onset period (Fig. 6.2). The increase in glacial transit speed on the first day of the onset period is mainly due to the increased pressure difference driving the water. The further increase on the second day is caused by the enlargement of the channel. Before the lake drained, the channel was inefficient but then developed quickly, as can be seen from the reduction of dispersion D and the increased fraction of mobile water β. However, contradictory to this are the large diurnal water level fluctuations in BH6 (located 50 m beside M4), which are commonly assumed to be caused by an efficient drainage system. The trace right at the beginning of the onset period shows a greatly reduced fraction of returned tracer mass M. This might be caused by water being pushed out laterally from the channel into storage areas. On the second day of the onset period the local storage areas may have been filled and the fraction of returned tracer mass increases again to previous values. The data from BH4 (Fig. 6.3b) also indicate the release of stored water: its water pressure drops 8 hours after the pressure in BH6 drops which could be due to water flowing out of storage keeping the pressure high. This 8 h time lag in the signal of BH4 measurements is also present before and after the drainage, indicating that storage-release processes also play a role during normal discharge regimes (c.f. Hock et al., 1999). The time lag also indicates that BH4 lies upstream of BH6 because otherwise the water pressure in BH6 should lag the pressure in BH4. Hence, water flow does not always follow the direction of the gradient of the calculated hydraulic potential (Fig. 6.1 and Chapter 3).

The bounds on the flow speed in the connection channel (Fig. 6.6) depend on the sinuosity σ of the channel and range from a maximum speed of $1.4\,\mathrm{m\,s^{-1}}$ for σ=1 to $2.7\,\mathrm{m\,s^{-1}}$ for σ=1.86. The inferred speeds on the first day of the onset period are slow ($<0.6\,\mathrm{m\,s^{-1}}$). Combined with the high dispersion, this suggests that the drainage system was not very efficient as could be the case for a braided flow path or flow through a network of englacial cracks (Fountain et al., 2005). The lower bounds on the flow speeds are always very low due to the poor constraint on the upper bound of $\hat{t}_{\mathrm{con}}$, but from the comparison to the model, it seems that the upper bounds on the flow speed are more relevant.

6.7.2 Comparison measurements and model

Even though the lake drained by overspilling into a moulin on its shore, the situation was similar to a subglacial outburst flood during the onset period. The main difference is that during a subglacial outburst, the water pressure is higher at the channel inlet which is then located at the lake bottom. However, this difference makes the used model (Clarke, 2003) not less applicable as the upper boundary condition can be adjusted accordingly and thus we can test it against our measurements.

Mod1 (Fig. 6.6a,b) shows that a good fit to the lake discharge can be achieved without matching the flow speeds inferred from the tracer experiments. Hence, discharge measurements alone are not enough to test the Spring-Hutter equations applied to a jökulhlaup. In order to match the inferred flow speeds, either the sinuosity/length of the connection channel (Mod2, Mod3) or the heat transfer (Mod4) need to be increased. However, on the first day of the onset period, the model cannot fit the inferred flow speeds while still matching the lake discharge and the inferred flow speeds on the second day. Thus, there is a qualitative difference in the drainage path between the first and the second day of the onset period. This is supported by the other observations discussed in the previous paragraph, in particular the decrease in tracer dispersion. The inability to model the flow speeds on the first day of the onset period may be due to the following reasons: the water does not initially flow through R channels (e.g., braided channels or englacial cracks); the Spring-Hutter equations are not valid for R channels at these low flow speeds and discharges; the geometry changes profoundly between the first and second day e.g., the sinuosity decreases considerably. Any of these reasons indicates that an accurate model of the very beginning of a jökulhlaup needs to go beyond the Spring–Hutter equations. So far only one jökulhlaup model does this and includes also sheet flow (Flowers et al., 2004) which probably could capture flow through a more distributed system with suitably chosen parameters.

On the second day of the onset period the model performs well if either the sinuosity/channel length is increased or if the heat transfer from the water to the channel wall is increased. A more sinuous or longer channel (Mod2, Mod3) leads to a reduced roughness and higher flow speeds to fit the discharge. However, because the inferred flow speed also depend on the sinuosity of the channel, the model results match up with the measurements. For Mod4, the heat transfer was increased, as it has been criticised that the outlet water temperature is overestimated by the Spring-Hutter equations (Jóhannesson, 2002; Clarke, 2003), however, Figure 6.7c shows that the water temperature is not significantly reduced. The use of a two-fold enhanced heat transfer coefficient (Eqn. 6.4) leads to a very high Manning roughness ($n_{\mathrm{man}} = 0.105\,\mathrm{m}^{-1/3}\,\mathrm{s}$) to keep flow speeds low in the larger channel. A high resistance to water flow can be caused by a channel which is low and broad. Hooke et al. (1990) introduced low and broad channels with the shape of a circular segment characterised by its central angle θ. Such a Hooke channel has a circular cross section for $\theta = 360°$ and a semicircular one for $\theta = 180°$. The hydraulic radius R_{h} (Eqn. 6.3) of a Hooke channel becomes smaller with decreasing θ for a fixed cross-sectional area S. The hydraulic radius in terms of S and θ is given by $R_{\mathrm{h}}(S,\theta) = \sqrt{S(\theta - \sin\theta)}/(\sqrt{2}(\theta + \sqrt{2 - 2\cos\theta}))$. A smaller hydraulic radius reduces water flow speed (Eqn. 6.2). Hence, the high Manning roughness of Mod4 can be reduced to an effective value of $n_{\mathrm{man}} = 0.049\,\mathrm{m}^{-1/3}\mathrm{s}$ (like Mod2) by the smaller hydraulic radius of a Hooke channel with a central angle of $\theta = 16.5°$ (this geometry also leads to higher closure rates but these are not important in these settings). This channel shape is very low and broad but could occur during the onset of a jökulhlaup if the drainage path evolved from a braided one, as suggested above.

The models Mod1, Mod2 and Mod4 produce virtually identical discharge hydrographs and are distinguished only by their water flow speeds. Hence, the comparison to measured flow speeds is needed for further model validation and leaves Mod2 and Mod4 as options. Unfortunately, it is impossible to discriminate between these two using our experimental data. This is because the flow speeds inferred from the tracer experiments are themselves dependent on the sinuosity. The water temperature at the outlet is almost identical (Fig. 6.7c) for Mod2 and Mod4, indicating that it is difficult to distinguish high sinuosity from enhanced heat transfer solely by temperature measurements. However, in situations where there are no direct flow speed measurements, low water temperatures at the outlet can indicate high sinuosity or enhanced heat transfer since Mod1 produces higher outlet temperatures than either Mod2 or Mod4. A model of the whole subglacial drainage system would not need the borehole water pressure data as a boundary condition, thus allowing a comparison for validation. However, many more assumptions would be needed to set up such a model and thus it is unlikely to yield more accurate results.

The presented interpretations are based on a model which was deliberately kept simple but still, there are a few potential shortcomings. An argument was presented to constrain the location of the connection channel to the grey area in Figure 6.1. However, it is plausible from the hydraulic potential that the connection channel could also pass between M1 and M2. Also, the connection channel presumably has tributaries, influencing its discharge, initial size and pressure. This would lead to increased tracer flow speeds, because in R channels the flow speed is an increasing function of discharge. Hence, the model, not taking into account tributaries, should underestimate rather than overestimate water flow speeds. The water pressure boundary condition at the connection channel outlet is insufficiently known. Figure 6.6g,h shows that the use of the previous year's subglacial water pressure data with large diurnal fluctuations as a boundary condition leads to variations in the modelled speeds and discharge that are greater than those observed in the measurements. In all likelihood, the diurnal fluctuations found in the pressure data recorded during the onset period were too small, whereas those from the previous year's data were too great (Fig. 6.4d). The additional water coming from the lake would keep the subglacial water pressure higher during the night, as was observed, for example, during the 2005 outburst on 11 and 12 June (Chapter 5) when the nightly pressure minima became less pronounced at lake discharges comparable to the ones encountered during the presented measurements. This higher subglacial water pressure at night would suppress the large modelled variations. This sensitivity on the pressure boundary condition at the connection channel outlet shows that the rest of the subglacial drainage system, dictating the subglacial water pressure, can have a great influence on the trigger and initial jökulhlaup evolution. Hence, to simulate the onset of a lake drainage, the prevailing conditions in the subglacial drainage system need to be taken into account. The model does not include storage–release processes for which there is clear evidence from tracer experiments and borehole water pressure data (see also Huss et al., 2007). They can influence the pressure and discharge conditions considerably, in particular during the onset. Water diverted into storage should lower the tracer flow speed by the fraction of diverted water. The inferred flow speeds obtained from the tracer measurements on the first day are about two to three times less than the modelled speeds. This could be caused by forcing one-half to two-thirds of the water into storage during this time. On the first day, tracer return mass diminished by half, suggesting that the low flow speed could be caused for the most part by storage processes.

6.8 Conclusions

For the first time water flow speeds calculated by a jökulhlaup model were compared to speeds inferred from dye tracer injections using the lake outlet. This showed that an ingenuous fitting to the discharge led to too high model flow speeds. During the first day of the lake drainage the inferred flow speeds were too low to be fitted at all, indicating that the water was not yet flowing in an R channel. Hence, to simulate the onset of a jökulhlaup it is necessary to go beyond the Spring-Hutter equations. Afterwards, the inferred flow speeds can be fitted by either increasing the sinuosity of the connection channel or by enhancing the heat transfer. For enhanced heat transfer the roughness needs to be increased to an improbably high value for a semi-circular channel but it can be reduced to reasonable values assuming a low and broad channel. However, the experimental data do not allow to discriminate between these two possibilities, leaving the field open for further research. In particular, a direct measurement of the location and sinuosity of en- and subglacial channels would be desirable as would be a better understanding of the heat transfer in an R channel. The former seems difficult to achieve whereas the latter could be achieved by means of laboratory experiments.

Chapter 7

Hazard assessment investigations in connection with the formation of a lake on the tongue of Unterer Grindelwaldgletscher, Bernese Alps, Switzerland

Abstract The surface of Unterer Grindelwaldgletscher glacier tongue has subsided by more than 200 m over the last 150 years. The surface lowering is not uniform over the glacier tongue but depends on the thickness of the uneven debris cover, which led to the formation of a depression on the tongue. A lake can form in this basin, which occurred for the first time in 2005. Such a glacier lake can drain rapidly leading to a so-called outburst flood. The lake basin has been increasing in size at an alarming rate and in 2008, it reached a volume which poses a significant flooding threat to the communities downstream, as was exemplified by an outburst of the lake in May 2008. The future evolution of the lake basin was extrapolated based on surface lowering rates between 2004–2008. An outburst flood model was tuned with the measured hydrograph from 2008 and then was run with the extrapolated lake bathymetries to simulate future lake outbursts and estimate their flood hydrographs. We discuss the rapidly increasing risk for Grindelwald and other communities, as well as the installation of an early warning system and possible prevention measures.

7.1 Introduction

Glacier lake outburst floods, also known as *jökulhlaups*, commonly occur in glaciated regions around the globe and present one of the greatest and most far-reaching glacier-related hazards. Lakes dammed by ice have a tendency to drain rapidly once an initial drainage pathway has been established (Roberts, 2005; Tweed and Russell, 1999), leading to floods in the valleys downstream. The outburst of such glacier lakes have caused extensive damage in the Swiss Alps

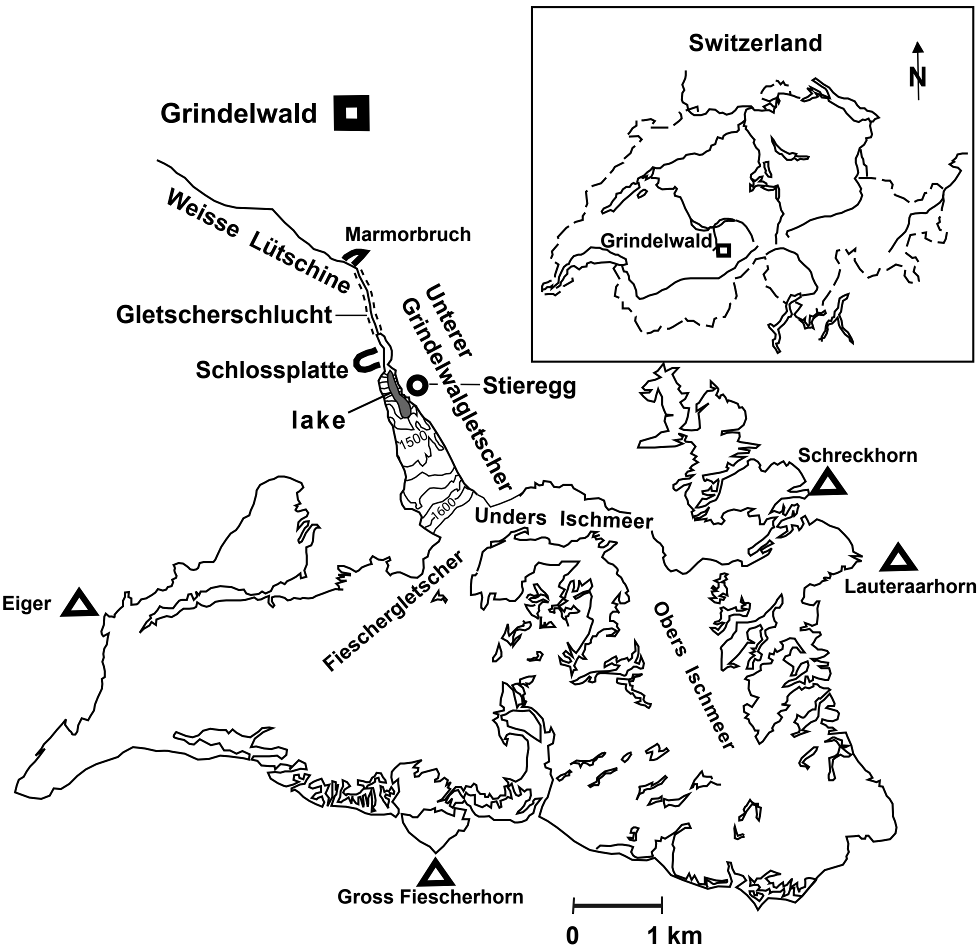

Figure 7.1: *Map of Unterer Grindelwaldgletscher with its two tributaries: Fieschergletscher (left) and Unders Ischmeer/Obers Ischmeer (right). The lake is located just south of "Schlossplatte" on the tongue of the glacier.*

(Raymond et al., 2003; Haeberli, 1983; Röthlisberger, 1981). The existence and development of these lakes is closely linked to the evolution of their damming glacier. Thus, in times of rapid glacier change, it must be expected that some of these lakes will cease to exist, others will change their behaviour and new ones will emerge.

The tongue of Unterer Grindelwaldgletscher (Fig. 7.1) is covered with an uneven layer of debris. The layer is thicker towards the terminus due to the ongoing collapse of an unstable rock face located there, with the result that the surface lowering rates are higher upglacier than right at the terminus. This led to the development of a topographical depression where a lake started to form in 2005. This basin has been growing in size ever since and poses an increasing threat to the communities downstream as the lake, which it can contain, potentially drains rapidly and causes floods. To make a hazard assessment of the situation, we looked at the future development of the glacier tongue and estimated future lake volumes. With these estimates, we calculated the expected peak discharges and advance warning times of such floods. These calculations were done with an existing model of glacier outburst floods (Clarke, 2003). The validity and limitations of our model results are discussed, as well as the implications of our findings for the damage potential to Grindelwald and communities further downstream, and possible preventative measures.

7.2 Methods

The surface topography of the glacier tongue was established with photogrammetric methods from aerial photos taken in autumn of 2006, 2007 and 2008, with an error of $\sim$0.1 m. From the resulting digital elevation models, the bathymetry of the lake basin was calculated and, thus, the potential lake volume. The bed topography was determined with ground penetrating radar (VAW, 2007); six profiles were acquired between the lower reaches of the lake to $\sim$1 km upglacier (Fig. 7.6a between 2150 and 3000 m). As radar measurements were not possible on the glacier tongue lying in the gorge, we interpolated the bed between the ice free part of the gorge and bed further upglacier, as determined by radar. We estimate that the presented bed topography has an error of $\pm$10 m where it was determined by radar and larger elsewhere.

The stage of the proglacial river was measured at Marmorbruch (Fig. 7.1), ca. 1.4 km below the glacier terminus with a radar. A stage-discharge relation was established with dye dilution methods, however, as the cross-section of the river bed is constantly changing, the error in the calculated discharge is around 20%. The lake level was measured with a pressure transducer installed in the lake. The main error source is the unprecisely known location of the sensor. Together with the bathymetry a lake discharge can be calculated for which we estimate an error of 20%.

7.3 Field site

The two glacier branches of Obers/Unders Ischmeer (between Schreckhorn and Fiescherhorn) and Fieschergletscher (between Fiescherhorn and Eiger) come together at the Zäsenberg to form Unterer Grindelwaldgletscher (Fig. 7.1). With a surface area of 19.6 km^2, it is the sixth largest glacier in Switzerland (status year 2004).

The evolution of Unterer Grindelwaldgletscher (Fig. 7.1) has been documented in a great number of historical illustrations and paintings dating back as far as the 17th century. The oldest illustration is a copperplate engraving (etching), done by J. Plepp before 1642 (Zumbühl, 1980). Since 1880, the position of the tongue has been determined every year until 1983, when it became impossible to take measurements as the terminus had retreated into the Gletscherschlucht, a deep and narrow gorge (Glaciological reports, 2009). Volume changes have been determined from 1861 onward based on the Siegfried and Dufour maps, and other maps and aerial photographs from the years that followed (Steiner et al., 2008). According to these findings, Unterer Grindelwaldgletscher lost $\sim$1 km in length and $\sim$1.56 km^3 in volume, equivalent to 60 m ice thickness loss on average over the entire glacier surface (Fig. 7.2).

7.3.1 The unstable rock face at the Schlossplatte

The surface lowering of the glacier tongue by more than 200 m since the little ice age exposed its flanking valley sides leading to their destabilisation due to the cessation of ice pressure. Consequently, at the Schlossplatte, $\sim 2\times 10^6$ m^3 of rock on the left side near the glacier terminus have become unstable (Figs. 7.1 and 7.3).

From July 2006 to August 2008, the rock face moved forward a distance of 51 m. During this two-year period, most of the moving rock mass disaggregated and repeatedly triggered

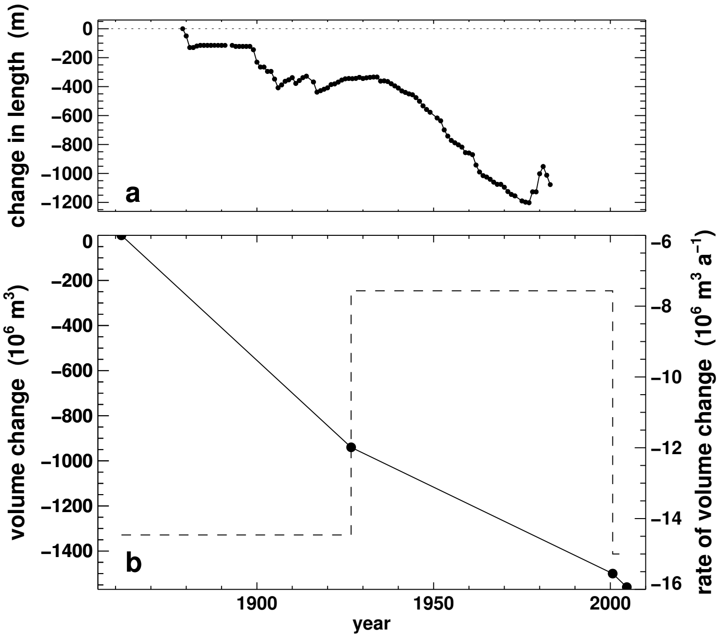

Figure 7.2: *Changes in length since 1880 (a), volume (b, solid line) and rate of volume change (b, dashed line) since 1860 of Unterer Grindelwaldgletscher. The terminus retreated into an inaccessible deep gorge and it has not been possible to determine its position since 1983 (Bauder et al., 2007; Steiner et al., 2008).*

rockfalls (Fig. 7.4). The debris remained on the glacier surface, with some of it spilling into the gorge in the proglacial area. By this process, the debris layer in the terminus zone of the glacier has been increasing in thickness. The slip plane of the unstable rock face lies at an unknown depth underneath the current glacier surface level, with a downward slope angle of $\sim 38°$ (source: GEOTEST, Oppikofer et al., 2008). In future, the remaining rock mass will probably continue to move towards the east side of the valley, but at a decreasing rate because of its further disaggregation (Fig. 7.4b).

7.3.2 Surface changes in the terminus zone since 2000

The tongue of Unterer Grindelwaldgletscher is located below 1500 m a.s.l. The inflow of glacier ice from the upper region has diminished drastically in the past decades due to higher summer temperatures and negative mass balances. The surface elevation of the glacier tongue has been dropping at an average rate of 5 m a^{-1} since 2000, translating into a volume loss of ∼3 million m^3 a^{-1} of ice between 2000 and 2008 (Fig. 7.5). It can be seen that the surface lowering is not uniform, which we attribute to the uneven debris layer on the glacier tongue. Direct point measurements and visual observations show that the debris layer is several meters thick near the Schlossplatte and 0–30 cm further upglacier. For debris layers thicker than a few centimetres, it was observed (Lundstrom et al., 1993) that the thicker the debris layer, the lower the rate of ablation of the underlying ice; with a 40 cm thick layer, ice ablation is reduced by 95%. It is evident (Fig. 7.5) that the glacier surface elevation remained largely unchanged in the area below the unstable rock face (northern part of the tongue), whereas upglacier it lowered very rapidly. This led to the formation of a depression on the glacier tongue. The ice flow in the lower region of the tongue appears to have been minimal (only a few m a^{-1}) in recent years, also favouring the formation of depressions on the glacier surface.

Figure 7.3: *The unstable rock face (Schlossplatte, marked) on the orographic left side of Unterer Grindelwaldgletscher at the foot of the eastern ridge of the Eiger mountain, the debris-covered tongue and the supraglacial lake in May 2008.*

7.3.3 Gorge geometry and terminus location

The terminus of Unterer Grindelwaldgletscher is situated in a long and narrow gorge, the Gletscherschlucht (Fig. 7.1). This gorge was explored on foot in March 2007. It was found that up to $\sim$1 km (as measured from the gorge entrance) it has a width of 10–30 m then narrows to a width of only 2–3 m at the 1.4 km point (Fig. 7.6). It was possible to proceed for another $\sim$15 m beyond a local snow-ice formation, where the gorge narrowed to $\sim$0.5 m in width, prohibiting further progress. Here, at Point PA (km 1.435, Fig. 7.6), there was no ice and no sign of the glacier terminus. The stream flow in the gorge could be clearly identified up to P1 (km 1.271) in our photogrammetric evaluations. The glacier terminus visible on the aerial photographs from autumn 2006 is designated as P2 (at km 1.510). The most likely glacier terminus (debris-covered or unrecognisable in the gorge) lies between P1 and P2. The floor of the gorge was ice-free up to the point reached at PA (between points P1 and P2). The length and the geometry of the remaining ice-free gorge floor is not known, as it could not be explored further. The same is true regarding the topography of the still ice-covered part of the gorge at the front section of the glacier tongue. It is only beyond the Schlossplatte that data on the glacier bed is available, based on our radar measurements (VAW, 2007).

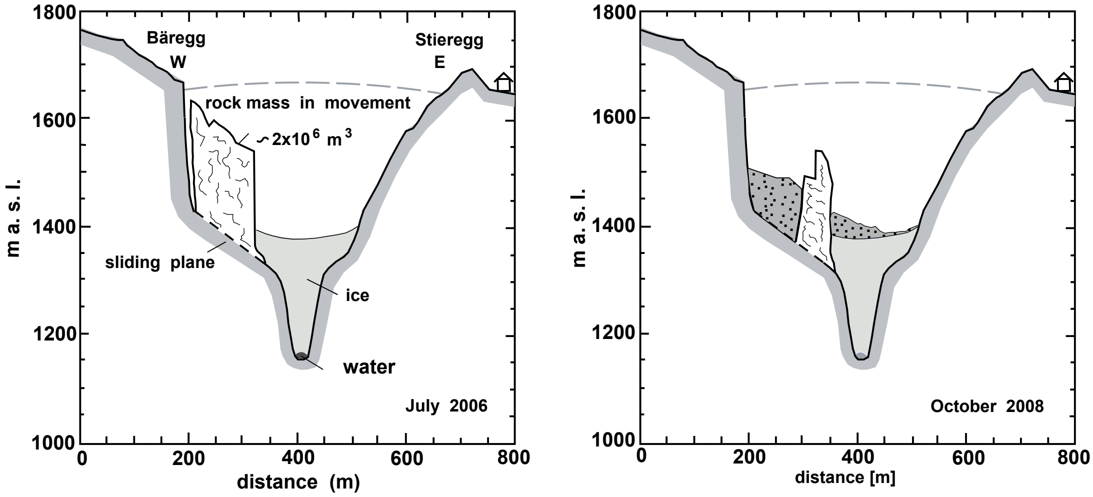

Figure 7.4: *Evolution of the unstable rock mass since July 2006. The lowest point of the glacier bed geometry was interpolated between the ice-free surface topography immediately downstream and results from radio-echo soundings performed upstream. However, the cross-section of the glacier and location of the sliding plane are not known.*

7.4 Lake development

The thinning of the tongue of Unterer Grindelwaldgletscher has been non-uniform due to the uneven thickness of the debris cover leading to the formation of a topographical depression on the tongue of the glacier where water can accumulate and form a lake (Fig. 7.3) (c.f. Gulley and Benn, 2007; Benn et al., 2001). The lake formed for the first time in 2005 and its basin has grown in size ever since (Table 7.1 and Fig. 7.7). The area and volume of this basin was determined based on measurements of surface topography. Its content corresponds to the maximal potential lake volume if the basin is filled completely. The photogrammetric analysis of aerial photographs taken at the end of summer in the years 2006, 2007 and 2008 allowed the determination of the potential lake size in spring of the following years (Fig. 7.7 and Table 7.1). The subsidence of the ice surface in the lake basin is faster than on the rest of the tongue (Fig. 7.5), thus, further accelerating the growth of the lake basin. This faster ablation of submerged ice is probably due to two effects, water can conduct heat efficiently by convection through a debris layer due to its density anomaly, furthermore, the debris on steeper slopes is washed away by the water, exposing bare ice. Conversely, the ice ablation in the vicinity of the unstable rock face at the terminus is negligible due to the thick debris cover which has led to the gradual formation of an ice dam in the years 2005–2009. In fact, the dam elevation has even increased between 2007 and 2009 due to the thickening debris cover caused by the ongoing collapse of the Schlossplatte (Table 7.1).

Due to ongoing climatic warming, Unterer Grindelwaldgletscher will continue to lose mass and become thinner, particularly in the region of the glacier tongue. Ablation will continue to occur at a non-uniform rate due to variations in the debris-layer thickness. There will be barely any melting of the ice dam near the terminus of the glacier tongue due to the thick layer of debris. In contrast, the rest of the tongue will become thinner at the rate of 5–10 $\mathrm{m\,a^{-1}}$, as observed between 2004 and 2008. By extrapolating the local surface lowering rates, shown in Fig. 7.5b, we predict the geometry of the future glacier tongue and, thus, an estimate of the future lake

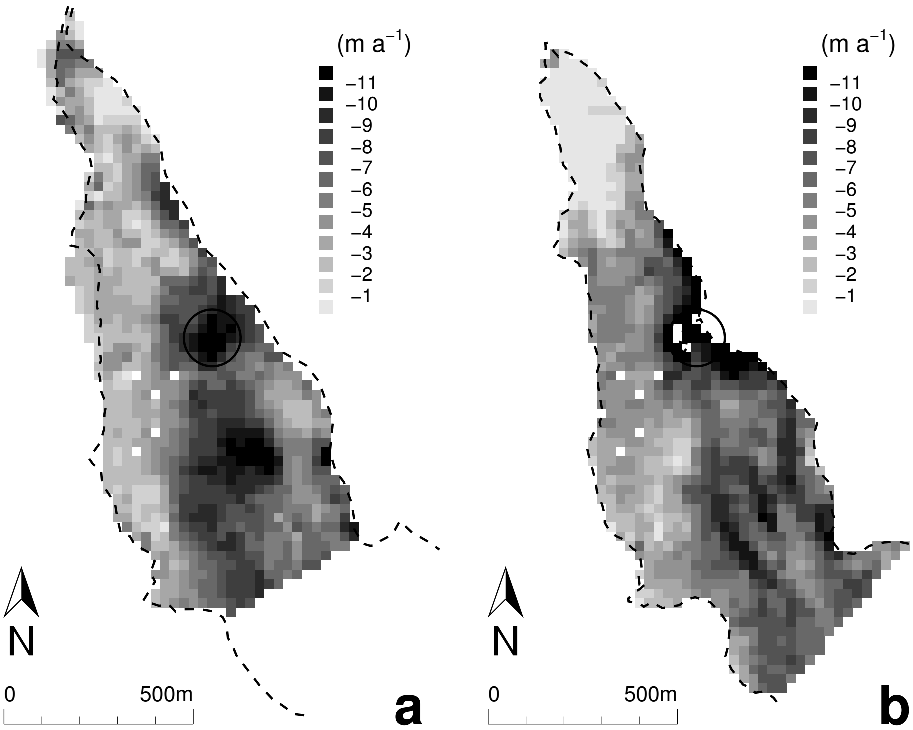

Figure 7.5: *Thickness changes on the tongue of Unterer Grindelwaldgletscher in the years 2000–2004 ($\overline{\Delta h}$ = –5.41 m a^{-1}, a), 2004–2008 ($\overline{\Delta h}$=–5.25 m a^{-1}, b). The deepest point of the newly formed lake is marked by a circle.*

basin volume and bathymetry can be calculated. It shows that the volume will increase from 2.6×10^6 m^3 in 2009 to an expected $8.9\pm1.8\times10^6$ m^3 in 2014. Table 7.2 summarises the expected basin volumes for the years 2010–2014.

7.5 Glacier dammed lake outburst floods

Glacier dammed lakes tend to empty suddenly and the resulting flood can inflict terrible damage on the valleys below. Lake dam failure can occur via two processes, either by flotation of the ice dam or by enlargement of a small dam breach (e.g. a crack) into a channel (Roberts, 2005). The first process can occur because the density of ice (900 kg m^{-3}) is smaller than that of water (1000 kg m^{-3}). Thus, once the filling level reaches around 9/10 of the ice dam height, the dam can be lifted and the water can escape. The second process is caused by the progressive enlargement of an en- or subglacial channel due to the dissipation of potential energy and the positive temperature of the conducted water. The model we used to predict flood magnitudes simulates the second process and will be discussed in the following section.

7.5.1 Modelling hydrographs

Nye (1976) offered the first theory explaining the drainage mechanism of glacier dammed lakes. This work was extended mainly by Spring and Hutter (1982), Clarke (2003) and Flowers et al.

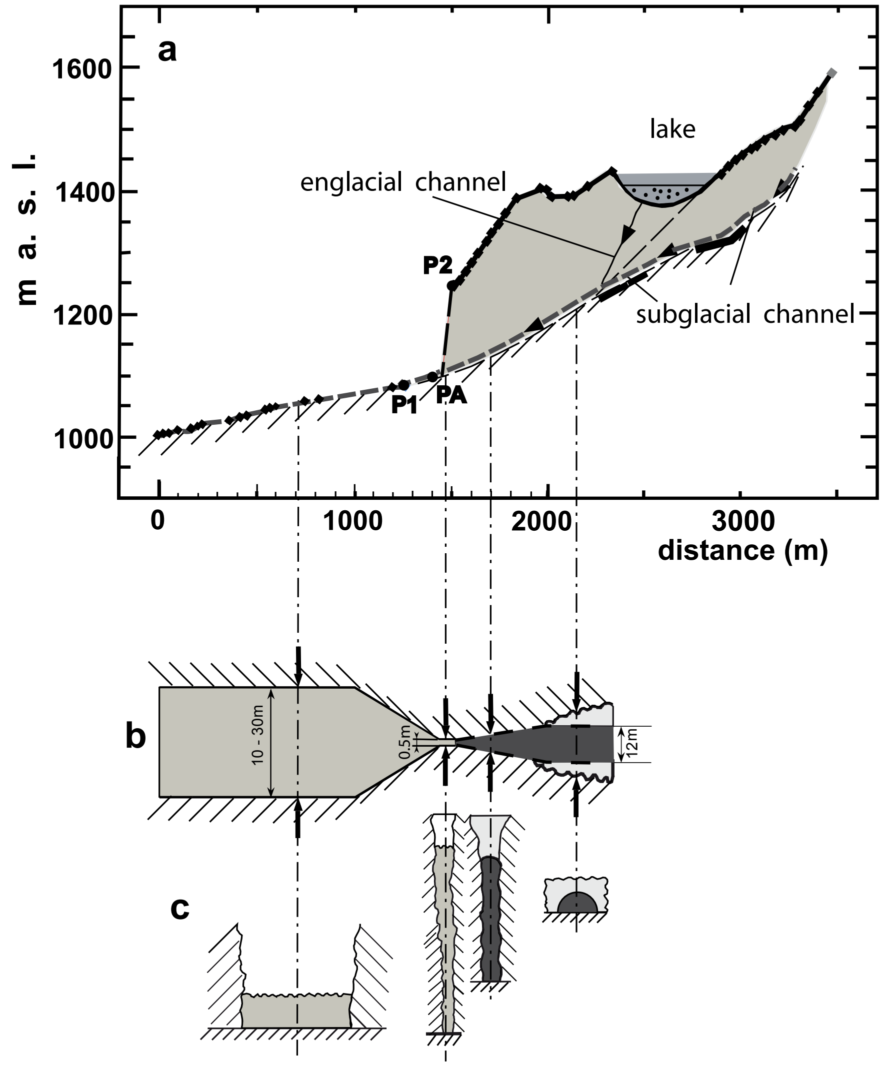

Figure 7.6: *Longitudinal profile of the glacier, the lake and the gorge (a), map plane view (b), and four cross-sections of the gorge (c), all share the same horizontal axis with distances measured from the lower terminus of the gorge. (a) The arrows indicate the en- and subglacial flow path of the water. Point P1: up to here it was possible to identify the stream bed clearly on the aerial photographs, but not further upstream. Point P2: glacier ice is visible on aerial photographs, but not further downstream. PA: it was possible to conduct reconnaissance of the gorge this far. The bed is marked with a thick line where it is known from radar measurements. (b) Schematic map view of the gorge: up to point PA mapped and thereafter an educated guess. (c) Diagram of the water flow at the glacier bed and in the gorge in four cross-sectional views. The dark-grey coloured water indicates subglacial pressurized flow conditions. Free surface runoff takes place beyond the glacier terminus, indicated by light-grey coloured water. The geometry of the two right cross-sections is an educated guess.*

(2004). Even though the model we use is based on the Spring-Hutter equations, for illustration, we give a brief introduction to the simpler Nye (1976) model for which Ng and Björnsson (2003) derived an approximate solution. The rate of change in discharge with time $\frac{dQ}{dt}$ is described in this theory using the following differential equation

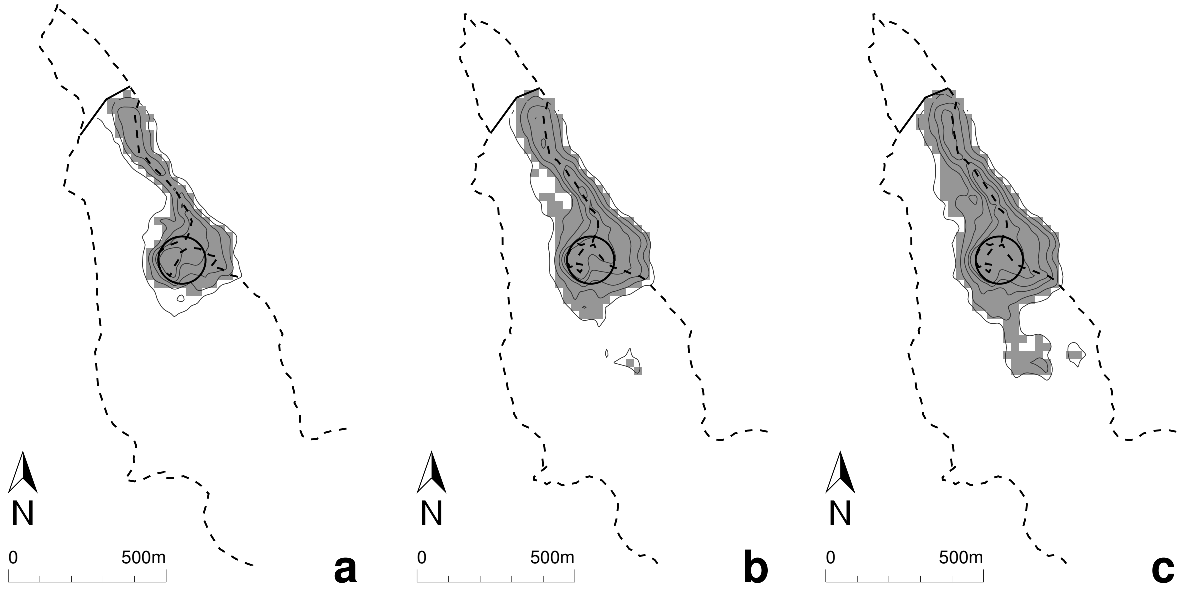

Figure 7.7: *The gray-shaded area gives maximal lake extent for the years 2007 (a, 0.034 km²), 2008 (b, 0.092 km²) and 2009 (c, 0.136 km²). The lake depth is given by the contour lines inside the lake area (interval 10 m). The centre of the lake is marked by a circle (identical to Fig. 7.5), the lake dam by a solid line and the glacier outline by a dashed line.*

$$\frac{dQ}{dt} = \underbrace{C_1 Q^{\frac{5}{4}}}_{\text{channel enlargement}} - \underbrace{C_2 Q \left(p_\mathrm{i} - p_\mathrm{w}\right)^3}_{\text{channel closure}}, \tag{7.1}$$

p_i and p_w are the ice and water pressure, C_1 and C_2 are constants depending on the geometry of the glacier and physical properties of ice and water. This equation states that the time evolution of discharge is governed by two opposing processes, one of which causes enlargement of the channel, the other of which causes closure. The channel enlarges because the ice of the channel wall melts due to dissipation of potential energy, whereas closure occurs because the ice creeps inward to fill the void. The steady state of this equation is unstable, thus, either a channel will enlarge progressively and lead to an outburst flood or it is sealed. This same behaviour is shared by the full theory (Nye, 1976) and by its extension (Spring and Hutter, 1982) also including the water temperature of the lake which can greatly affect peak discharge.

7.6 Modelled lake outbursts

We employed Clarke's (2003) model, which uses a modified version of the Spring-Hutter equations, to simulate the outburst floods of the lake on Unterer Grindelwaldgletscher. The modifications of the Spring-Hutter equations are minor, such that they become numerically stable. This model, unlike the simpler one presented in the last section, includes water temperature as a variable which is important for our setting, as the lake water can be quite warm. As input, the model needs the geometry of the bed, ice and channel (Fig. 7.6), the hypsometry of the lake basin (derived from photogrammetry and future estimates, Fig. 7.5), the lake temperature T and

Table 7.1: *Dam crest elevation h_{dam}, lake basin surface area and volume for the years 2007, 2008 and 2009 based on the surface topography determined from aerial photographs taken in fall of the previous year. "Year": summer season for which the indicated lake size was determined, "Survey": date when the aerial pictures were taken.*

Year	Survey (date)	h_{dam} (m a.s.l.)	Surface area (km^2)	Volume ($10^6\ m^3$)
2007	5 Sep 2006	1396.6	0.034	0.24
2008	12 Sep 2007	1402.3	0.092	1.30
2009	18 Aug 2008	1407.3	0.136	2.61

Table 7.2: *Predicted lower bound on the future lake basin surface area and volume for the years 2010–2014 for a dam crest elevation of h_{dam}=1407 m a.s.l.*

Year	Surface area (km^2)	Volume ($10^6\ m^3$)
2010	0.17	3.5
2011	0.21	4.5
2012	0.24	5.7
2013	0.28	7.3
2014	0.30	9.0

the roughness of the channel n_{man}. The model uses the Manning roughness description which relates water flow speed to the pressure difference (Chow et al., 1998). Initial conditions are the water-level of the lake and the channel size. The boundary condition is the water pressure at the glacier terminus (c.f. Fig. 7.6), i.e. the height of the water-level inside the gorge. The model then calculates the time evolution of the channel diameter, discharge and lake level.

We first ran the model for the 2008 outburst. For that outburst, we have measurements of the lake level, bathymetry (therefore, also lake discharge), proglacial discharge and lake temperature T. We fitted the model to the hydrograph by varying n_{man}. Hydrographs for the potential outburst in the years 2009–2014 were calculated by assuming the predicted lake bathymetry and using the same n_{man} and T as for 2008. The parameters n_{man} and T are poorly constrained and we analysed the sensitivity of the model for a range of those parameters for the expected 2014 flood. Furthermore, in the case of large outburst floods, the narrow gorge (Fig. 7.6) has a damming effect and causes the water-level in the gorge to rise. The resulting back pressure lowers the lake discharge. We did not model the flood routing in the gorge, which would be needed to calculate the water-level at the glacier terminus. Instead, a simple sensitivity analysis for the 2014 flood was performed by prescribing several fixed water-levels in the gorge as lower boundary condition, ranging from 0 m to 200 m.

7.6.1 Outburst 2008

The first serious outburst flood occurred in 2008. The lake filled during spring and on 30 May it drained within a few hours, attaining a peak discharge of 80 m^3 s^{-1}. At the onset of the outburst, the lake was barely half full, having a volume of 0.75×10^6 m^3. Afterwards, during the summer 2008, the lake basin remained empty most of the time but in August it suddenly refilled within a few hours. This suggests that water was entering the lake from the subglacial drainage system as supraglacial streams entering the lake could not have filled it as rapidly. However, in August the lake did not empty fast enough to cause another flood.

We fitted the outburst flood model to the discharge hydrographs of both of the lake and of the proglacial stream of the May 2008 outburst (Fig. 7.8). It is clear that the model is far from perfect, with the measured hydrograph rising more quickly than the modelled one. Nevertheless, it correctly reproduces the peak proglacial discharge.

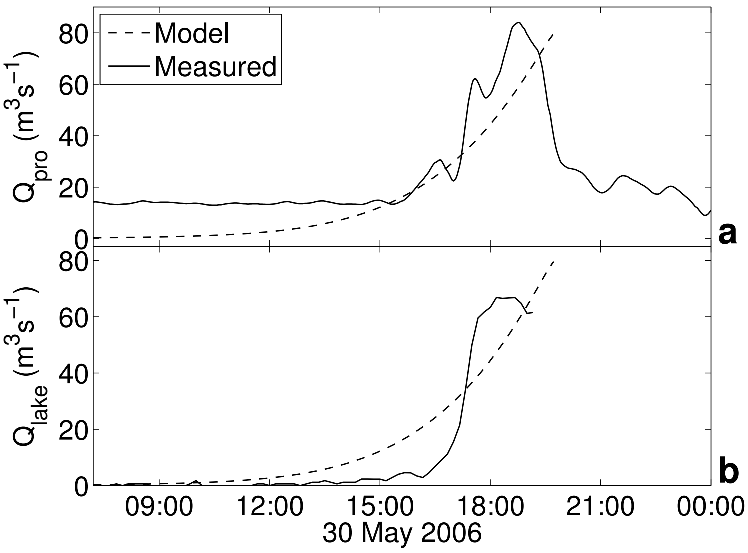

Figure 7.8: *Comparison of the measured and modelled outburst hydrographs in May 2008. (a) proglacial discharge, (b) lake discharge (note that when the Q_{lake} time series stops, the lake is not empty yet). Model parameters: lake volume 0.75×10^6 m^3, lake water temperature 2.0 °C, Manning channel roughness 0.025 m$^{-1/3}$ s.*

7.6.2 Future outbursts

With the parameters obtained from fitting the model to the 2008 outburst, we ran the model for the known bathymetries of 2008 and 2009 and for the ones predicted for the years 2010–2014, assuming a completely filled lake and, of course, an identical outburst mechanism. Figure 7.9 shows the calculated hydrographs; they are similar to each other but have an increasing peak discharge.

We calculated an advance warning time Δt by assuming that an alarm can be raised once the lake level has dropped by 0.5 m, and then calculated the time until lake discharge reached 80 m^3 s^{-1} when damage would start to occur (c.f. Sect. 7.7.3). In Fig. 7.10, the maximal discharge $Q_{\max}$ and Δt is plotted against the year of the flood. $Q_{\max}$ increases from 130 to

590 $m^3\,s^{-1}$ and Δt decreases from 5.5 h down to 3.3 h. The two model parameters, channel roughness n_{man} and lake temperature T, are likely to vary from year to year. We took the model run for 2014 as base case with T=2.0 ° C and $n_{\mathrm{man}} = 0.025\,\mathrm{m}^{-1/3}$ s and varied either T or n_{man} to study the sensitivity of the model to these parameters. Figure 7.11a shows plots of $Q_{\max}$ and Δt against n_{man}. $Q_{\max}$ decreased considerably from 1200 to 220 $m^3\,s^{-1}$ with n_{man} increasing from 0.01 to 0.08 $\mathrm{m}^{-1/3}$ s and, thus, Δt increased from 0.6 to 17 h. Figure 7.11b shows that $Q_{\max}$ increased from 380 to 960 $m^3\,s^{-1}$ with $1 < T < 4$ °C, and, thus, Δt decreased from 7.5 to 1.1 h. The gorge is very narrow (∼0.5 m) near the terminus of the glacier which causes the water-level to rise considerably at high discharge, thus, exerting a back pressure on the water flowing inside the glacier. Taking the same base case as above, we increased the water-level in the gorge from 0 to 200 m. This decreased $Q_{\max}$ (Fig. 7.12) from 600 to 320 $m^3\,s^{-1}$ and consequently Δt increased from 3.2 to 7.3 h.

7.7 Discussion

The lake basin, which formed on the tongue of Unterer Grindelwaldgletscher, will increase in volume in the future and, thus, presents an ever-growing threat to the community of Grindelwald and others further downstream. The proglacial stream, Weisse Lütschine, flows through Grindelwald Grund, where the terminal station of the Jungfraubahnen is located in addition to other infrastructure. Firstly, we discuss the model performance, then we assess the hazard potential of the lake for floods in Grindelwald based on model results, and recommend strategies for averting damage to people and infrastructure.

7.7.1 Choice of outburst flood model

There are two reasons we chose to use Clarke's (2003) model: first, this model and its predecessors are established models of glacier lake outburst floods and have been applied to several different outbursts (Nye, 1976; Clarke, 1982, 2003) which showed that they can perform adequately. Second, a more physically complex model would have been difficult to construct and run because of the following factors. The exact physical details responsible for the outbursts are poorly known and they would be difficult to experimentally investigate. Furthermore, the responsible mechanisms can vary between drainage events as is illustrated by the lake drainages in 2008: once it drained rapidly and once slowly, without producing a flood. Also, a more complex model would likely require more input data like, e.g., the geometry of the glacier bed or the sediment layer thickness at the bed. However, measurements of these quantities are not feasible.

Thus, the results of this study are only valid for one of the many possible drainage mechanism and its resulting hazard potential. We think that the modelled mechanism, or slight variations thereof as discussed below, can produce the potentially largest outburst floods in the time frame considered in this study. Therefore, it is the relevant mechanism to be considered for the presented hazard evaluation.

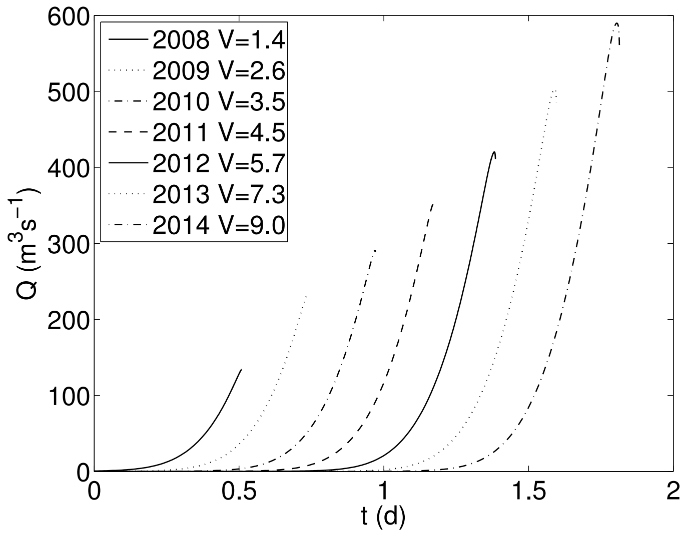

Figure 7.9: *Predicted outburst hydrographs at the glacier terminus for the years 2008–2014 assuming a completely filled lake basin and using model parameters as in Fig. 7.8. The timing is only relative and the hydrographs are offset for ease of viewing. The legend gives the year and the lake volume V (10^6 m^3).*

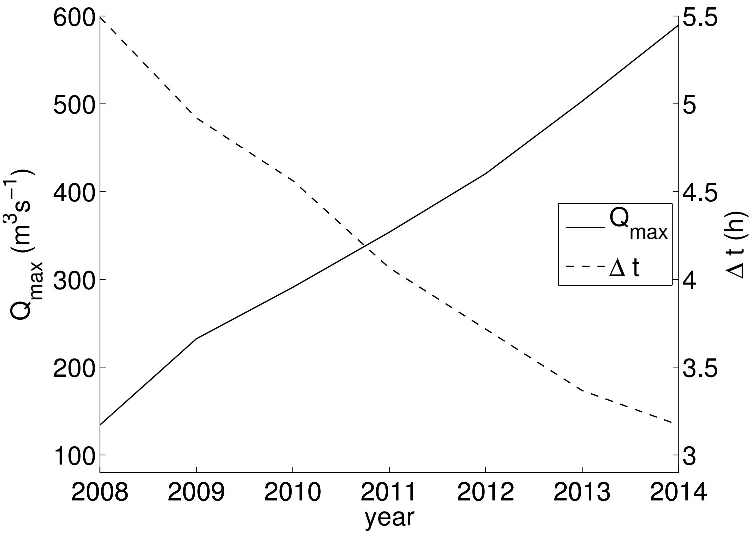

Figure 7.10: *Predicted maximal discharge ($Q_{\max}$) and advance warning time (Δt) for the years 2008–2014 assuming a completely filled lake basin and model parameters as used for Fig. 7.8.*

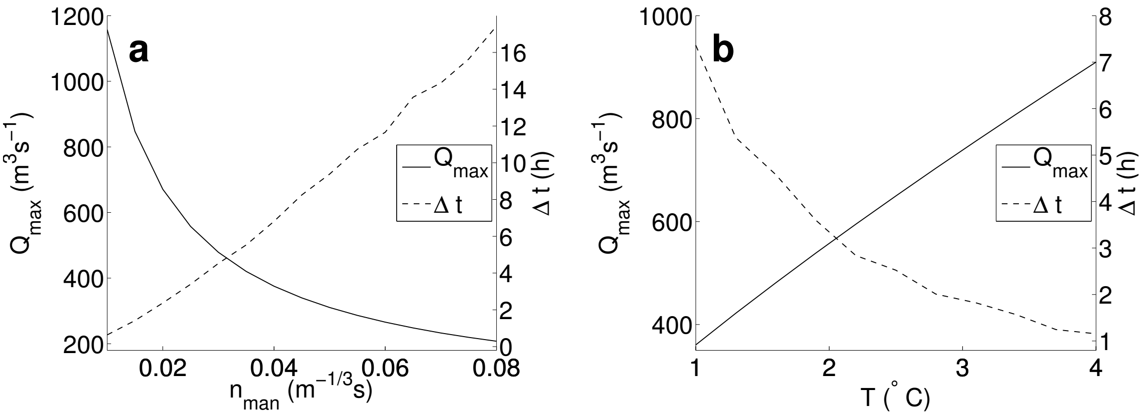

Figure 7.11: *The model sensitivity (a) to changes in Manning channel roughness* n_{man} *and (b) to changes in the lake water temperature* T*. Left axis gives maximal discharge* $Q_{\max}$ *and right axis advance warning time* Δt*.*

7.7.2 Model performance

The outburst in 2008 gave us a chance to calibrate the unknown channel roughness parameter n_{man} by fitting the modelled to the measured hydrograph. Figure 7.8 shows that the fit is not so accurate, in particular the lake outflow hydrograph rises much faster than the modelled one. This could be due to a number of factors and their combination: (a) we know that there is an already existing subglacial drainage system in place conducting the surface meltwater to the glacier terminus (see Fountain and Walder, 1998, for a review of the glacial drainage system). Figure 7.6 shows the main drainage system channel (annotated by subglacial channel) and the channel connecting the lake to it (annotated by englacial channel). At the beginning of the outburst only the connection channel would have to open up, which it could do much faster due to its shorter length. Once the lake discharge surpasses the capacity of the main drainage system, the channel of the main drainage system will have to enlarge too. Thus, this mechanism would lead to a faster-rising hydrograph at the onset of the flood and to a slightly higher peak discharge. (b) The onset of the lake outflow could be due to a crevasse opening and connecting to the subglacial drainage system, which would lead to an even faster increase in initial discharge than the triggering mechanism (a).

Especially at higher discharges, as can be expected in the years after 2010, the narrow geometry of the gorge below the terminus of the lake will influence the lake discharge hydrograph. Results show that the channel can attain a maximum diameter of ~12 m for the highest discharge values. If the width of the gorge segment, which is still underneath the glacier, is less than this maximal channel diameter (at least in places), then the emptying of the lake will take place more slowly and the peak discharge will be reduced compared to normal conditions. It is not feasible to quantify this effect but it is likely to be minor compared to the other influences (e.g. lake water temperature, discussed below). In the ice-free part near the glacier terminus, the gorge narrows to ~0.5 m. As a result, with increasing discharge, the water-level in the gorge at the glacier terminus will rise above the level of the subglacial channel. In this case, the water pressure head at the end of the subglacial channel does not, as previously assumed, correspond to atmospheric pressure but to the water-level in the gorge. We estimate the maximal water-level in the gorge for the 2014 outburst using the following argument: the calculated cross-section of the subglacial channel at the glacier terminus has a maximum area of $50\,\text{m}^2$. If the flow velocity of water in

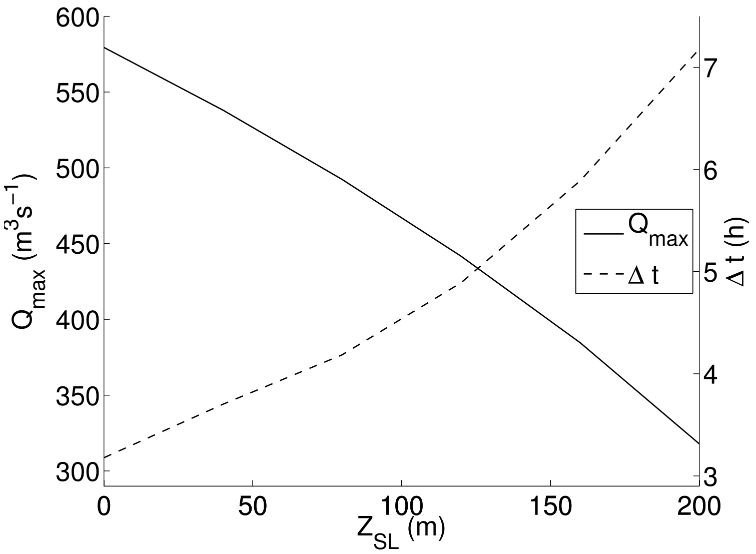

Figure 7.12: *The model sensitivity to changes in water-level in the gorge Z_{SL}. Change in maximal discharge (left axis), change in advance warning time (right axis).*

the adjoining 0.5 m wide gorge remains the same as in the subglacial channel, then the height of the free water-level has to be $\sim$100 m above the level of the channel at the terminus. The exerted back pressure diminishes calculated peak discharge (Fig. 7.12) from 600 to 450 $\mathrm{m^3\,s^{-1}}$ for a water-level of 100 m in the gorge.

The two important model parameters of channel roughness n_{man} and lake temperature T are not well constrained. For the first, we cannot estimate its band of variation as we have only witnessed one outburst flood so far. The latter is dependent on the weather conditions prior to the flood and on how much ice is exposed inside the lake basin. Thus, we conducted a sensitivity analysis of the model based on the model run of 2014 for quite a wide range of these parameter (Fig. 7.11), which shows that both parameters have a major effect on both the modelled peak discharge Q_{max} and advance warning time Δt. Based on our current knowledge, it seems prudent to assume a value of n_{man} in the range $0.015 < n_{\mathrm{man}} < 0.045\,\mathrm{m^{-1/3}\,s}$ (0.025 $\mathrm{m^{-1/3}\,s}$ in 2008) which leads to a considerably uncertainty of the calculated Q_{max} between 800 and 350 $\mathrm{m^3\,s^{-1}}$. The lake temperature can and should be measured and high values will indicate the danger of a more intense outburst. The temperature range $1 < T < 4\,^{\circ}\mathrm{C}$ is realistic for the lake (2 °C in 2008) which leads to a range of calculated $380 < Q_{\mathrm{max}} < 960\,\mathrm{m^3\,s^{-1}}$ in 2014. Note that a higher Q_{max} automatically means a shorter Δt due to the shorter duration of the whole flood and, thus, outbursts with a greater damage potential also have shorter advance warning times.

The uncertainties in the model predictions are considerable. However, at the moment, with only one observed outburst flood, nothing would be gained by applying a more complicated model, e.g. taking the above-mentioned processes (a) and (b) into account. The ongoing lowering of the lake basin will make the connection channel to the main drainage system shorter and, thus, item (a) is likely to become more important in the future.

The time of the outburst and the lake level at that point cannot be predicted based on any current theories and it is likely that this will remain so (Chapter 7.8). Thus it is possible that the basin on Unterer Grindelwaldgletscher will never fill completely before drainage initiates and, thus, peak discharges will remain below what we have predicted.

7.7.3 Hazard assessment for Grindelwald

The flood defences of the Weisse Lütschine have been constructed to safely conduct discharges of up to $120\,m^3\,s^{-1}$ of which typically $40\,m^3\,s^{-1}$ are due to background discharge. Thus, excluding times of already heightened discharge of the Weisse Lütschine due to strong precipitation, a peak lake discharge of $80\,m^3\,s^{-1}$ can be conducted without leading to damage. This is the peak discharge of the 2008 outburst and, thus, it is evident that a larger lake basin, already one of the size expected in 2009, poses a considerable threat to Grindelwald, as damage will occur at higher discharge and people will need to be evacuated. Thus, peak discharge $Q_{\max}$ prediction and also, for evacuation purposes, the advance warning time Δt estimates are necessary. For the flood in 2008, the measured Δt is 02:05 h and the calculated one is 7 h. This shows, as discussed in the previous section (processes (a) and (b)), that the flood rises faster in the initial stages than predicted by the model. Thus, all the advance warning times should be divided by a safety factor of three. A complementary early warning system could be based on measurements of the subglacial water pressure, which increases rapidly as an outburst commences. It could support the primary system which relies on data from lake level measurements.

As of spring 2009, Grindelwald will have to anticipate major damage to its infrastructure from floods due to the lake. The exact peak discharge cannot be determined as we cannot predict the filling level at which an outburst will occur (it is most likely somewhat random). Furthermore, we cannot predict how many outburst floods will occur per year as the lake can refill after emptying, as illustrated by the episode in August 2008. All in all, we estimate the likelihood of a major flood as being very high. Furthermore, in the years beyond 2010, the potential discharges are large enough to inflict very serious damage in all downstream communities.

7.7.4 Preventive measures

From spring 2008 onwards, the expected floods due to the drainage of the glacier lake were estimated to cause damages in the Lütschental as well as further downstream. An early warning system has been installed in the glacier lake, which continuously records the lake water-level with a water pressure sensor. As soon as a critical lake level decrease is recorded, a warning message is automatically sent to the person in charge of the regional natural hazard prevention. This system worked perfectly during the flood of the lake drainage on 30 May 2008.

To avert future destructive floods, the lake level should be kept as low as possible such that the potential lake water volume remains small (<0.5 million m^3). To achieve this goal, the Bernese authorities decided to build a 2.1 km long drainage tunnel on the right side of the gorge from Marmorbruch to the lake (Fig. 7.1). The tunnel will exit onto the glacier surface behind the debris-covered ice dam at the lowest possible level, so that the water of the lake can drain through the tunnel. The anticipated completion date is October 2009. It is planned to regularly adjust the tunnel exit to the lowering glacier surface in the following years. The tunnel is designed to allow large construction machines to reach the glacier to artificially level the surface in order to allow water to drain through the tunnel or to make a breach in the debris-covered ice dam, in the event that such measures prove necessary in the future. The early warning system and the tunnel construction work are described on the website http://www.gletschersee.ch.

7.8 Conclusions

New natural hazards can emerge due to the retreat of glaciers, as in the case of Unterer Grindelwaldgletscher where a new supraglacial lake has recently formed. This ice-dammed lake is unstable and can drain rapidly, leading to dangerous floods. We conducted a hazard assessment of the lake on Unterer Grindelwaldgletscher and predicted ranges of future maximal lake volume, flood discharge and advance warning times.

The latter were shown to be long enough so that, with a suitable alarm system, a timely evacuation should be feasible. However, from 2009 onward, floods with a high potential for destruction are to be anticipated and, thus, the construction of a 2.1 km long drainage tunnel was initiated in order to limit the lake volume below a critical level.

Conclusion

En- and subglacial processes are one of the final frontiers of glaciological research. Their experimental investigation is a formidable task because no direct observations are possible due to the inaccessibility of the sites where these processes take place and because the time and length scales over which these processes occur are short. The aim of the Gornergletscher project is to shine light on some of these processes by using jökulhlaups as natural experiments that allow the study of the non-equilibrium behaviour of subglacial processes due to the large perturbation caused by the heightened discharge. Our measurements on Gornergletscher were extensive, ranging from surface flow speed observations, to seismological measurements and to dye tracer experiments. All these measurements give us information about the en- and subglacial environment but—as mentioned above—none of them are direct observations of the processes occurring at the glacier bed and within the ice. Thus, models of the processes as well as models of their effects on the glacier are needed to interpret the observations.

This thesis focuses on the glacier drainage system, an important component of the en- and subglacial environment, as it conducts water, the perpetrator of most of these processes. To investigate the subglacial drainage system, I used tracer experiments, measurements of subglacial water pressure in boreholes and measurements of lake and proglacial discharge. Again, these measurements are not direct observations and needed to be interpreted with suitable models.

I presented the first comprehensive dye tracer study of a jökulhlaup for which I conducted over 200 injections during three field seasons. They yielded information on the seasonal evolution, the influence of the jökulhlaup and the catchment structure of the drainage system. I observed that the maximal tracer transit speeds occur not during the peak of the jökulhlaup but on the following day when the lake had already emptied and subglacial water pressure had dropped which is interpreted with tracer retardation inside the injection moulin (Chapters 2, 5).

The lake overspilled in 2006 into a moulin on its shore and drained steadily over the course of three weeks. This special type of drainage allowed me to inject tracer directly into the lake water. I conducted a series of tracer injections over two diurnal discharge cycles using the moulin into which the lake drained. With these high frequency injections and their comparison to similar, existing measurements (Schuler et al., 2004), using a normal moulin, I could distinguish between the influence of the en- and subglacial flow path on measured tracer transit speeds. I showed that several injections per day and near continuous moulin and proglacial discharge measurements are needed to be able to make this distinction (Chapter 4).

The first one and a half days of the supraglacial overspill drainage of Gornersee in 2006 were identical to a subglacial outburst as the flow conditions in the moulin were fully pressurised. I compared flow speeds inferred from measurements to results from Clarke's (2003) jökulhlaup model. This is the first time that such flow speed data is available making this kind of comparison possible and the results showed that the modelled flow speeds are too high. To match the inferred flow speeds on the second day after the onset, either a sinuous channel or an enhanced heat transfer needed to be prescribed. However, during the first 12 hours, the measured flow speeds were lower than what the model could produce leading to the conclusion that initially water did not flow through a R channel (Chapter 6).

The newly formed supraglacial lake on Unterer Grindelwaldgletscher shows that due to glacier change new glacier lakes can develop rapidly. The destructive potential of this lake is considerable and our group participated in a hazard assessment study. The future evolution of the lake size, the peak discharge and the advanced warning time were estimated. Due to this assessment, a 2.1 km long tunnel through the bedrock on the glacier's eastern flank was constructed with the aim to drain the lake, thus keeping the water volume below hazardous levels (Chapter 7).

Our understanding of the glacier drainage system is far from complete and further field experiments are needed. Such studies should aim to gather as large a dataset as possible and include many different types of measurements as only then theories can be put to a stringent test. In this thesis it became clear that the following areas, among others, require to be studied in more depth with field or laboratory experiments:

a) The sinuosity and roughness of R channels are unknown and, as I showed in Section 4.5.1, it is difficult to separate their effect on tracer transit speed.
b) It has been found before (Jóhannesson, 2002; Clarke, 2003) and here again (Sec. 6.7.2) that the heat transfer in R channel models is not accurate.
c) Subglacial water flow speeds have never been measured.
d) The location of en- and subglacial channels are unknown.

These issues could be addressed by the following experiments:

a) This is probably the most difficult of above questions to answer. If at all possible, a highly dynamical situation would be needed, like a jökulhlaup, to distinguish between effects of sinuosity and roughness on tracer experiments and on measurements of subglacial water pressure.
b) Accurate temperature measurements of the lake and proglacial water are important; a laboratory study of water flow through its solid phase should be conducted; ice erosion on R channel walls might be an important process, especially at high discharges, and thus ice content in the proglacial stream should be quantified,
c) With an extensive hot water drilling campaign it might be possible to drill into a subglacial channel to inject tracer into it; care should be taken to locate the channel exactly as otherwise the injections will not yield representative results. This scheme will produce measurements of residence time and together with point (a) and (d) a deduction of subglacial flow speed will be possible.
d) Advances in geophysical techniques might make it possible to map channels, e.g. high frequency radar or active source seismology conducted by introducing explosives into moulins (Sec. 6.5.3).

An accurate model of the Gornergletscher and the Unterer Grindelwaldgletscher jökulhlaups—and in fact of the early stages of any jökulhlaup—will need to take the prevailing subglacial drainage system into account, in particular the existing R channels but also en- and subglacial storage areas. However, the prediction of jökulhlaup flood magnitudes and onset time remains difficult or impossible. For Unterer Grindelwaldgletscher, my predictions of maximal discharge for 2008 were successful and lay within the large range of predicted peak discharges. Some of this large range is due to external factors, in particular the lake water temperature plays an important role and can vary a lot due to meteorological conditions. Conversely, to predict the onset time of a jökulhlaup seems almost impossible, at least for the two lakes our group studied. I think that small scale processes, e.g. the development of a small crack, may either be sufficient or not to initiate a drainage proceeding by enlargement of en- or subglacial channels, like it occurred on Gornergletscher in 2005 and 2008 but not in the other years. If this drainage mechanism fails to take place, Gornersee often fills to above flotation level of the ice dam (2004, 2006, 2007) and once more, it seems that there are some small scale processes governing whether water can penetrate beneath the dam and lift it (2004, 2007) or not (2006). It seems unlikely that measurement techniques allowing the detection of these small scale processes will be developed anytime soon.

Thus, the only viable solution for hazard prevention, barring large scale constructions like digging a drainage tunnel, is to monitor the lake level with a high temporal resolution and trigger an alarm as soon as the level starts to drop. In the case of Unterer Grindelwaldgletscher this gives advanced warning times of several hours and on Gornergletscher of as much as a day.

Appendix A

Outline and comparison of the events during the jökulhlaups 2004–2008

Our group has studied the Gornergletscher jökulhlaups intensively in the years 2004–2008. Each year a one to two month long field campaign was conducted involving up to 15 people. Gornersee exhibited a very complex drainage behaviour in these five years, each year the drainage was somewhat different. The drainage mechanisms can be broadly classified in the following categories:

a) A *subglacial* outburst initiated by the *flotation of the ice dam*. This leads to a initially rapidly rising lake discharge levelling out during the later stages of the outburst. It takes about 3-7 days to empty the lake.

b) A *subglacial* outburst initiated by *enlargement of en- or subglacial R channels*. This leads to a progressively increasing lake discharge until the lake is empty, usually within 3-7 days.

c) A *supraglacial overspill* outburst initiated when the lakes starts spilling over into a moulin. The lake levels then lowers by incising a canyon into the ice. This type of drainage is slow, at least in the case of Gornersee, and last about 3 weeks.

Here I summarise the events in these five years in the Table A.1 and with a plot of the key observations which are the lake and additional proglacial discharge due to the jökulhlaup, the amount of water stored en- or subglacially, the water level in a borehole drilled to the bed, the uplift and flow speed of the glacier at a stake. The locations of the used boreholes and the stake are marked in the map in Figure A.1. A more extensive summary of the events in 2004 and 2005 is given by Huss et al. (2007).

In 2004 (Fig. A.2), the lake filled to its maximal possible volume and started overflowing along the middle moraine on 1 July. On the same day a large calving event took place lowering the lake level by 0.3 m. During the night of 2 July, subglacial lake drainage initiated, lake discharge rose rapidly on 2 and 3 July and diminished again afterwards. Proglacial discharge started to rise on 3 July and reached its maximum on 6 July. The drainage was triggered by flotation of the ice dam as is suggested by the rapidly rising lake discharge and an up to 2 m surface uplift of the ice dam (Weiss, 2005).

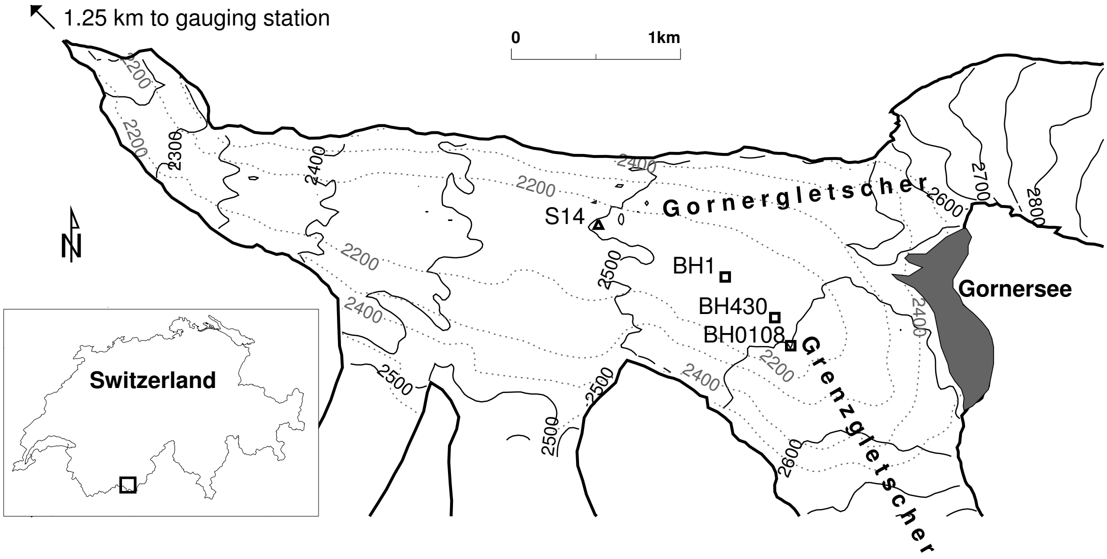

Figure A.1: *Overview map of Gornergletscher with solid contours of surface elevation and dashed of bed elevation. Three boreholes are marked (BH1, BH430 and BH0108) and stake 14 (S14).*

In 2005 (Fig. A.3), the lake filled up to around a third of its maximal possible volume when the jökulhlaup initiated, which was on 9 June. This is one of the earliest recorded onsets of the jökulhlaup. The lake outflow increased progressively until the lake was empty on 15 June. This progressively rising discharge suggests that lake drainage proceeded by melt enlargement of sub- or englacial channels. In the proglacial stream the lake water was registered between 13 and 16 June. Huss et al. (2007) (Fig. 8) show from lake level records and meltwater input into the lake that there was a leak several days prior to the jökulhlaup.

In 2006 (Fig. A.4), the lake filled until its shore reached the small moulin M4 (Fig. 2.2) into which the lake spilled over. The moulin adjusted its capacity from 0.1 to 5 $m^3\,s^{-1}$ in the first 1.5 days of the lake drainage. During this time the moulin was filled to its top and pressurised channel flow was occurring, like during the onset of a typical jökulhlaup. This onset period is the focus of Chapter 6. After these 1.5 days the moulin had adjusted its drainage capacity, the water level in the moulin lowered and the lake discharge was limited by the height of the spillway. The lake level then lowered by incising a canyon into the ice. The lake level subsidence was slightly more than 1 m per day and the discharge was varying diurnally between 2 and 5 $m^3\,s^{-1}$. It took around three weeks to empty the lake. At the end of the lake drainage the canyon was about 200 m long, 5 m wide and up to 50 m deep.

In 2007 (Fig. A.5), the lake filled until its shore reached the moulin BH6 on 4 July, close to the one into which it drained the previous year. It spilled over into this moulin until subglacial lake drainage initiated on 7 July. The main outburst happened during the next two days when the bulk of the lake water drained into a crevasse which had opened at around mid height of the lake basin. During the main outburst, a peak lake discharge of 15 $m^3\,s^{-1}$ was attained. On 9 July, the lake level had dropped to the height of this crevasse and discharge again was by supraglacial overspill. During the next five days subglacial drainage and supraglacial overspill alternated twice again until the lake was empty on 15 July. The proglacial discharge rose to almost 30 $m^3\,s^{-1}$ at the end of the main outburst and less during the subsequent events.

Table A.1: *Table summarising the key observations on the lake drainages in the years 2004–2008*

Year	Lake drainage onset mechanism	Date of onset	Duration (d)	Peak lake discharge ($m^3\,s^{-1}$)	Peak proglacial discharge ($m^3\,s^{-1}$)	Lake Volume ($10^6\,m^3$)
2004	Flotation	1 July	5	17	40	4.0
2005	Channel enlargement	9 June	6	10	20	1.5
2006	Supraglacial overspill	5 July	21	6	35	3.9
2007	Flotation	4 July	8	15	27	3.7
2008	Channel enlargement	19 June	5	30	20	2.0

In 2008 (Fig. A.6), the lake outburst proceeded similarly to 2005. The lake started to drain on 18 July as can be seen from the rise of subglacial water pressure, lake discharge increased progressively until the lake was empty on 22 July. This progressive increase shows that the flood proceeded by enlargement of englacial channels. Proglacial discharge was increased from 21 until 24 July.

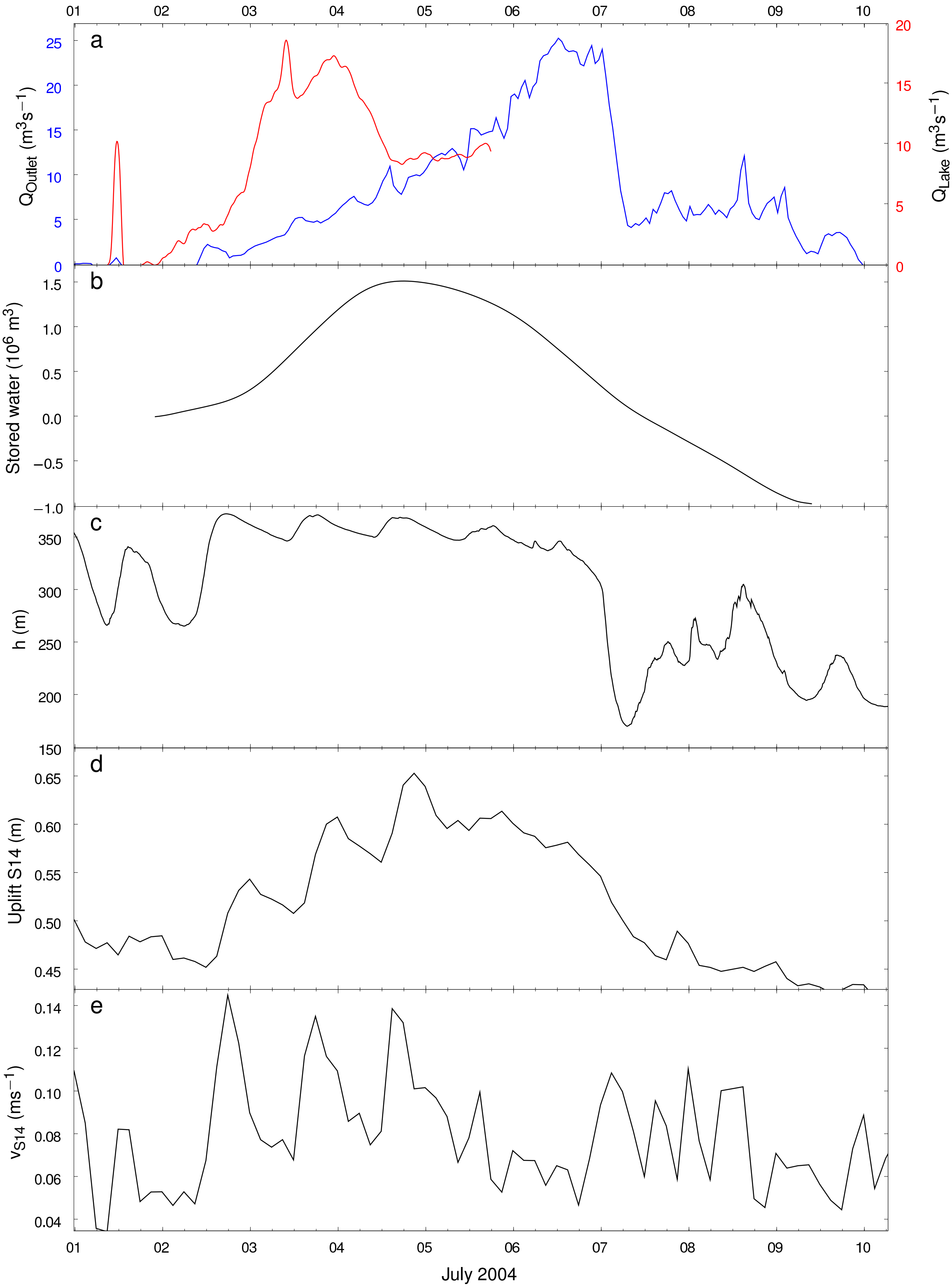

Figure A.2: *Compilation of the key measurements of the 2004 Gornergletscher jökulhlaup: (a) additional proglacial discharge (blue, left scale) and lake discharge (red, right scale); (b) volume of englacially stored water; (c) water level in borehole BH430; (d) ice uplift and (e) flow speed at stake 14.*

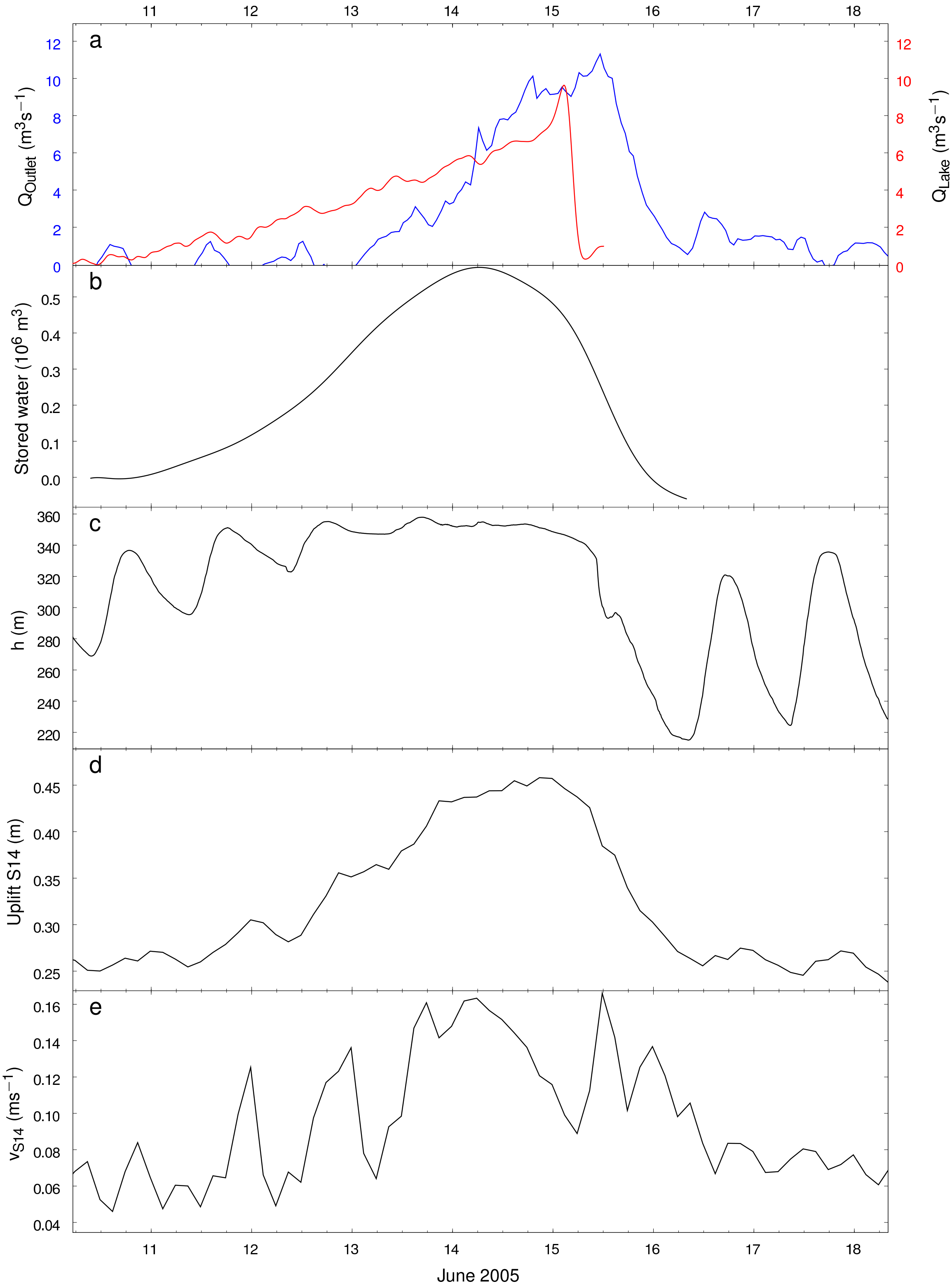

Figure A.3: *Compilation of the key measurements of the 2005 Gornergletscher jökulhlaup: (a) additional proglacial discharge (blue, left scale) and lake discharge (red, right scale); (b) volume of englacially stored water; (c) water level in borehole BH1; (d) ice uplift and (e) flow speed at stake 14.*

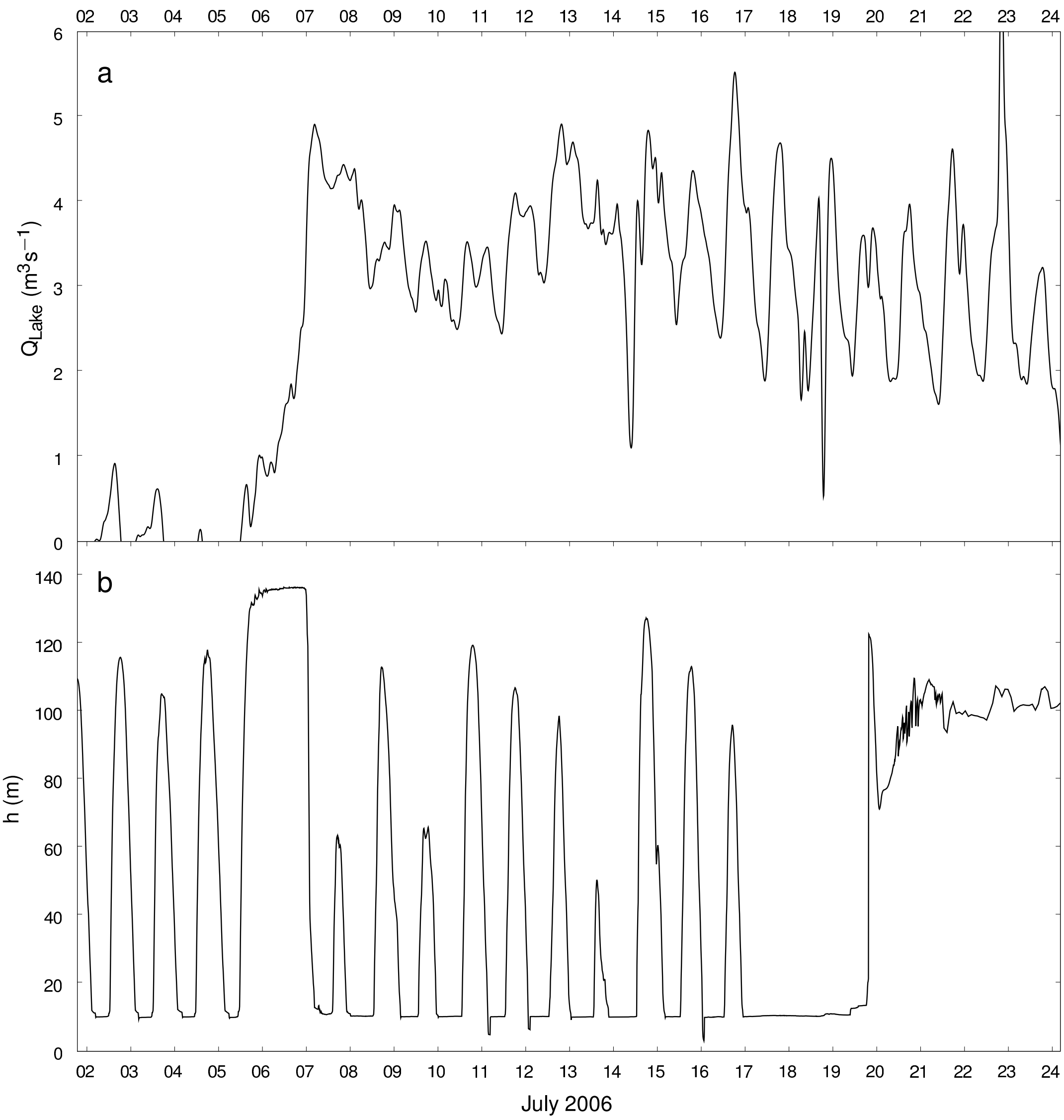

Figure A.4: *Lake discharge (a) and water level in borehole BH1 (b) located 50 m beside the drainage moulin.*

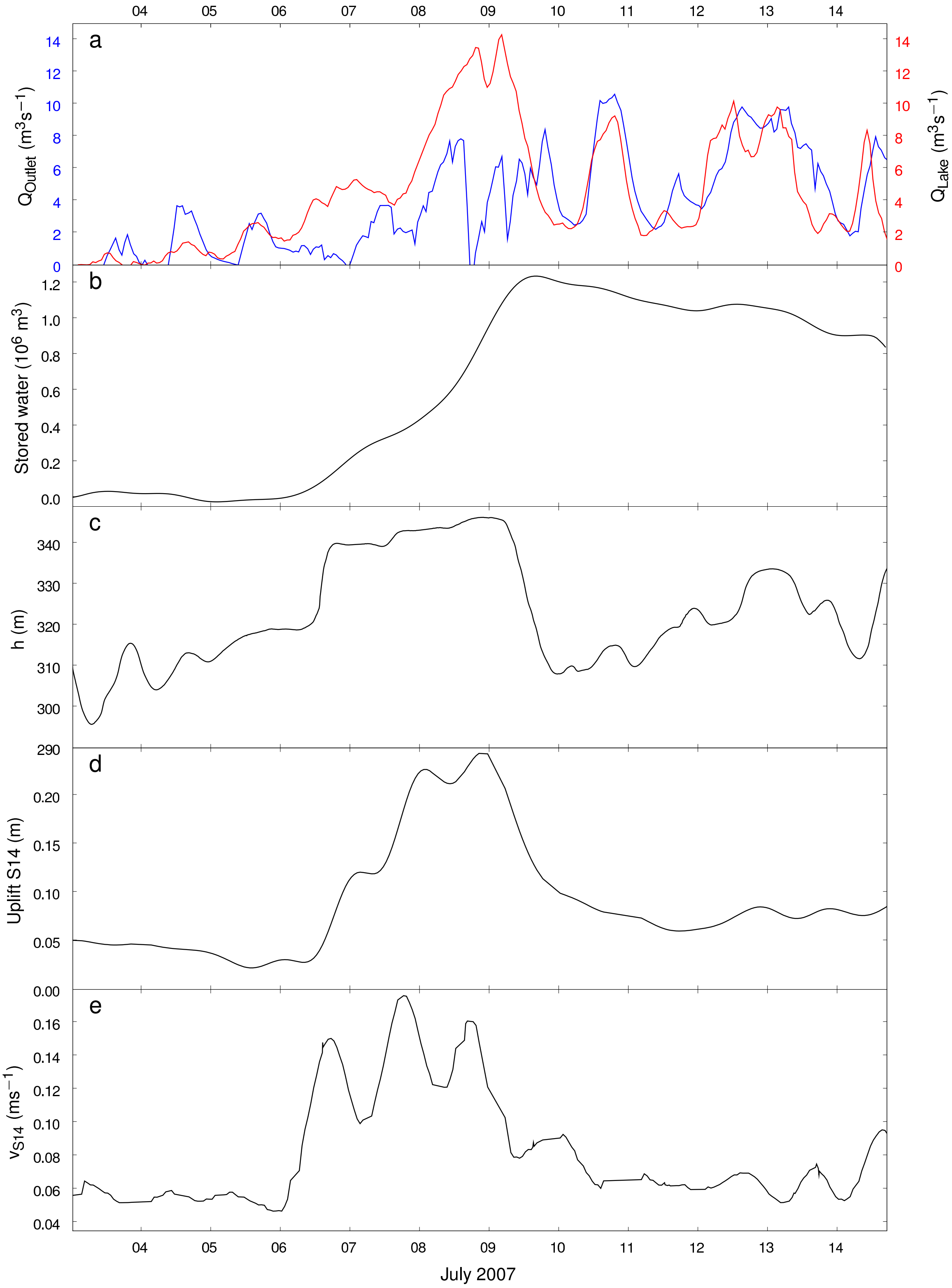

Figure A.5: *Compilation of the key measurements of the 2007 Gornergletscher jökulhlaup: (a) additional proglacial discharge (blue, left scale, unreliable on 9, 10 July and after 14 July) and lake discharge (red, right scale); (b) volume of englacially stored water; (c) water level in borehole BH1; (d) ice uplift and (e) flow speed at stake 14.*

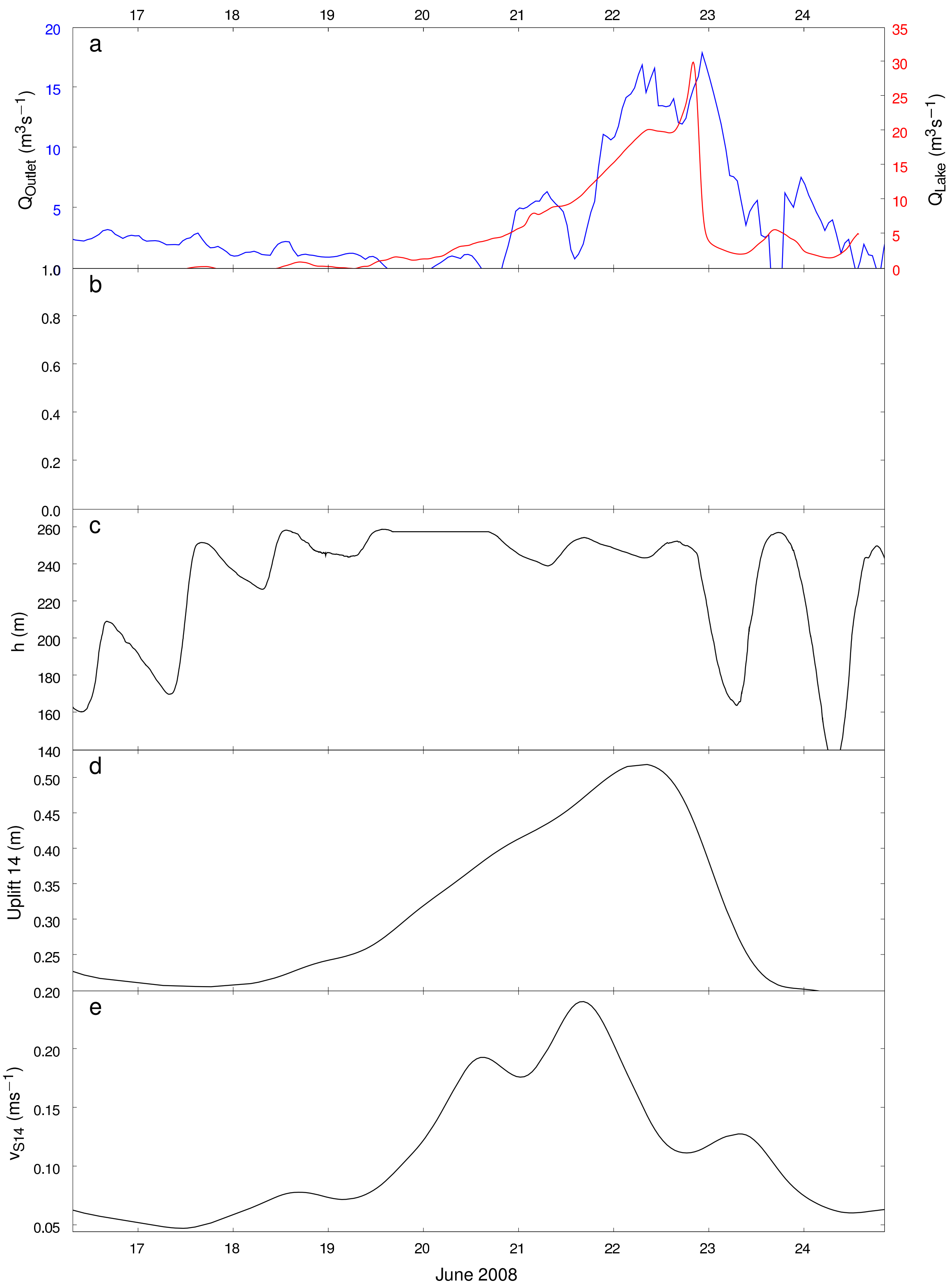

Figure A.6: *Compilation of the key measurements of the 2008 Gornergletscher jökulhlaup: (a) additional proglacial discharge (blue, left scale, not accurate) and lake discharge (red, right scale); (b) volume of englacially stored water could not be calculated; (c) water level in borehole BH0108; (d) ice uplift and (e) flow speed at stake 14.*

Appendix B

Tips for dye tracer studies on glaciers

When I started my PhD, little did I know. I was looking for practical advice on how to conduct dye tracer experiments on glaciers and did not find much. Here I want to give a short summary of the experiences I gained during three field seasons doing more than 200 injections. In the first season, Alexandre Loye, doing his Master's thesis with me, was of invaluable help and more on our measurement setup and calibration procedure can be found in his thesis (Loye, 2006).

Tracing strategy

First of all one should consider whether dye tracer experiments are the right thing to do. Their quantitative interpretation is not easy and necessitates many additional measurements (mainly moulin and proglacial discharge). Thus tracer measurements, like so many other experimental techniques, are rather work intensive.

Where to inject

Where to inject depends, of course, on the aims of the study, however the following should apply to most. Choose your moulin/moulins and stick with them. Tracer experiments from different moulins cannot be compared to each other without conducting numerous injections using in both moulins. I committed the mistake of switching moulins in 2007 when supraglacial overspill drainage commenced and I started tracing the lake outlet. However, these injections were more or less useless standing by themselves. Instead I should have continued to tracer the moulins I was tracing before. Then the injections series displayed in Figure 5.5 would be more complete.

When to inject

The simple answer is: several times a day. The frequency of injections is limited by three constraints, first tracer breakthrough curves should not be overlapping, second by the keenness of the experimenters and third by financial constraints. Several measurements over a discharge cycle are needed to properly quantify the influence of inflow modulation (c.f. Chapter 4). If I had to track the changes in the glacier drainage system over a period of a few weeks, I would employ the strategy described in Section 4.5.5.

What dye

Fluorescent dyes are good as they are detectable at very low concentrations. For smaller glaciers salt can also be used (Kohler, 1995). I used Uranine (a.k.a. Fluorescein) and Rhodamine WT. Most of the dye I used was bought as aqueous solution. The bottling of the dye is a very messy affair but much less so then when working with powder (it is a good idea to have a Master's student doing that work). When using solution, shake the container well before the bottling. Note that Uranine's fluorescence is dependent on pH in a range which could be encountered in the proglacial stream (depending on the geology).

How much dye

A first estimate for the necessary amount tracer mass M is

$$M = f\,Q\,\frac{c}{2}\,\Delta t, \tag{B.1}$$

where f is the fraction of the injected mass returned ($\sim$0.5), Q is the proglacial discharge, c is the desired peak concentration and Δt is the width of the breakthrough curve at half peak concentration. Also, it should be considered to use a well developed moulin situated not too far from the terminus for the first injection to get an idea of the prevailing conditions in the glacier drainage system.

Dye tracing jökulhlaups

Dye tracing during jökulhlaups poses additional complications to the experimental procedure: due to heightened water discharge the amount of dye injected needs to be increased. The flooding at the terminus makes the detection of the dye difficult as loss of the equipment ought to be avoided. These two constraints would make it almost impossible to trace large jökulhlaups like e.g. Grimsvötn. The Gornersee jökulhlaups, however, are suited as peak discharges are small at around $40\,\mathrm{m^3\,s^{-1}}$.

Other measurements

Additional hydrologic measurements are indispensable to interpret tracer experiments. The two most important ones are discharge into the moulin and proglacial discharge. The former is needed to be able to assess the importance of inflow modulation (c.f. Chapter 4) the latter is needed to calculate the mass of returned tracer and to assess the hydraulic conditions in the main drainage system. Both these discharges can be measured with dye dilution methods using salt or fluorescent tracer (naturally, using the latter one needs to make sure not to interfere with the actual tracer experiments). The proglacial discharge of some glaciers is measured at water gauging sites. If possible, a glacier with such a facility should be chosen. Nevertheless, it would be prudent to verify the discharge data of the gauging station by dye dilution experiments. Discharge into the moulin might be estimated over longer periods with a melt model after being calibrated with dilution measurements. To run a melt model the surface catchment area of the moulin needs to be mapped periodically and air temperature data is needed (best off-ice). Furthermore, discharge into the moulin might affect the tracer transit even hours after the injection if discharge is low.

The weather conditions are the main influences on the glacier drainage system and can influence the tracer transit until detection. Thus they should be recorded when doing injections. Any other measurements of the glacier drainage system are also useful to interpret tracer experiment results, in particular subglacial water pressure measured in boreholes.

Tracer detection

Location

Detection of the dye should be done near to the terminus before any other streams merge with the proglacial stream. If there are two or more streams exiting the glacier then separate dye detection in all of them would be interesting (this would necessitate individual discharge measurements as well). If detection is some distance below the terminus, then one should consider doing tracer experiments in the proglacial stream to be able to estimate the residence time in the proglacial stream (as was done with Eqn. 6.1).

The location should be safe to work at as discharge in the proglacial stream can increase rapidly, due to e.g. outbursts of subglacial water pockets. A man-made structure is often ideal, e.g. a gauging station, and often has the additional advantage of mains electricity.

Instruments

I used a Turner 10-Au flow-through fluorometer and a BackScat submersible fluorometer. In 2005 I also used an automatic water sampler. The Tuner 10-Au was quite sensitive to turbidity and it was lucky that I also measured turbidity so that I could correct for this effect. The BackScat was measuring flawlessly. If I had to buy a fluorometer it would be the BackScat equipped to measure both rhodamine and uranine. If buying a fluorometer make sure it works well in very turbid water. I once had my hand on one which was utterly useless in mildly turbid water.

To measure the tracer concentration, the proglacial water and the detection apparatus need to be brought into contact. Ideally, the setup up does not need constant surveillance. I used a submersible pump to feed water through the Turner 10-Au fluorometer (via a barrel, see Loye, 2006). It pumped around $30\,\mathrm{l\,min^{-1}}$. I have tried to use a suction pump but it did not work for long: the suction parts of the pump were quickly eroded by the suspended sediment rendering the pump unable to prime. Water flow in any hoses and pipes used should be fairly fast as otherwise sediment deposition will clog them. Also, when syphoning water, air bubbles can stop the flow. Apparently Thomas Schuler (2002) experienced both of those problems when he was syphoning water through the Turner 10-Au on Unteraargletscher. The BackScat is a submersible fluorometer. For it to work it needs to be submersed and there needs to be enough water below the sensor ($\sim$20 cm). This kind of fluorometer will be easier to install in most situations as it can be brought to the water and not vice versa. The only problem is to find a suitable pool, which water gauging stations normally have, but which can also be found in proglacial streams.

Calibration

Calibration should be practised at home but eventually done for real in the field, using water from the proglacial stream. If you buy predissolved dye then it is easiest to make your calibration standards as volume of predissolved dye to volume of water and not bother with net dye weight contained in the solution. Always used distilled water to make the standards. It is also prudent to recalibrate the fluorometer now and then (in particular if one is interested in the returned tracer mass). When doing the calibration at home, be sure to use water which is not chlorinated as this can destroy the dye. I used a barrel to calibrate both fluorometer in the field. It needs to be big enough to allow the BackScat to have enough water underneath its sensor. I prepared a calibration solution which when adding 1 ml to the barrel resulted in 10 ppB dye concentration.

Evaluation

The evaluation has been discussed in great depth in this thesis and thus there is not much to add. Important is to be clear about the concepts introduced in Sections 5.2 and 6.2 and that the measurements of moulin and proglacial discharge are indispensable for any interpretation.

Bibliography

Anderson, S. P., Walder, J. S., Anderson, R. S., Kraal, E. R., Cunico, M., Fountain, A. G., and Trabant, D. (2003). Integrated hydrologic and hydrochemical observations of Hidden Creek Lake jökulhlaups, Kennicott Glacier, Alaska. *Journal of Geophysical Research*, 108(F1):6003, doi:10.1029/2002JF000004.

Aschwanden, H. and Leibundgut, C. (1982). Die Markierung des Wasser des Gornerseeausbruchs mit drei Fluoreszenztracern. In Leibundgut, C. and Weingartner, R., editors, *Tracermethoden in der Hydrologie, Beiträge zur Geologie der Schweiz*, volume 28, pages 535–549.

Bartholomaus, T. C., Anderson, R. S., and Anderson, S. P. (2008). Response of glacier basal motion to transient water storage. *Nature Geoscience*, 1:37–37.

Bauder, A., Funk, M., and Huss, M. (2007). Ice volume changes of selected glaciers in the Swiss Alps since the end of the 19th century. *Annals of Glaciology*, 46:145–149.

Benn, D. I., Wiseman, S., and Hands, K. A. (2001). Growth and drainage of supraglacial lakes on debrismantled Ngozumpa Glacier, Khumbu Himal, Nepal. *Journal of Glaciology*, 47(159):626–638.

Bingham, R. G., Nienow, P. W., Sharp, M. J., and Boon, S. (2005). Subglacial drainage processes at a High Arctic polythermal valley glacier. *Journal of Glaciology*, 51:15–24.

Bird, R. B., Stewart, W. E., and Lightfoot, E. N. (1960). *Transport Phenomena*. John Wiley, New York.

Björnsson, H. (1998). Hydrological characteristics of the drainage system beneath a surging glacier. *Nature*, 395:771–774.

Chow, V., Maidment, D., and Mays, L. (1998). *Applied Hydrology*. McGraw-Hill Series in Water Resources and Environmental Engineering. McGraw-Hill.

Clarke, G. C. K. (1996). Lumped-elements analysis of subglacial hydraulic circuits. *Journal of Geophysical Research*, 101(B8):17547–17559.

Clarke, G. C. K. (2005). Subglacial processes. *Annual Review of Earth and Planetary Sciences*, 33:247–276.

Clarke, G. K. C. (1982). Glacier outburst floods from “Hazard Lake”, Yukon Territory, and the problem of flood magnitude prediction. *Journal of Glaciology*, 28(98):3–21.

Clarke, G. K. C. (2003). Hydraulics of subglacial outburst floods: new insights from the Spring-Hutter formulation. *Journal of Glaciology*, 49(165):299–313.

Collins, D. N. (1979). Quantitative determination of the subglacial hydrology of two Alpine glaciers. *Journal of Glaciology*, 23(89):347–362.

Fischer, U. H., Braun, A., Bauder, A., and Flowers, G. E. (2005). Changes in geometry and subglacial drainage derived from digital elevation models: Unteraargletscher, Switzerland, 1927–1997. *Annals of Glaciology*, 40:20–24.

Fisher, D. (1973). Subglacial leakage of summit lake, british columbia, by dye determinations, in symposium on the hydrology of glaciers. *International Association of Hydrological Sciences*, 95:111–116.

Flowers, G., Björnsson, H., Pálsson, F., and Clarke, G. (2004). A coupled sheet-conduit mechanism for jökulhlaup propagation. *Geophysical Research Letters*, 31:L05401.

Flowers, G. E. (2008). Subglacial modulation of the hydrograph from glacierized basins. *Hydrological Processes*, 22:3903–3918.

Flowers, G. E. and Clarke, G. K. C. (1999). Surface and bed topography of Trapidge Glacier, Yukon Territory, Canada: digital elevation models and derived hydraulic geometry. *Journal of Glaciology*, 45(149):165–174.

Fountain, A. G. (1993). Geometry and flow conditions of subglacial water at South Cascade Glacier, Washington State, U.S.A; an analysis of tracer injections. *Journal of Glaciology*, 39(131):143–156.

Fountain, A. G., Jacobel, R. W., Schlichting, R., and Jansson, P. (2005). Fractures as the main pathways of water flow in temperate glaciers. *Nature*, 433(7026):618–621.

Fountain, A. G. and Walder, J. S. (1998). Water flow through temperate glaciers. *Reviews of Geophysics*, 36(3):299–328.

Fowler, A. C. (1999). Breaking the seal at Grímsvötn. *Journal of Glaciology*, 45(151):506–516.

Glaciological reports (1881–2009). The Swiss Glaciers, 1880–2004/05. Technical Report 1-126, Yearbooks of the Cryospheric Commission of the Swiss Academy of Sciences (SCNAT). published since 1964 by Laboratory of Hydraulics, Hydrology and Glaciology (VAW) of ETH Zürich, http://glaciology.ethz.ch/swiss-glaciers/.

Gulley, J. and Benn, D. (2007). Structural control of englacial drainage systems in Himalayan debris-covered glaciers. *Journal of Glaciology*, 53(182):399–412.

Haeberli, W. (1983). Frequency and characteristics of glacier floods in the Swiss Alps. *Annals of Glaciology*, 4:85–90.

Hock, R. (1999). A distributed temperature-index ice- and snowmelt model including potential direct solar radiation. *Journal of Glaciology*, 45(149):101–111.

Hock, R., Iken, A., and Wangler, A. (1999). Tracer experiments and borehole observations in the overdeepening of Aletschgletscher, Switzerland. *Annals of Glaciology*, 28:253–260.

Hooke, R. L., Laumann, T., and Kohler, J. (1990). Subglacial water pressures and the shape of subglacial conduits. *Journal of Glaciology*, 36(122):67–71.

Hubbard, B. and Nienow, P. (1997). Alpine subglacial hydrology. *Quaternary Science Reviews*, 16:939–955.

Huss, M., Bauder, A., Werder, M., Funk, M., and Hock, R. (2007). Glacier-dammed lake outburst events of Gornersee, Switzerland. *Journal of Glaciology*, 53(181):189–200.

Iken, A., Fabri, K., and Funk, M. (1996). Water storage and subglacial drainage conditions inferred from borehole measurements on Gornergletscher, Valais, Switzerland. *Journal of Glaciology*, 42(141):233–248.

Jóhannesson, T. (2002). Propagation of a subglacial flood wave during the initiation of a jökulhlaup. *Hydrological Sciences Journal*, 47(3):417–434.

Kamb, B. (1987). Glacier surge mechanism based on linked cavity configuration of the basal water conduit system. *Journal of Geophysical Research*, 92(B9):9083–9100.

Käss, W. (1998). *Tracing Technique in Geohydrology*. A.A. Balkema, Rotterdam/Brookefield.

Kessler, M. A. and Anderson, R. S. (2004). Testing a numerical glacial hydrological model using spring speed-up events and outburst floods. *Geophysical Research Letters*, 31:L18503.

Kohler, J. (1995). Determining the extent of pressurized flow beneath Storglaciären, Sweden, using results of tracer experiments and measurements of input and output discharge. *Journal of Glaciology*, 41(138):217–231.

Lang, H., Leibundgut, C., and Festel, E. (1979). Results from tracer experiments on the water flow through the Aletschgletscher. *Zeitschrift für Gletscherkunde und Glazialgeologie*, 16(2):209–218.

Loye, A. (2006). Gornergletscher — Evolution of the drainage system during a jökulhlaup as revealed by dye tracer experiments. Diplomarbeit, Abteilung für Glaziologie, VAW (unpublished), ETH–Zürich.

Lundstrom, S., McCafferty, A., and Coe, J. (1993). Photogrammetric analysis of 1984-89 surface altitude change of the partially debris-covered Eliot Glacier, Mount Hood, Oregon, U.S.A. *Annals of Glaciology*, 17:167–170.

Mathews, W. H. (1965). Two self-dumping ice-dammed lakes in British Columbia. *Geographical Review*, 55(1):46–52.

McAdams, W. (1951). *Heat transmission*. McGraw-Hill, 2nd edition.

Ng, F., Liu, S., Mavlyudov, B., and Wang, Y. (2007). Climatic control on the peak discharge of glacier outburst floods. *Geophysical Research Letters*, 34:L21503.

Ng, F. S. L. and Björnsson, H. (2003). On the Clague-Mathews relation for jökulhlaups. *Journal of Glaciology*, 49(165):161–172.

Nienow, P. W., Sharp, M., and Willis, I. C. (1996). Velocity-discharge relationships derived from dye tracer experiments in glacial meltwaters: implications for subglacial flow conditions. *Hydrological Processes*, 10:1411–1426.

Nienow, P. W., Sharp, M., and Willis, I. C. (1998). Seasonal changes in the morphology of the subglacial drainage system, Haut Glacier d'Arolla, Switzerland. *Earth Surface Processes and Landforms*, 23:825–843.

Nye, J. F. (1976). Water flow in glaciers: jökulhlaups, tunnels and veins. *Journal of Glaciology*, 17(76):181–207.

Oppikofer, T., Jaboyedoff, M., and Keusen, H. R. (2008). Collapse at the eastern Eiger flank in the Swiss Alps. *Nature Geoscience*, 1:531–535. doi:1038/ngeo258.

Piccini, L., Romeo, A., and Badino, G. (2002). Moulins and marginal contact caves in the Gornergletscher, Switzerland. *Nimbus*, 23–24:94–99.

Raymond, C. F. and Nolan, M. (2000). Drainage of a glacial lake through an ice spillway. In *Debris-covered glaciers (Proceedings of a workshop held at Seattle, Washington, USA, September 2000)*, pages 199–207. IAHS Publ. no. 264.

Raymond, M., Wegmann, M., and Funk, M. (2003). Inventar gefährlicher Gletscher in der Schweiz. Mitteilung 182, Versuchsanstalt für Wasserbau, Hydrologie und Glaziologie der ETH Zürich.

Renaud, A. (1936). Les entonnoirs du glacier de Gorner. *Denkschriften der Schweizerischen Naturforschenden Gesellschaft*, 71(1):pp. 27.

Riesen, P. (2007). Investigation of glacier flow during two ice-dammed lake outburst events on Gornergletscher, Valais, Switzerland, by using a three-dimensional numerical model. Diplomarbeit, Abteilung für Glaziologie, VAW (unpublished), ETH–Zürich.

Roberts, M. J. (2005). Jökulhlaups: a reassessment of floodwater flow through glaciers. *Review of Geophysics*, 43(RG1002):doi:10.1029/2003RG000147.

Roberts, M. J., Russell, A. J., Tweed, F. S., and Knudsen, O. (2000). Ice fracturing during jökulhlaups: implications for englacial floodwater routing and outlet development. *Earth Surface Processes and Landforms*, 25:1429–1446.

Röthlisberger, H. (1972). Water pressure in intra– and subglacial channels. *Journal of Glaciology*, 11(62):177–203.

Röthlisberger, H. (1981). Eislawinen und Ausbrüche von Gletscherseen. In *P. Kasser (Ed.), Gletscher und Klima - glaciers et climat, Jahrbuch der Schweizerischen Naturforschenden Gesellschaft, wissenschaftlicher Teil 1978*, pages 170–212. Birkhäuser Verlag Basel, Boston, Stuttgart.

Ryser, C. (2009). The polythermal structure of Grenzgletscher, Valais, Switzerland. Masterarbeit, Abteilung für Glaziologie, VAW (unpublished), ETH-Zürich.

Schuler, T. (2002). Investigation of water drainage through an alpine glacier by tracer experiments and numerical modeling. Technical Report 177, Mitteilungen der Versuchsanstalt für Wasserbau, Hydrologie und Glaziologie der ETH Zürich.

Schuler, T. and Fischer, U. H. (2003). Elucidating changes in the degree of tracer dispersion in a subglacial channel. *Annals of Glaciology*, 37:275–280.

Schuler, T., Fischer, U. H., and Gudmundsson, G. H. (2004). Diurnal variability of subglacial drainage conditions as revealed by tracer experiments. *Journal of Geophysical Research*, 109:F02008.

Schuler, T. V. and Fischer, U. H. (2009). Modeling the diurnal variation of tracer transit velocity through a subglacial channel. *Journal of Geophysical Research*, 114. doi:10.1029/2008JF001238.

Smedt, F. D., Brevis, W., and Debels, P. (2005). Analytical solution for solute transport resulting from instantaneous injection in streams with transient storage. *Journal of Hydrology*, 315:25–39.

Spring, U. and Hutter, K. (1982). Conduit flow of a fluid through its solid phase and its application to intraglacial channel flow. *International Journal of Engineering Sciences*, 20:327–363.

Stearns, L. A., Smith, B. E., and Hamilton, G. S. (2008). Increased flow speed on a large East Antarctic outlet glacier caused by subglacial floods. *Nature Geoscience*, 1:827 – 831.

Steiner, D., Zumbühl, H. J., and Bauder, A. (2008). Two Alpine glaciers over the last two centuries: a scientific view based on pictorial sources. In Orlove, B., Wiegandt, E., and Luckman, B., editors, *The Darkening Peaks: Glacier Retreat, Science, and Society*, pages 83–99. University of California Press. International and Interdisciplinary Workshop on Mountain Glaciers and Society, held in Wengen, Switzerland, October 6-8, 2004.

Sugiyama, S., Bauder, A., Huss, M., Riesen, P., and Funk, M. (2008). Triggering and drainage mechanisms of the 2004 glacier-dammed lake outburst in Gornergletscher, Switzerland. *Journal of Geophysical Research*, 113:F04019.

Sugiyama, S., Bauder, A., Weiss, P., and Funk, M. (2007). Reversal of ice motion during the outburst of a glacier-dammed lake on Gornergletscher, Switzerland. *Journal of Glaciology*, 53(181):172–180.

Thorarisson, S. (1939). The ice dammed lakes of Iceland with particualr reference to their values as indicators of glacier oscillations. *Geografiska Annaler*, 21:216–242.

Toride, N., Leij, F., and van Genuchten, M. T. (1999). The CXTFIT code for estimating transport parameters from laboratory or field tracer experiments, version 2.1. Technical Report 137, U.S. Salinity Laboratory, U.S. Department of Agriculture, Riverside, California.

Tweed, F. S. and Russell, A. J. (1999). Controls on the formation and sudden drainage of glacier-impounded lakes: implications for jökulhlaup characteristics. *Progress in Physical Geography*, 23(1):79–110.

van Genuchten, M. T. and Wierenga, P. (1976). Mass transfer studies in sorbing porous media, I, Analytical solutions. *SSSAJ*, 40:473–481.

VAW (2007). Unterer Grindelwaldgletscher; Glaziologische Abklärungen im Zusammenhang mit der Seebildung. Bericht im Auftrag des Oberingenieurkreis I des Kantons Bern; Nr. 7945.21.2; (unpublished).

Waller, R. I., Russel, A. J., van Dijk, T. A. G. P., and Knudsen, Ó. (2001). Jökulhlaup-related ice fracture and supraglacial water release during the November 1996 jökulhlaup, Skeidarárjökull, Iceland. *Geografiska Annaler*, 83A(1–2):29–37.

Walter, F. (2009). *Seismic Activity on Gornergletscher during Gornersee Outburst Floods*. PhD thesis, ETH Zürich. No. 18184.

Walter, F., Clinton, J., Deichmann, N., Dreger, D., Minson, S., and Funk, M. (2009). Moment tensor inversion of icequakes on Gornergletscher, Switzerland. *Bulletin of the Seismological Society of America*, 99(2A):852–870.

Walter, F., Deichmann, N., and Funk, M. (2008). Basal icequakes during changing subglacial water pressures beneath Gornergletscher, Switzerland. *Journal of Glaciology*, 54(186):511–532.

Weiss, P. (2005). Gletscherdynamik vor und nach der Entleerung des Gornersees im Sommer 2004. Diplomarbeit, Abteilung für Glaziologie, VAW (unveröffentlicht), ETH–Zürich. pp. 149.

Werder, M. A., Bauder, A., Funk, M., and Keusen, H. R. (2010). Hazard assessment investigations in connection with the formation of a lake on the tongue of the Unterer Grindelwaldgletscher, Bernese Alps, Switzerland. *Natural Hazards and Earth System Sciences*, 10(2):227–237.

Werder, M. A. and Funk, M. (2009). Dye tracing a jökulhlaup: II. Testing a jökulhlaup model against flow speeds inferred from measurements. *Journal of Glaciology*, 55:899–908.

Werder, M. A., Loye, A., and Funk, M. (2009). Dye tracing a jökulhlaup: I. Subglacial water transit speed and water-storage mechanism. *Journal of Glaciology*, 55:889–898.

Werder, M. A., Schuler, T. V., and Funk, M. (submitted). Short term variations of tracer transit speed on alpine glaciers. *The Cryosphere*.

Wingham, D. J., Siegert, M. J., Shepherd, A., and Muir, A. S. (2006). Rapid discharge connects Antarctic subglacial lakes. *Nature*, 440:1033–1036.

Zumbühl, H. (1980). Die Schwankungen der Grindelwaldgletscher in den historischen Bild- und Schriftquellen des 12. bis 19. Jahrhunderts. *Denkschriften der Schweizerischen Naturforschenden Gesellschaft*, 92. 279 S. + Anhang.

Acknowledgements

To the successful completion of this thesis many people, of the VAW and others, contributed and my gratitude is extended to all of them. First and foremost, I would like to thank Martin Funk —my supervisor and boss— for making this PhD possible, for putting together such a fantastic project as the Gornergletscher-project, for allowing and supporting the large amount of field work I did, for sending me to summer schools and conferences, for always listening to my ideas, for making good suggestions and for providing input to my work. It has been a great pleasure working with him and spending good times in the field and in the Arvenstübli.

The other important scientific influence on me was Thomas V. Schuler. His PhD thesis was the first scientific glaciological text which I ever looked at, as I downloaded and read it to prepare myself for the job interview at VAW; this and my smart attire got me my PhD place. I would like to thank him for the good collaboration we had, for the numerous interesting conversations, for having me over in Oslo, for reading through my paper manuscripts and for being on my thesis committee.

I would like to thank Prof. Dr. Paolo Burlando for serving as a co-referee for my thesis and for his helpful comments to improve my thesis. Prof. Dr.-Ing. Hans-Erwin Minor and Prof. Dr. Robert Boes, I would like to thank for making the VAW such a good place to do my PhD at.

Many people have contributed to this thesis, be it with help during field work, office work, research or by distracting me when I did not manage to do that myself. Special thanks goes to the Gorner-crew for having made the field work such a great experience, both from a scientific and personal point of view. Alexandre Loye, doing his dimploma thesis with me, helped greatly in the first field season with making sure the tracer experiments worked; without him things would never gone as smoothly as they did. Fabian Walter and Patrick Riesen, the two other PhD students on the Gorner-project, made the field work one of the greatest experiences of my life. They both helped me with my work, with their assistance and advice, and were superb company when relaxing in the evenings, the "Seenachtsfest" springs to mind. Furthermore, to work with them on this project, also in the office, was stimulating and fun. Of course there were many others contributing. Bruno Nedela was our camp boss, painter, mountaineering advisor, tourist liaison officer, cook and excellent friend. Matthias Huss, Boris Müller and Patrick Weiss got the Gorner-campaign running in 2004 and set the bar high for Fabian, Patrick and me. Christina Bucher showed us how to correctly operate the theodolite (sorry, total station) and helped with lots of field work. And of course, I would like to thank the rest of the Gorner-crew for all their work and help during preparation and measurements and for the good times we had: Andy Aschwanden, Carolin Antoni, Andreas Bauder, Ruzica Dadic, Nicolas Deichmann, Olaf Eisen, Urs Fischer, Valentin Gischig, Huw Horgan, Albin Kretz, Martin Lüthi, Roger Rüegg, Claudia Ryser, Cornelius Senn, Shin Sugiyama, Steve Szoradi and Thomas Wyder.

The project, including my salary, was funded by the Swiss National Science Foundation (Grant-No. 200021-103882/1 and 200020-111892/1). Grande Dixence SA, Hydro Exploitation SA, the Swiss Military and the Hochalpine Forschungsstationen Jungfraujoch und Gornergrat helped with logistics and accommodation. Grande Dixence SA provided the discharge data from the proglacial stream Gornera, which were key data for my work. Michael Schurter lent me his BackScat fluorometer, which recorded most of the tracer experiments. I would like to thank

Garry Clarke and Gwenn Flowers for providing their computer programs which proved invaluable for my work. Regine Hock put a lot of work into making the two papers on "Dye tracing a jökluhlaup" what they became. Susan Braun-Clarke proof-read most of this thesis.

The good atmosphere and productive work environment at VAW is due to my good office mates, Marie Rousselot and Jed Brown, the Gorner-crew and the rest of the glaciological team: Hermann Bösch, Pierre Dalban, Jerome Failletaz, Daniel Farinotti, Jakob Helbing, Kolumban Hutter, Arne Keller, Antoine Pralong, Mélanie Raymond, Aurel Schwerzmann, Tetsuo Sueyoshi, Martin Truffer, Giuliana Turi and Stephanie Usselmann. I thank them for their help, the work they did for me, the inspiring discussions and the times in the Arvenstübli.

The team of the VAW Werkstatt has always been helpful and I would like to thank in particular Stefan Gribi, Daniel Gubser, Roger Lörtscher, Rolf Meier and Robert Pöschl for their help with equipment, electronics and transport systems. I am grateful to Christoph Ortmanns whos advice was valuable for the setup of the fluorometers.

I would like also to thank my friends: Lukas Frei and Dave Keen for conversations about statistics, computers and for other things, like drinking beer; Graham Tyldesley and Dirk Wallis for all the mountaineering we did in Scotland, the Alps and Peru; Ralf Petter for all the gnarly snowboarding and for having me as Godfather of his son Felix, who, incidentally, was born on the day of my defence; and all my other friends in Scotland, Switzerland and elsewhere for the quality times we had together during the years of my PhD, it would only have been half the fun without them.

I thank Ursula Meili for all the love she gave me, for the patience she had with me during the final throes of my PhD, for accompanying me on my postdoctoral academic pursuits and for making the future look so bright.

And my parents, I would like to thank, to have made all this possible with their support and love.